



Title	Behavior of Fe colloids in mine drainages of circumneutral and acidic pH : Implications from geochemical trends and Fe isotopes
Author(s)	Chikanda, Frances Semida
Citation	北海道大学. 博士(工学) 甲第14683号
Issue Date	2021-09-24
DOI	10.14943/doctoral.k14683
Doc URL	http://hdl.handle.net/2115/86930
Type	theses (doctoral)
File Information	Frances_Semida_Chikanda.pdf



[Instructions for use](#)

Behavior of Fe colloids in mine drainages of circumneutral and acidic pH: Implications from geochemical trends and Fe isotopes

A dissertation submitted in partial fulfillment of the requirements for the degree of
Doctor of Philosophy in Engineering

By

FRANCES SEMIDA CHIKANDA



Division of Sustainable Resources Engineering
Graduate School of Engineering, Hokkaido University, Japan

September 2021

Abstract

Mine drainages are increasingly attracting attention with regards to their contribution to toxic elements in river systems. Common to mine drainages, besides other toxic elements such as As, Zn, Pb and Cd, is Iron (Fe). Fe commonly exists in abundance in most mine drainages, resulting in the commonly known yellow boy, which are Fe minerals that form through the life of the drainage. The presence of Fe in such forms is influenced by the dynamics of Fe, which allow it to be in its ferrous state at anoxic conditions, but once conditions change to oxic, the Fe oxidizes and forms Fe minerals. Abundant in the environment are Fe nanoparticles, which are a very common form of Fe. Fe nanoparticles are remarkably abundant, and studies have widely reported their increased reactivity that is attributed to their increased surface area, but also, high mobility. These nanoparticles have been reported to sequester toxic elements in mine drainages, and act as transport vectors for Fe and the other elements, thereby affecting the elements' cycles. This therefore makes mine drainages significant players in contributing to global element cycles. Despite their significance, very few field studies have been carried to elucidate the detailed behavior of the nanoparticles in mine drainages. Therefore, this study was focused on highlighting the behavior of the nanoparticles in mine drainages, to clarify their impact on other toxic elements in the drainage and their contribution to element cycles.

The study was carried out at two mine drainages, Ainai and Shojin river, to cover a wider scope of the behaviors of nanoparticles in mine drainages. This is because mine drainages vary significantly in their geochemical characteristics. The study utilized two fractions of wastewater, dissolved and colloidal fractions to understand the water chemistry, supported by Fe isotopic fractionations and geochemical modelling to further explore the formation, behavior and transportation of the Fe nanoparticles. Understanding these behaviors allowed us to give an insight on the circulation of Fe in other aquatic systems.

Ainai mine drainage is a near-neutral pH drainage (avg 7.1), that utilizes aeration to treat, Fe, As and Zn. Wastewater is released from an underground mine, that is rich in ferrous Fe, to a drain about 1 km long, before being disposed off in a nearby river. The Ca-SO₄ type water, is quickly oxidized, resulting in ferric Fe, which then forms ferrihydrite colloids. The colloids are aggregated to over 300 nm when they begin to settle from the drainage towards the downstream. When the Fe colloids form as the primary colloids, As is incorporated into the Fe colloids, thereby being removed together with the Fe colloids. A variation in behaviors with seasons exists in that, in the rainy season, the colloids aggregate quickly due to increased interactions and are removed faster than in dry season when their aggregation is slower, then the colloids remain longer in the drainage.

On the other hand, Shojin river is an acidic drainage (avg 3.1), whose waste water is released with abundant ferric Fe. Wastewater (pH 3.1) containing Fe, As, Pb, Cd and other toxic elements is released, which then mixes with natural river water (pH 6.9), therefore resulting in an increase in pH after mixing. The dilution of the wastewater by river water plays a significant role in reducing the toxic elements to about a fourth of the original concentrations. Following dilution, an increase in pH occurs, which initiates hydrolysis of the ferric Fe, and due to the presence of sulphate in the wastewater, schwertmannite colloids are formed, also sorbing As during the process. Unlike at Ainai, the colloids at Shojin river display a dissolution behavior that results in a release of Fe and As. However, further downstream, the colloid formation picks up due to increase in pH, thereby effectively removing the toxic elements from the drainage, through aggregation and deposition. The different formation processes of the colloids are seen as a trigger for the variations in the processes occurring in the drainage and one that is highly affected is the aggregation rate. Quantitative calculations showed a faster aggregation rate at Ainai, compared to Shojin river and this was due to the quicker formation kinetics at Ainai, compared to those of Shojin river, given the low pH, which slows down reaction kinetics.

A novel approach of utilizing Fe isotopes of the water fractions is reported. At Ainai, the redox related, oxidative precipitation of the Fe colloids resulted in notable fractionations between the dissolved and colloidal fractions. The dissolved fraction had significantly lighter $\delta^{56}\text{Fe}$ values, compared to the colloidal fraction, which had relatively heavier values. Seasonal variation showed a difference in the oxidation rate, but which was, in either case, a difference that highlights the oxidative precipitation at Ainai mine drainage. When compared to Rayleigh fractionation model, a misfit was observed, which was attributed to colloids unaccounted for in the model, and hence reflected the colloids that were transported from the upstream of the drainage. The misfit was estimated quantitatively to reflect the number of colloids transported at the given distance. Finally, from the Fe isotopes, it was evident that the major phase of Fe being transported was in form of Fe colloids and remained the same unless extreme changes occurred. At Shojin river on the other hand, minimal fractionations were observed in the $\delta^{56}\text{Fe}$ values, because of the non-redox associated processes at Shojin river, during the formation of the colloids. Minor fractionations were however observed which reflected the precipitation and dissolution of the colloids.

In conclusion, the study highlights the significance of Fe colloids in mine remediation and the findings from this research can be implemented to increase the efficiency of mine drainage designs. Furthermore, the variations with season are important to consider in detail to ensure full time efficiency of the drainage because seasonal effects cause a variation in element concentrations, flowrates, and aggregation rates of the colloids. Since Fe colloids are stable at neutral pH, while some instability is observed at low pH, close monitoring at low pH is required to avoid re-release of toxic elements to the water. At a

larger scale, the abundance of Fe colloids in mine drainage systems is confirmed and it is seen that the transportation of the colloids may be a route through which Fe is supplied to rivers. This highlights why the rivers are high suppliers of Fe to oceans, and more importantly, the size fraction that is transported should always be in check to avoid mis-estimations of the amount of Fe supplied to oceans by rivers, that is transported from mine drainage systems.

Acknowledgements

I would like to extend my deepest gratitude to my professor, Associate Professor Tsubasa Otake for his support throughout my studies and stay in Japan. His support and effort towards grooming me into the person and professional that I have become is highly appreciated. Alongside his tremendous support, I will always appreciate the academic and social support that Professor Tsutomu Sato always offered. His encouragement for me to always improve my research remains a fundamental part of my study path. I am forever grateful for the academic guidance, motivation and inspiration that my professors gave me throughout this journey.

Secondly, my studies in Japan were highly enriched by my colleagues, the members of Environmental Geology. All of them contributed in one way or another, towards the attainment of my degrees. Particularly, I would like to thank Prof. Yoko Ohtomo for her constructive analysis during my study period. I would like to appreciate Ms. Akane Ito, my academic supporter during the initial stages of my studies and paved an encouraging path towards my study life. Ms. Aoi Koide, who set the background for my doctoral research, and her direct assistance in my experiments.

My research was a combination of field work, experiments, and data reconciliation, all of which were done with colleagues, mostly from the Environmental Geology laboratory. Specifically, Sereyroith Tum and Tatsuya Matsui, with whom I shared a research group, also highly assisted in my studies. I would also like to recognize Ms. Ayaka Murofushi and Mr. Edward Nhlane for their support during the project in Malawi. Some external institutions that assisted with data obtaining include the Nanomaterials department in Frontier for Research (FE-SEM, TEM), and Research Institute for Humanity and Nature, RIHN (Fe isotope data). All these, and many others made my research possible and a success.

Last but not least, I would like to extend my heartfelt appreciation to my husband, Hermes Dinala, who always supported my dreams and made sure I achieve my best at all times and my son Roman Yuki, who is my recent great motivation. I appreciate my mother, Playsant Munthali, who has always been an inspiration to me, and made sure that I succeed in life. My family and friends that helped me balance my academic and social life. And most importantly, I thank God for granting me the wisdom and grace throughout my studies.

Table of Contents

Abstract	i
Acknowledgements	iv
List of tables	ix
List of Figures	ix

Chapter 1: General introduction

1.1	Background	1
1.1.1	Fe colloid formation and toxic element uptake	3
1.1.2	Formation of Fe colloids at circum-neutral pH	5
1.1.3	Formation of Fe colloids in acidic condition	6
1.1.4	Isotopic Fe fractionations as indicators for Fe cycling	7
1.2	Problem statement	8
1.3	Objectives of the study	8
1.4	Approaches and methodologies	9
1.5	Structure of thesis	11

Chapter 2: Formation of Fe colloids and Zn-Fe Layered Double Hydroxides as sequestration agents for toxic elements in the circumneutral Ainai mine drainage

2.1	Introduction	13
2.2	Description of study area: Location, geology, and drainage system	14
2.3	Materials and methods	16
2.3.1	Field sampling: Water and solid samples	16
2.3.2	Analytical methods	17
2.4	Results	18
2.4.1	On-site and element concentrations of water samples	18
2.4.2	Dissolved and colloidal fractions of the toxic elements in the drainage ..	22
2.4.3	Characterization of the Fe colloids	25
2.4.4	Characterization of Zn colloids	30
2.5	Discussion	31
2.5.1	General characteristics of water samples	31

2.5.2	Formation of the Fe colloids in the drainage and removal of As	32
2.5.3	Colloid mineralogy responsible for sequestration of toxic elements	34
2.5.4	Aggregation and deposition of the Fe colloids	34
2.5.5	Removal of Zn by Zn-Fe Layered Double Hydroxides.....	36
2.6	Summary	37

Chapter 3: Formation of Schwertmannite colloids in the acidic Shojin river and their impact on metal sequestration

3.1	Introduction	39
3.2	Description of study area: Location, geology, and drainage system.....	40
3.3	Materials and methods	43
3.3.1	Field sampling: Water and solid samples	43
3.3.2	Analytical methods	43
3.4	Results	44
3.4.1	On-site and general water characteristics	44
3.4.2	Colloidal and dissolved fractions of Fe, As and Pb.....	47
3.4.3	Characterization of Schwertmannite colloids and other mineralogy in the drainage	50
3.5	Discussion	56
3.5.1	General water characteristics.....	56
3.5.2	Formation of schwertmannite colloids in the drainage and their sequestration of toxic elements	57
3.5.3	Dominant mineralogy for sequestration of toxic elements.....	61
3.6	Summary	62

Chapter 4: A comparison of colloid behavior in the Ainai and Shojin river drainages

4.1	Introduction	64
4.2	Methodology	64
4.3	Results	65
4.3.1	A comparison in the colloid formation from field observations	65
4.3.2	Colloid mobility at Ainai and Shojin drainages	66
4.4	Discussion	69
4.4.1	Key variations in the geochemical characteristics of Ainai and Shojin rivers.	

4.5	Summary	70
-----	---------------	----

Chapter 5: Fe isotope systematics associated with the formation and transportation of Fe colloids in Ainai and Shojin mine drainages

5.1	Introduction	71
5.2	Materials and methods	72
5.2.1	Purification of Fe solution	72
5.2.2	Analytical methods	73
5.3	Results	73
5.3.1	Isotopic fractionations in the dissolved and colloidal fractions of Ainai mine drainage and Shojin river	73
5.4	Discussion	76
5.4.1	Relationship between the colloid formation and isotopic fractionations of the dissolved and colloidal fractions.	76
5.4.2	Flux of Fe inferred from Fe isotopes and colloid behavior	82
5.5	Summary	87

Chapter 6: Theoretical simulations of Ainai and Shojin mine drainages using geochemical modelling and thermodynamic calculations

6.1	Introduction	89
6.2	Methodology	89
6.2.1	Thermodynamic modelling.....	89
6.2.2	Transport modelling	90
6.2.3	Theoretical estimation of aggregation and deposition.....	91
6.3	Results	92
6.3.1	Geochemical simulations of Ainai mine drainage and Shojin river.....	92
6.3.2	Simulation of colloid transportation by Phreeqc	93
6.3.3	Theoretical estimations of aggregation and deposition kinetics.....	95
6.4	Discussion	98
6.4.1	Fe systematics of Ainai mine drainage with Shojin river system with respect to their geochemical characteristics	98
6.4.2	Transportation of the colloids as a function of pH	99

6.4.3	Aggregation and deposition kinetics of Ainai mine drainage and Shojin river	102
6.5	Summary	104

Chapter 7: General conclusions and implications

7.1	Conclusions from the study	105
7.2	Implications of the study	107

References.....	111
------------------------	------------

Appendix	119
-----------------------	------------

List of tables

Table 2-1. Data summary of on-site parameters of Ainai mine drainage measured during field work.....	19
Table 2-2. Fe, As and Zn concentrations in dissolved and colloidal fractions in July and October.	24
Table 3-1. Results of on-site measurements from the Shojin river	46
Table 3-2. Main anion chemistry of the Shojin river mine drainage.....	47
Table 3-3. Fe, As and Zn concentrations in dissolved and colloidal fractions in July and October.	48
Table 4-1. A comparison of geochemical characteristics of Ainai and Shojin	65
Table 5-1. Summary of the Fe isotopic fractionation values in the different fractions of total, dissolved and colloidal fractions at Ainai drainage and Shojin river.....	75
Table 6-1. Parameters used to calculate aggregation rate at Ainai and Shojin.	97

List of Figures

Figure 1-1. An estimated global accounting for all natural, incidental, and engineered nanomaterials on or in Earth's surface and atmosphere (Hochella et al., 2019).....	3
Figure 1-2. Definition of the truly dissolved, dissolved, colloidal and particulate Fe by size.....	4
Figure 1-3. A summary of the sampling and analytical approaches applied in this research work.....	10
Figure 2-1. (a) A schematic representation of Ainai mine drainage showing the sampling points (S1–S6), reservoir (P1), and settling pond (P2) with an inset map showing the location in Japan; (b) pipe releasing water from underground to concrete drain; (c) concrete drain inside the tunnel; (d) upper exterior drain (S1); (e) unconcreted upper to middle drain, (f) concreted lower drain; (g) reservoir pond (P1).	15
Figure 2-2. A summary of the sampling and analytical approaches applied in this research work.....	16
Figure 2-3. Average fluid compositions for July and October. (a) Down-drain pH and alkalinity trends and (b) stiff diagram.	20
Figure 2-4. Average trends of the (a) Precipitation and flow rates at Ainai mine; (b) Fe ²⁺ concentration (pack test) and turbidity in July 2016 and October 2018.....	21
Figure 2-5. Trend displayed by (a) turbidity and (b) Fe ²⁺ concentrations from pack test in July and October.....	21
Figure 2-6. Amount of organic carbon in the Ainai wastewater samples	22
Figure 2-7. Distribution of (a) Fe, (b) As, (c) Zn and (d) Si concentrations in dissolved and colloidal fractions as a function of distance from the mine.....	25

Figure 2-8. XRD profiles of (a) sediment samples from S1 and S5 and (b) suspended solids from P1.....	26
Figure 2-9. Fe colloids on a 200kDa ultrafilter	27
Figure 2-10. Size and aggregation variations of Fe colloids in the Ainaï mine drainage.	27
Figure 2-11. (a) An FE-SEM (secondary electron) image of colloid aggregates collected on ultrafilters and (b) the electron dispersive spectra of the colloids.....	28
Figure 2-12. TEM images of the ferrihydrite colloids. (a) Colloid aggregate and (b) magnified colloid aggregate showing the 3 to 5 nm colloids that compose the larger 100 nm colloids.	29
Figure 2-13. Size distribution of the colloids in Ainaï mine drainage observed in FE-SEM and TEM images.....	29
Figure 2-14. Field emission–SEM images of Zn LDH in (a) a natural sample from S3 suspended solids; and (b) a synthetic sample (c) EDS spectrum of the Zn-Fe LDH from synthesized sample and (d) EPMA peaks of the synthesized sample in (c).....	31
Figure 2-15. Colloidal concentrations of Fe in July and October as a function of distance from the mine.	36
Figure 2-16. A graphical summary of the Ainaï mine drainage.....	38
Figure 3-1. Schematic of the Shojin river drainage, showing the sampling points. Insert map is the location of Shojin river in Hakodate area.	41
Figure 3-2. Pictures of the Shojin drainage. SW1 shows the SW1 sampling point and the limestone bed, SR1 is the river water before mixing, SW2 is the second source of wastewater, SR2 is after mixing of the waste and river waters and SR7 is further downstream of the drainage.....	42
Figure 3-3. Trends of (a) pH, Fe ²⁺ and (b) turbidity from upstream to downstream	45
Figure 3-4. Anion concentrations of the Shojin river drainage.	47
Figure 3-5. Concentrations of (a) total Fe, (b) total As, and (c) total Pb. Fe, As and Pb in dissolved and colloidal fractions are shown in (d), (e) and (f) respectively. pH is shown as yellow triangles in the Fe plot. “Total” in all the element plots refers to concentrations obtained as the sum of the colloidal and dissolved fractions. In the fraction distribution plots, the wastewater sources (SW1 to 4) are eliminated because their concentrations are too high and hence decrease the visibility of the trends of colloid formation from SR2 onwards.....	49
Figure 3-6. XRD profile of the sediments collected at SR2. Sh: Schwertmannite.	51
Figure 3-7. The mineralogy identified in the solid particle analyses carried out on Shojin river samples. (a) An aggregation of the Fe colloids, (b, c and d) up-close images of the bulbous, fibrous schwertmannite colloids (e) goethite occurring on an aged aggregate surface of the schwertmannite colloids, and (f) goethite crystals amongst colloid aggregates and other minerals.	53
Figure 3-8. Colloids collected on the 200 kDa ultrafilters of SR2 and SR5.	54
Figure 3-9. An up-close observation of the schwertmannite colloids collected on the 200 kDa ultrafilter. (a) A secondary electron image of colloid aggregates, (b) the EDS spectra from SEM showing the elemental composition of the colloids and (c) a TEM image of the colloids.....	55

Figure 3-10. (a) Chemical and (b) channel structures of schwertmannite (Zhang et al., 2018).....	59
Figure 3-11. Removal of Pb as a function of pH calculated by a surface complexation model (GWB)	60
Figure 3-12. A graphical summary of the remediation process at Shojin river	63
Figure 4-1. A comparison in correlation of the Fe and As in dissolved and colloidal fractions at (a) Ainai mine drainage and (b) Shojin river.....	66
Figure 4-2. Colloids transported from the upstream as a function of distance. The arrows represent the settling rate at the two study sites.	68
Figure 4-3. Fe colloid concentrations and size variations at Ainai and Shojin. Brown structures are the Fe colloids, while the yellow circles represent the incorporated As..	68
Figure 5-1. Photographic images showing (a) separation of Fe solution through resin and (b) final solution collected in micro vials for analysis	73
Figure 5-2. Fe isotope variation of total, dissolved and colloidal Fe of Shojin river drainage. The light gray shade shows the region for $\delta^{56}\text{Fe}$ of Fe sulphides (Sharma et al., 2001).....	77
Figure 5-3. The isotopic fractionation pattern of Fe in Ainai mine drainage in the (a) rainy and (b) dry seasons.	79
Figure 5-4. Fractionation pattern of Ainai Fe with respect to Rayleigh fractionation model at various fractionation factors ($\Delta=1.5$ and 2%).	82
Figure 5-5. Fe isotopic values of various Fe sources including rivers.	83
Figure 5-6. (top) A relationship of the measured vs modelled data of the Ainai mine drainage. The arrows represent the misfits between the modelled and actual data. (bottom) The $\delta^{56}\text{Fe}$ plot displaying the area whose integration gives the $\delta^{56}\text{Fe}$ that is attained as a result of colloids transported from upstream to the particular site.	87
Figure 6-1. (a) Solubility diagram of Shojin river and (b) Stability diagram of Fe species in Ainai mine drainage.	92
Figure 6-2. Colloids transported from the upstream as a function of distance.....	93
Figure 6-3. Comparison of field and modelling data of colloid formation and transportation of Fe colloids at Ainai mine drainage and Shojin river.....	94
Figure 6-4. A variation in the aggregation rates at Ainai mine drainage and Shojin river.	96
Figure 6-5. The aggregation process of colloids based on Brownian's motion.	103
Figure 7-1. New proposed design for Ainai mine drainage implied from our findings.	108
Figure 7-2. The proposed design of the sedimentation pond at Ainai mine drainage..	109
Figure 7-3. Colloid mobility at circumneutral and acidic pH mine drainages along with their isotopic signatures.	110

1 Chapter 1: General introduction

1.1 Background

Mine drainages are an increasing source of toxic elements in the environment (Fu and Wang, 2011), due to wastewater released from underground workings or tailings. Since the increase in demand for mined materials continues to grow due to industrialization, mine-related water contamination is expected to increase. Effluent from mine contamination contain a wide variety of contaminants, that require treatment approaches suited to the contamination. To treat such wastewater, various treatment methods have been applied to mine drainage, all involving long-term and expensive processes. Considering the long term treatment that is commonly required in mine drainages, natural remediation processes, (i.e., passive treatment systems), are becoming the preferred option (Zipper et al., 2014). Natural remediation approaches utilize naturally occurring geochemical, biological, and physical processes (Zipper and Skousen, 2014) to treat the contaminated water, thereby making it a cheaper option than its active treatment counterpart. However, since the processes in natural remediation are mostly naturally occurring, a deep understanding of the processes is required for the development of efficient treatment of the mine drainages. Furthermore, for the sustainability of mining, development of passive water treatment systems, that employ natural remediation, is key. Therefore, this research focused on semi-passive and passive treatment systems in order to understand the systems in detail and establish ways to improving the passive treatment systems for sustainable mining.

Worth noting is that the geochemical characteristics of wastewater in the mine drainages, such as pH, redox conditions, dissolved chemical composition, and organic-matter content (Nordstrom, 2011) occur in a wide variation, and may also differ with season. As a consequence, it is necessary for designing efficient treatment systems, to understand the processes and factors that affect natural remediation. The most common types of mine drainage wastewaters are acidic (Dold, 2014), usually referred to as acidic mine drainage (AMD). AMD usually occurs due to interactions of water, and rocks containing sulphur-bearing minerals forming sulphuric acid and dissolved iron and other metal ions (Dold, 2014). Reactions occur that result in pH ranges of about 2 to 8, and leave the waters in a contaminated state, i.e., with high concentrations of metal ions. To achieve remediation, most mine drainage that is highly acidic e.g. pH below 4, is mixed with other water sources to attain a circumneutral pH (Jung et al., 2012), which helps to precipitate toxic elements with other oxides out of the water systems. However, field studies highlighting the processes that play key roles in achieving efficient remediation in these mine drainages are scarce, especially with regards to nanoparticle behavior.

Nanoparticles are generally defined as particulate matter with at least one dimension that is less than 100 nm (Christian et al., 2008). This definition, being based on spatial dimensions, allows for inclusion of ultrafine particles as well as colloids, however, makes the understanding of these particles complex and highly heterogeneous. (SCENIHR, 2006). These particles occur in a wide range and their remarkable abundance in the environment has drawn attention to their contribution to global cycles of e.g. Iron (Fe), Carbon (C) and Nitrogen (N), that are relevant to human life and the environment. Varying widely from engineered, biological and environmental nanoparticles, they all play significant roles in the environment, but in this research, focus is given to the environmental nanoparticles that occur in mine drainages. These nanoparticles are supplied to oceans via various sources, such as aerosols, wind and glaciers, however the largest suppliers have been reported to be river systems (Figure 1-1. An estimated global accounting for all natural, incidental, and engineered nanomaterials on or in Earth's surface and atmosphere Hochella et al., 2019). These river systems have further been reported to be highly affected by mine drainages, and in mine drainages, an abundance of toxic elements cannot be denied. Consequently, this potentially leaves river systems that are affected by mine drainages as significant sources through which transportation of toxic elements to oceans can be understood.

Among the many (toxic) elements, Fe is usually abundant in the mine drainage systems, thereby drawing the attention of this research to Fe nanoparticles. Understanding of Fe nanoparticles has been reported to give insight on the behavior of other (toxic) elements (e.g. Fritzsche et al., 2011; Gledhiir and Buck, 2012; von der Heyden and Roychoudhury, 2015), because of the ability of Fe to sorb other elements, affecting their fate and thereby warranting a detailed study. Furthermore, Fe nanoparticles in mine drainages besides being remarkably abundant and affecting other elements, have been reported to be highly mobile and can therefore act as transport vectors for other elements within the mine drainages and beyond. Thus far mine drainages have highly affected (contaminated) river systems around the world (Byrne, 2019), and as a result, mine drainages are recognized as one of the biggest contributors of toxic elements to the rivers and hence oceans.

The transportation of these colloids is highly dependent on their physiochemical properties and distribution, which vary widely depending on system. Tracing the mobility of these elements has been done by a couple of approaches, however, Fe isotopic fractionations are an emerging approach that has high potential to achieve the same. Fe leaves isotopic signatures depending on their source, and may fractionate with distinct processes, hence, they have been utilized in this research as tracers for the mobility of the Fe colloids. Furthermore, this approach has been applied to infer on Fe mobility on a global scale.

It is based on these backgrounds, that the current research was carried out. Specifically, the behavior of Fe nanoparticles in mine drainages were studied, their formation, aggregation, deposition, and transportation behaviors, using field measurements, water and sediment analyses, geochemical modelling and Fe isotopic fractionations. Seeing as the studied aspects fall in several sub-categories, each aspect is explained below.

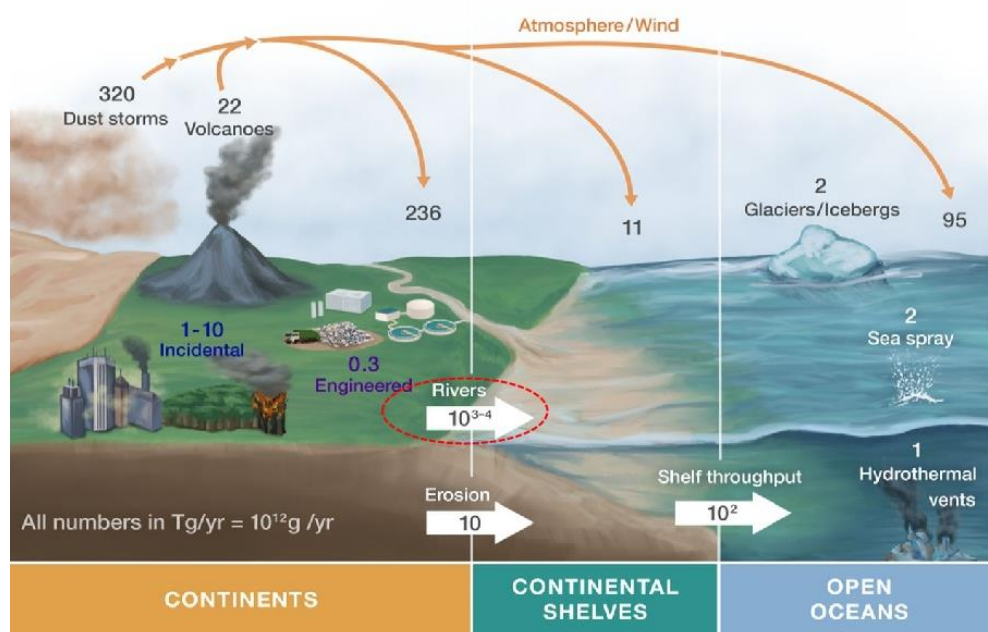


Figure 1-1. An estimated global accounting for all natural, incidental, and engineered nanomaterials on or in Earth's surface and atmosphere (Hochella et al., 2019)

1.1.1 Fe colloid formation and toxic element uptake

Iron is generally ubiquitous in mine drainages, along with other toxic elements (Pokrovsky and Schott, 2002; Schemel 2000). The thermodynamic characteristics of Fe allows it to affect the mobility of toxic elements such as arsenic (As), zinc (Zn), lead (Pb), and copper (Cu), because it exists as Fe^{2+} in relatively anoxic environments but can oxidize to Fe^{3+} and form Fe oxyhydroxides under oxidizing conditions (Whitney King, 1998). In oxic and neutral-pH environments, Fe^{3+} exists predominantly in the oxyhydroxide form, facilitating the formation of Fe-rich colloids (1 nm to 100 nm) (Liao et al., 2017; Gledhiir and Buck, 2012). Nonetheless, colloidal Fe may exist in environments of acidic pH, as well, therefore our investigation was carried out in both acidic and near-neutral systems.

Mine drainages are usually abundant in Fe (Williamson et al., 2006), among other elements. The dynamics of Fe allow it to be ferrous Fe in anoxic and oxidize to ferric Fe in oxic environments, therefore facilitating the formation of Fe (oxy) hydroxides. Studies regarding these (oxy) hydroxides have been widely carried out (e.g. Dold, 2014; Sverjensky and Fukushi, 2006; Khamphila et al., 2017), however preceding, co-existing or even dominating species in these systems are the Fe colloids (Boye et al., 2010). Fe-rich nanoparticles range in size from 1 to 100 or 200 nm, have large surface areas and are therefore very reactive. These particles are also resistant to settling by gravity, therefore act as geochemical vectors for transporting other toxic elements in the drainages (Pokrovsky and Schott, 2002). The presence of these Fe colloids has been reported to affect the fate of other toxic elements; therefore, an investigation is carried out at Aina mine drainage and Shojin river to clarify the formation of the Fe colloids, their formation dynamics, their impact on the co-existing (toxic) elements.

For a long time, 0.45 to 0.2 μm filtration was used to separate particulate from dissolved particles, however, this dissolved phase contains Fe colloids and truly dissolved Fe (Figure 1-2). This has raised concerns for determination of size fraction cut-offs that may be safe in determining water chemistry. Considering the abundance and large surface area of colloids, which Jung et al. (2012) correlated with an increased reactivity than bulk suspended solids, their sequestration of other toxic elements is reported to be higher and requires detailed understanding. Experimental studies have also highlighted this (Sharma et al., 2010; Mokhter et al., 2018). However, due to the diverse geochemical characteristics of treatment systems, field evidence concerning the formation and behavior of Fe colloids, and their significance in removing toxic elements from mine drainage, still requires clarity.

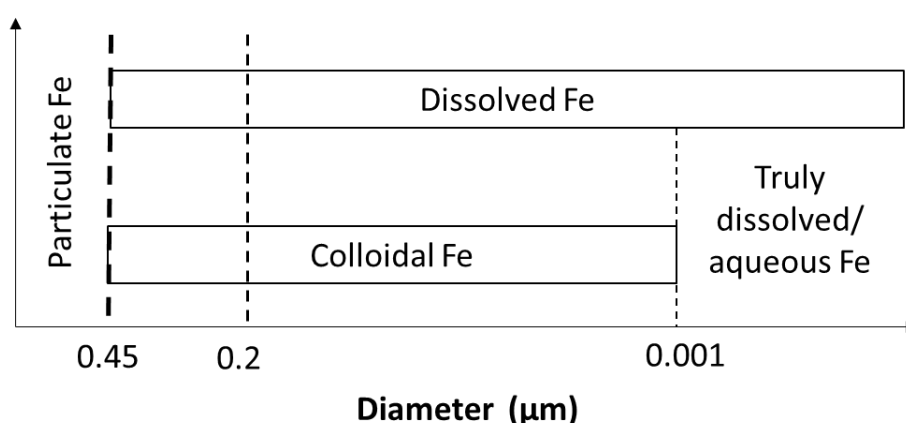


Figure 1-2. Definition of the truly dissolved, dissolved, colloidal and particulate Fe by size.

In this study, the colloids were defined as particles of sizes 0.2 microns to 200 kDa (to represent particles under 5 nm), while truly dissolved are below 200 kDa. The reason for the cut off chosen for the colloids best reflects the particles that remain suspended in water and resist gravitational settling, hence can be transport media for other elements. Beyond this size, studies have shown that particles will quickly settle and therefore are mostly referred to as particulates and are therefore not a point of consideration in this study.

Colloid deposition/transportation behavior has been a topic of discussion for a while. The traditional size definition resulted in some elements being underestimated in water systems, and since these colloids exhibit characteristic properties, that differ from the dissolved or particulate matter, studying the behavior of these colloids requires detailed studies. Colloids are resistant to gravitational settling, and studies of their formation and aggregation rates should account for the time they remain in the system (Pokrovsky and Schott, 2002; Wang et al., 2016). Whereas deposition of colloids is possible once the aggregates become large enough, aggregation rates may vary between systems and depending on the aqueous chemistry. The estimation of aggregation rate is therefore a major aspect to consider in the design of passive treatment systems.

Sequestration of toxic elements in mine drainage by nanoparticles has been widely studied (e.g. Hao et al., 2018)(Babakhani, 2019)(Ritter et al., 2006) Processes such as competitive adsorption and precipitation kinetics in mine drainage usually result in the formation of a variety of mineral phases that are able to sequester toxic elements (Plumlee et al., 1997; Nguyen et al., 2019). In addition to Fe colloids as a dominant medium for remediation, layered double hydroxides (LDHs) have also gained popularity due to their efficiency, flexibility, and ability to reduce concentrations of metals such as Zn and Cu (Xu et al., 2013; Okamoto et al., 2010). Previous studies have reported natural occurrences of LDHs and their synthesis, particularly in the presence of Fe (Morimoto et al., 2015a; Hongo et al., 2008). However, clarity is still lacking regarding the characterization of LDHs and factors crucial for their formation and stability, as might be provided by comparisons of field and experimental observations.

1.1.2 Formation of Fe colloids at circum-neutral pH

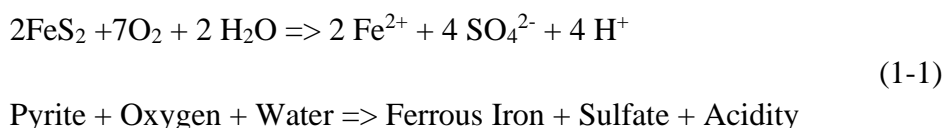
Acidic mine drainages (AMD) occur in wide range of pH values that range from 2 to 8 (Skousen *et al.*, 2017). The generation of AMD is a result of interaction of water with rocks that have been exposed due to mining activities. In these drainages, the geology, mineralogy groundwater chemistry varies, thereby resulting in the variation of the nature of mine drainages. These geochemical variations control the geochemical processes that occur in the drainages. In this section, focus is given to mine drainages of circum-neutral pH and the processes that dominate the systems. Nevertheless, in most mine drainage, iron oxide minerals are ubiquitous and a subgroup of them is term hydrous ferric oxides (HFO). These HFO consist of a wide variety of amorphous minerals are represented by

the general formula a $\text{Fe}_2\text{O}_3 \cdot n\text{H}_2\text{O}$, a common mineral being ferrihydrite (Plumlee, Logsdon and Filipek, 2020).

Ferrihydrite is yellow to reddish-brown mineral common to mine drainage at near neutral pH (Bowles and Oxides, 2021). It has a large surface and high reactivity, making it a significant mineral when it comes to self-remediating systems (Plumlee et al., 1997). Previous studies have reported a high efficiency in the remediation by ferrihydrite and the formation of these minerals was also investigated. It was reported that the ferrihydrite forms from smaller particles that are formed from keggin group of tetrahedra and octahedra within a unit cell, that form from Fe, O and H. The precursor, nanoparticles are usually more reactive and are very abundant, making them significant players in the self-remediating process. Despite the abundance, further clarity is still required with regards to the behavior of the colloids at circum-neutral pH.

1.1.3 Formation of Fe colloids in acidic condition

As earlier mentioned, mine drainages vary in geochemical characteristics hence a detailed background of the colloids in acidic conditions is reviewed. Acid mine drainage (AMD) is generated when sulphide minerals are exposed to oxygen and water as summarized in the general equation below (Akcil and Koldas, 2006) :



As pointed out in the previous section, and evident from the above equation, AMD is commonly abundant in Fe, varying from Fe^{2+} to Fe^{3+} depending on the source and characteristics of the drainage. Depending on the nature of the mineralogy, which is commonly sulphide minerals, SO_4^{2-} is also common in these drainages. These ions exist along with other ions that vary widely and include toxic elements and heavy metals. The pH of these mine drainages also varies, however, in most cases, they are highly acidic from the protons supplied during the mineral dissolution. The pH plays a significant role in the state of the drainage since at low pH, the solubility of many elements is high and with an increase in pH, precipitation is likely to occur with a high stability. Among other factors, the pH is one of the most significant factors that determine the remediation approach that will be applied in a mine drainage.

The presence of Fe in the drainages allows for the formation of secondary Fe minerals, because of the thermodynamics of Fe. Fe has the ability to form a wide variety of minerals

that have the ability to sequester other toxic elements from the drainage thereby aiding in the remediation process. Depending on the pH, the Fe mineralogy may vary. Schwertmannite has been reported as the most common Fe mineral in AMD, with the variable chemical formula of $\text{Fe}_8\text{O}_8(\text{OH})_{8-2x}(\text{SO}_4)_x \cdot n\text{H}_2\text{O}$ ($1 \leq x \leq 1.75$) (Cruz-Hernández et al., 2017; Fernandez-Martinez et al., 2010). Schwertmannite is a poorly crystalline mineral, that has a high specific area and tunnel structure that acts as an important sink for trace metals, therefore playing a significant role in determining their fate. Schwertmannite occurs in a wide variety of sizes and in this research, particularly, the formation and role of schwertmannite colloids is investigated.

At low pH, the formation of stable nanoparticles may be challenged and result in dissolution behaviors, and hence release of the toxic elements that were sorbed by the sequestration media. Nonetheless, colloids may still exist in these systems and therefore are worth a detailed investigation. Schwertmannite forms through two main pathways; Fe^{3+} hydrolysis or biotic and/or abiotic oxidation of Fe^{2+} . Various experimental studies have been carried out to follow these formation pathways, however, very few studies have investigated the schwertmannite colloids in the actual field.

1.1.4 Isotopic Fe fractionations as indicators for Fe cycling

Having clarified the behaviors of Fe and the colloids in these mine drainages, an estimation of Fe flux was then considered. A combination of geochemical trends and Fe isotopic fractionations was taken to achieve this. Fe has four stable isotopes ^{54}Fe (5.8%), ^{56}Fe (91.8%), ^{57}Fe (2.1%) and ^{58}Fe (0.3%) (Poitrasson, 2006), and fractionations of the isotopes occur with respect to various processes that Fe in the solution or mineral undergoes. The emergence of better analysis has allowed for more precise and accurate analyses to distinguish fractionations of the various isotopes in a wide variety of terrestrial samples. Factors that control the fractionation processes include mineral weathering, mineral precipitation and dissolution and redox processes among others (Fantle and DePaolo, 2004; Bergquist and Boyle, 2006). In these aquatic systems, Fe may change its redox state, or change from e.g., dissolved to colloidal phase, therefore resulting in observable isotopic fractionations. The presence or absence of organic matter in the reactions also determines the nature of fractionation that may happen. The distinct differences in $\delta^{56}\text{Fe}$ that have been observed for riverine particles and colloids make the Fe isotopes a suitable tracer for source and Fe mobility. Therefore, we infer the geochemical trends and isotopic fractionations to the Fe mobility on the mine drainages and the global Fe cycle.

Iron, the fourth most abundant element in the crust is an essential micronutrient whose circulation in Earth's surface environments (e.g., lithosphere, atmosphere hydrosphere,

biosphere) is very important. Fe exists in various phases i.e. truly dissolved, colloidal, and particulate state, and its form of existence highly determines its availability especially as a micronutrient (Escoube et al., 2015). It further exists in either ferric or ferrous state, which significantly controls its characteristic behavior. These phases of Fe are crucial because they significantly affect its circulation, and in turn, the Fe cycle and supply to oceans affects the marine geochemistry and the global Fe and C cycle (Boyd and Ellwood, 2010). Fe is summarized to be sourced mainly from, among others, the continental shelf, hydrothermal vent, aerosols (atmospheric deposition), glaciers and rivers (Raiswell and Canfield, 2012). Some of these supplies, e.g. hydrothermal vents, vary insignificantly at short timescales, thereby contributing very little to the overall cycle of the Fe. This leaves rivers as one of the major contributors of Fe to oceans. Rivers have been fed and affected by different sources, but in the recent years, mine drainage has been reported as the highest supplier of (toxic) elements to rivers due to a significant increase in wastewater produced from mine waste (Norsuzila et al., 1989). Among other elements, Fe which is a common abundant element in mine drainages, is highly supplied to rivers by these drainages, thereby affecting the flux of Fe to the oceans and hence the global cycle.

1.2 Problem statement

Having reviewed previous work and findings related to Fe colloids, it is evident that gaps exist with regards to their understanding. One extensive gap is highlighted due to the diversity of environments, reaction pathways and many other factors that are undergone during their formation. Nonetheless, their significance in the remediation of mine drainages cannot be over emphasized. Based on the background, this research aimed to address the following questions.

- a. How do colloids form in mine drainages of circum-neutral and acidic conditions?
- b. What reaction pathways do they follow, and what geochemical factors determine their behavior in the drainages?
- c. How do these colloids affect other (toxic) elements in the drainages?
- d. How do processes such as aggregation and deposition play a role in determining the behavior of the colloids in the drainages?
- e. How can a novel method, i.e., Fe isotopic fractionation, be utilized to understand the behavior of Fe colloids and infer the findings to the global Fe cycle?

1.3 Objectives of the study

The overall objectives of this research are to highlight the formation processes of Fe colloids and their role in transporting or removing toxic elements in mine drainages of

acidic and circumneutral pH. Furthermore, the significant processes that are related to the behavior of the colloids are investigated to assist in understanding the colloids and the fate of the toxic elements. Finally, Fe isotopic fractionations of the mine drainages from upstream to downstream were analyzed to utilize the fractionations and Fe concentration variations to highlight the colloid transportation and Fe flux at a larger scale.

Particularly, in chapter 2, we studied a circumneutral passive treatment system that utilizes aeration to remove Fe, As, and Zn from underground wastewater drainage from Aina mine, Japan, considering both dissolved and colloidal fractions. The progression of elements from dissolved to colloidal states and their fate were studied. Specific objectives were to; (1) clarify the formation, semi-quantitative aggregation, and deposition behaviors of Fe colloids at circumneutral pH; (2) examine their application to As and Zn sequestration from mine drainage over two seasons and (3) investigate the formation of LDHs by comparing natural and synthetic samples and factors affecting their formation and stability. The concentrations of metals in the drainage system from the mine provided insight into the behavior of the metals involved, and highlighted factors that determine the fate of toxic elements in mine drainage.

Similarly, in chapter 3, studying the acidic drainage highlights; (1) the formation, semi-quantitative aggregation, and deposition behaviors of Fe colloids at acid pH and (2) the sequestration methods for As by the Fe colloids.

The objectives met in chapter 4 are how the cycling of Fe is understood using Fe isotopic fractionations while the geochemical modelling in chapter 5 simulates our field findings for easier implementations.

1.4 Approaches and methodologies

Fe is an abundantly occurring element that significantly influences the biogeochemistry of other elements and hence significant element cycles (Tagliabue et al., 2017). As earlier reported, Fe is particularly abundant in mine drainages, and in these systems also plays a significant role in determining the fate of other elements. Fe has been reported to have high reactivity and interactions with other elements, irrespective of its form, i.e. dissolved, colloidal and particulate, however, the increased surface area associated with the colloids makes them the most reactive with the other elements (Conrad et al., 2019). Furthermore, the resistance to gravity settling of the colloids complements the attention that they draw when studying the behavior of Fe in the mine drainages as well as other aquatic systems. Previous studies have also highlighted the repeated sedimentation, resuspension, and recycling of Fe, making its mobility a complex phenomenon. It is based on these backgrounds that the initial approaches in chapters 2 and 3 were developed. Fe colloids

were particularly the point of focus, as these have clearly shown to play active roles in the systems of interest.

Therefore, Fe behavior was studied in particular with focus on the dissolved and colloidal fractions of the Fe. This enabled a clear understanding of the Fe in the mine drainages, and hence an implication to Fe circulation in other systems.

In addition to the standard circulation of Fe implied from the dissolved and colloidal fractions, attention has grown towards the application of Fe isotopic fractionations to highlight the behavior of the Fe, in both dissolved and colloidal fractions. Factors that control Fe isotopic fractionations include the redox related reactions such as oxidation of ferrous to ferric Fe, difference in isotopic fractionation from the sources, formation of organic complexes with Fe, and many others. Considering that these processes are inevitable during the mobilization or circulation of Fe in the systems, Fe isotopic fractionations are an ideal approach to be applied to understand the behavior of Fe in the drainages. The development of advanced analytical methods further complements the ability of the approach to meet the research objectives.

Finally, a simulation by geochemical modelling has been an approach utilized to complement study findings. In this research, despite the extensive fieldwork approach that was initially taken, a simulation of the systems by geochemical modelling provided a more detailed understanding and further expectations of the geochemical processes that dominate the drainage systems. This allows a confirmation of the field findings and increases an understanding and applicability of our research findings. A detailed explanation of the methodologies is given in each respective chapter, however, a general summary of the methodologies applied in the study is shown below (Figure 1-3).





Sampling sites	On-site measurements	Sampling		Lab analyses
Ainai mine drainage Shojin river	pH, DO, ORP, EC, Fe ²⁺ , Temp, Flow rate, Turbidity	Solution samples (colloidal)  1 > 0.2 μm Particulate < 0.2 μm Dissolved	Sediments  Suspended particles 	IC: Anion ICP-AES: Major elements (Fe, Ca, Mg...) ICP-MS: Trace elements (As, Zn, Pb, Cd) SEM, TEM, XRD: Precipitate characterization MC-ICP-MS: δ ⁵⁶ Fe
		 2 > 200 kDa, < 0.2 μm Colloidal < 200 kDa Truly dissolved		

Figure 1-3. A summary of the sampling and analytical approaches applied in this research work.

1.5 Structure of thesis

This thesis comprises of seven chapters and an appendix. Chapter 2 was published in the Science for the Total Environment. Overall, this thesis summarizes the behavior of colloidal Fe in mine drainages, due to the limited number of studies that is linked to the wide diversity of the mine drainages. In addition to that, the fate of Fe is clarified through understanding Fe isotopic fractionations in the systems. This thesis provides insight on the behavior of Fe, in determining the fate of other elements that it co-exists within the drainages, as well as the fate of the Fe itself, accounting for the global circulation of Fe in the environment. The contents of the thesis according to chapter are listed below:

Chapter 2 and 3 show general behavior of Fe colloids from field observations and analyses. Keeping in mind that colloidal particles (1 to 100 nm) are highly reactive and abundant in aquatic systems, their presence, formation mechanisms and other behaviors were investigated. Water samples sampled in different fractions were analyzed for their metal concentrations and the abundance of the colloids was confirmed. Formation mechanisms were also established, in accordance to the mineral (i.e. ferrihydrite in circum-neutral and schwertmannite in acidic drainages) were clarified. Their relationship to the elements they coexist with was also clarified which shows the fate of the elements.

Chapter 4 is a comparative chapter, discussing the variation of colloid transport in the circum-neutral Ainai mine drainage, with the acidic Shojin river. Since the two immediately previous chapters stand alone to describe the behaviors of the colloids in the respective drainage systems, chapter 4 integrates the two chapters to aid with an understanding from a comparative point of view. Among the other concepts addressed in this chapter, one aspect that is highlighted is the transportation of the colloids following their formation, because this is an important aspect to highlight when developing efficient drainage systems.

Chapter 5 highlights the circulation of Fe in various systems as inferred from colloid behavior and isotopic Fe fractionations. Fe isotopic fractionations have been reported in different environments. The isotopic ratios were considered from the upstream to downstream of the drainages, to follow the source, fractionation along the course (since mineral formations are occurring), and towards the downstream (where deposition is highly expected to dominate). These fractionations have been interpreted to the behavior of Fe in the drainages.

Chapter 6 shows experimental simulations and theoretical calculations that support findings and provide applicability of our findings. Quantitative calculations that complement the findings are also shown in this chapter. Geochemical modelling, that is recognized as an important tool in geochemistry among other fields, is extensively applied to show how our findings, particularly with colloid transport, surface complexation and other approaches may be applied in other fields.

Chapter 7 gives a conclusive summary of the thesis. Implications of the study carried out are also highlighted to show how the findings would be utilized for development or improvement of wastewater treatment systems. The findings may also be applicable in other fields.

2 Chapter 2: Formation of Fe colloids and Zn-Fe Layered Double Hydroxides as sequestration agents for toxic elements in the circumneutral Ainai mine drainage

The contents of this chapter were accepted for publication in Science for the Total Environment.

Chikanda, F., Otake, T., Koide, A., Ito, A. and Sato, T. 2021. The formation of Fe colloids and layered double hydroxides as sequestration agents in the natural remediation of mine drainage. DOI: <https://doi.org/10.1016/j.scitotenv.2021.145183>

2.1 Introduction

Iron colloids have been confirmed to form in systems in which Fe is present. Given that these colloids play significant roles in transporting other elements, the possibility of Fe colloids playing significant roles in Ainai mine drainage is investigated. In its circumneutral state, Ainai mine drainage poses as a good study site as most drainages are neutralized before the wastewater is released, therefore the understanding obtained here will give insight on the behavior of Fe colloids in a wide variety of drainages.

Mine drainages are majorly in acidic conditions, but in most of the treatment methodologies, one significant concept is the adjustment of waste water pH to near-neutral or neutral pH (Sánchez et al., 2006). Depending on the drainage, self-mitigating capacity is observed, and allows and adjustment of the pH to a state where the metals are efficiently remediated. Processes such as aeration, oxidation of ferrous to ferric Fe and microbial activity (Nordstrom, 2011) may naturally play a role in this geochemical evolution and allow for efficient natural remediation. Ainai is one system that shows a natural capacity to remediate its contamination, however, the detailed geochemical processes that govern the natural remediation still lack detailed clarity. Furthermore, since mine drainages vary in the properties mentioned above, field investigations, which provide an understanding of geochemical processes, also lack in many mine drainages, especially with regards to nanoparticles.

Ainai mine drainage, despite being rich in Fe like many other drainages, has been reported to have As and Zn as elements that require treatment at the drainage. Arsenic and Zinc are “heavy metals” (Adriano, 2001), that pose chronic health problems in human beings therefore, their concentrations in water should be closely monitored. The WHO limit for As and Zn are 10 µg/L (World Health Organization, 2018) and 5 mg/L (Mohod and Dhote, 2013) . Despite their individual characteristic behaviors in the presence of sorbents, As and Zn have both been proven to be removable by Fe. Therefore, depending

on the conditions of the drainage, Fe that is present in the drainage has the ability to sorb and control the fate of the other elements.

Given that only aeration is applied to the drainage for the treatment of the toxic elements, further relying on the presence of Fe to initiate the precipitation of Fe oxyhydroxides, and therefore sorb the toxic elements, an investigation is carried out utilizing field measurements and laboratory analysis, and thereby aiming to clarify the processes responsible for the natural remediation of the Fe, As and Zn from the drainage.

Based on this background, the objectives of this chapter are (i) to clarify the formation, aggregation, and deposition behaviors of Fe colloids at circumneutral pH; (2) examine the role of the colloids on As and Zn sequestration from mine drainage over two seasons; and (3) investigate the formation of LDHs by comparing natural and synthetic samples and factors affecting their formation and stability. The concentrations of metals in the drainage system from the mine provided insight into the behavior of the metals involved, and highlighted factors that determine the fate of toxic elements in mine drainage in the presence of Fe colloids.

2.2 Description of study area: Location, geology, and drainage system

The abandoned Ainai mine is in the northern part of Kosaka town, ~600 m northeast of Omori Mountain, in the Hokuroku district, Akita prefecture, Japan. Sulfide ores containing Zn, Pb, and Cu (e.g., sphalerite, galena, chalcopyrite) were mined from the Kuroko-type volcanogenic massive sulfide deposit (Lu et al., 2019), which was formed in association with submarine bimodal volcanisms in the middle Miocene (Kinoshita and Takeuchi, 1964; Yamada and Yoshida, 2011). Contaminated water has flowed from the mine since its closure and requires treatment before discharge.

Aeration has been used to oxidize and precipitate Fe along with As and Zn. This natural remediation involves a 1000 m drain that runs from the underground tunnel through two treatment ponds to connect with a tributary of the Kosaka River at altitudes of 260–300 m (Figure 2-1a). Wastewater flows from the underground mine in pipes (Figure 2-1b), through a concrete drain inside a tunnel (Figure 2-1c), is released to an outside drain (Figure 2-1d), which has steps to improve aeration (Figure 2-1e), then connects to a concrete drain (Figure 2-1f) before being stored in a reservoir (Figure 2-1g) and sedimentation ponds prior to release to the river. Sediments that accumulate in the ponds are transferred periodically to a nearby area.

Ainai mine drainage is located in a sub-frigid humid climate, with four distinct seasons. Abundant snowfall and monsoons have been reported in the region (Lu et al., 2019).

Besides winter, when the drainage is covered by snow, precipitation at Ainai is highest in July, and lowest in October. Snow falls from October until mid-February (Japan Meteorological Agency, 2018). Therefore, July and October are referred to as the rainy and dry seasons, respectively, at some points in this thesis for simplicity.

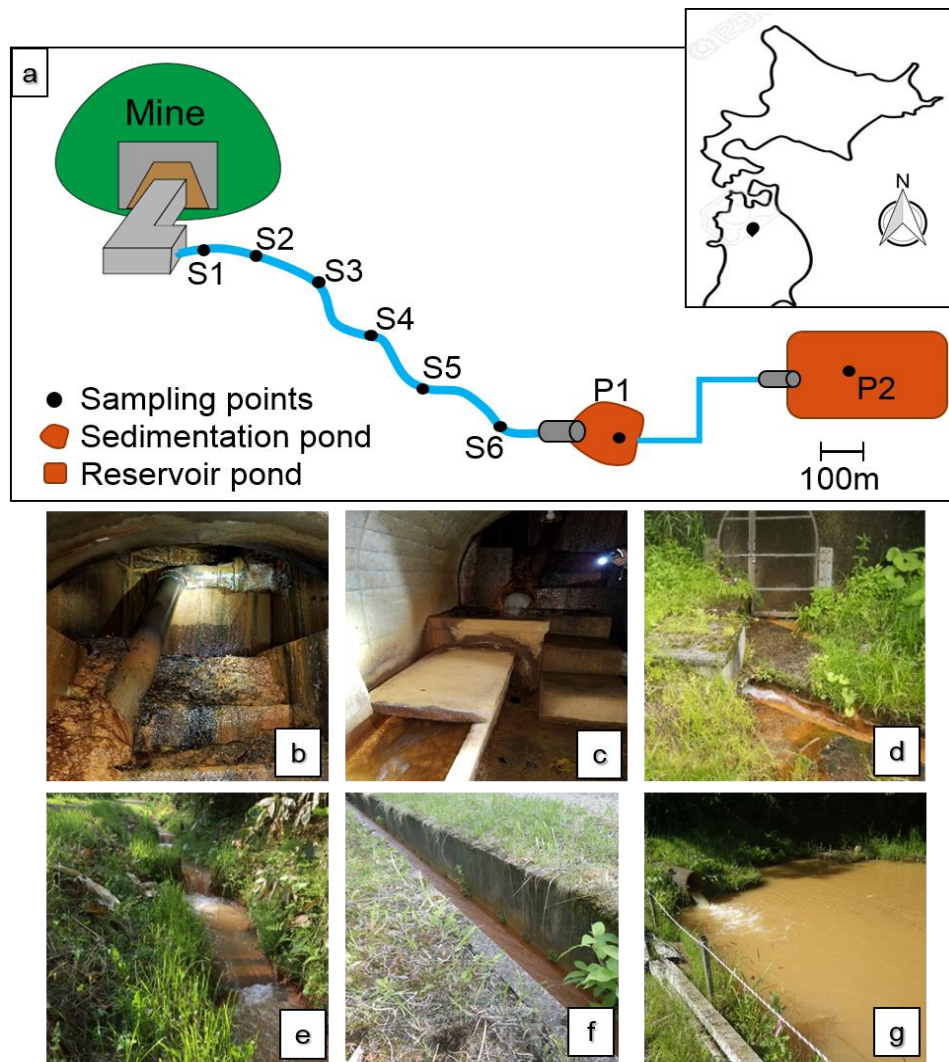


Figure 2-1. (a) A schematic representation of Ainai mine drainage showing the sampling points (S1–S6), reservoir (P1), and settling pond (P2) with an inset map showing the location in Japan; (b) pipe releasing water from underground to concrete drain; (c) concrete drain inside the tunnel; (d) upper exterior drain (S1); (e) unconcreted upper to middle drain, (f) concreted lower drain; (g) reservoir pond (P1).

2.3 Materials and methods

2.3.1 Field sampling: Water and solid samples

Field surveys were conducted at Aina mine in July 2016 and Oct 2018 and at Shojin in July 2019 and August 2020. Samples of water, suspended solids, and sediments were collected from the upstream to downstream in both systems, to represent the processes occurring in the drainages. A summary of the methodology approach is summarized in Figure 2-2.

Water was sampled through three types of filters, 0.2 μm PTFE membrane filter (Advantec 25HP020AN), 200 kDa ultrafilter (Advantec USY-20) and As filters (Sep-Pack cartridge: As exchange column), to provide four types of samples: 0.2 μm membrane-filtered, non-acidified sample for anion analyses; acidified 0.2 μm membrane-filtered sample; and 200 kDa ultra-filtered sample and samples to be analyzed for As speciation, with the latter three being acidified by 1 vol.% HNO_3 (ultrapure grade, Kanto chemicals) for cation analyses. Here, we define the dissolved and colloidal fractions as follows: (1) ultra-filtered (200 kDa) water samples contain the dissolved fraction; (2) membrane-filtered (0.2 μm) samples contain the colloidal and dissolved fractions; (3) the difference between (1) and (2) provides the colloidal fraction. Samples were collected in 50 mL polypropylene bottles, pre-rinsed with 6 vol.% HNO_3 overnight, and stored at $\sim 4^\circ\text{C}$ pending analysis. On-site measurements were undertaken for Fe^{2+} concentrations, dissolved oxygen (DO), pH, electrical conductivity (EC), turbidity, temperature, oxidation-reduction potential (ORP), and alkalinity of water samples. A pack test was used for Fe^{2+} concentrations; Eh (Redox potential of the normal hydrogen electrode) was calculated as $\text{Eh} = \text{E} + 206 - 0.7 \times (\text{T} - 25)$ (E: oxidation - reduction potential (mV), T: temperature



Sampling sites	On-site measurements	Sampling	Lab analyses
Aina mine drainage (S1 to P2)	pH DO ORP EC Fe^{2+} Turbidity Temperature Flow rate Distance between sites Drainage dimensions	Solution samples <ul style="list-style-type: none"> Colloidal fraction: $> 200 \text{ kDa}, < 0.2 \mu\text{m}$ Dissolved fraction: $< 200 \text{ kDa}$ 	IC: Anions (Cl^- , SO_4^{2-} ...) ICP-AES: Major elements (Fe, Ca, Mg ...) ICP-MS: Trace elements (As, Zn, Pb, Cd)
		Sediments 	Suspended particles 
2 samplings -July -October			

Figure 2-2. A summary of the sampling and analytical approaches applied in this research work.

(°C)). Alkalinity was determined by HNO₃ titration of water samples filtered through a 0.45µm PTFE membrane filter. A Gran-function plot was applied to obtain HCO₃⁻ concentrations from alkalinity. Distances from each sampling site and flowrates were measured on site. Sediments samples were also collected at most sampling points using a shovel while suspended particles were collected by pumping 0.5 L to 1 L of water through 0.2 µm mixed-cellulose-ester filters (Advantec A020A047A).

2.3.2 Analytical methods

Anion and cation analyses: Non-acidified water samples were diluted 10 times and analyzed by ion chromatography (IC; Metrohm IC861) using Multi-anion Standard Solution 1 (Wako Pure Chemical Corporation) for calibration. Acidified samples were diluted 40 times and analyzed for major and trace elements by inductively coupled plasma–atomic emission spectroscopy (ICP–AES; Shimadzu ICPE-9000) and ICP–mass spectrometry (ICP–MS; Thermo Scientific iCap Qc). Standards were prepared from a multi-standard solution (Wako). In, Ru and Rh and were used as internal standards for ICP–MS analysis. Oxide formation during analysis was monitored by the CeO/Ce ratio and maintained at <0.5% and He collision mode was utilized to avoid molecular interference from ⁴⁰Ar³⁵Cl⁺ on ⁷⁵As⁺.

Microscopic observations: Sediment and suspended particulate samples were dried at room temperature and the minerals present were determined by X-ray diffraction (XRD; Rigaku XRD Multi-Flex) using Cu Kα radiation (λ = 0.15406 nm) with an accelerating voltage of 30 kV and beam current of 20 mA, in the 5°–70° range, scanned at 2.0° min⁻¹. The morphology and chemical composition of the suspended particulates were analyzed by field-emission scanning electron microscopy with an energy-dispersive X-ray spectrometer (FE–SEM–EDS; JEOL JSM-6500F). Samples were prepared for transmission electron microscopy (TEM; JEOL JEM-2010) by dispersion in ethanol (with ultrasonication) and placed on a Cu grid with a film. Minerals were identified using Crystal Structures Libraries (HULINKS).

Total Organic carbon (TOC): The water samples were analyzed for their total organic carbon concentrations. The amount of total carbon was assumed to reflect the total organic carbon since the solution that was used for analysis was obtained after alkalinity (filtered by a 0.45µm filter and added HNO₃, followed by titration). Raw (unfiltered) samples were also analyzed for comparison; however, some precipitation was observed upon arrival at the laboratory and for fear of particles blocking the analysis machine, the samples were filtered by a 0.45µm filter before analysis. The values were expected to reflect all C in the solution but seemed slightly lower, so possibly C was incorporated in

the aggregates that were filtered out. As a result, the sample obtained from alkalinity was used to measure the amount of total organic carbon in the samples.

2.4 Results

2.4.1 On-site and element concentrations of water samples

Results of the on-site measurements of Ainai mine drainage are reported in Table 2-1. Ainai mine drainage is a neutral to alkaline (pH 6.20 to 7.91) system and pH increases down-drain with decreasing alkalinity (Figure 2-3a). The HCO_3^- concentration (measured from the alkalinity) decreases down-drain (246.2 to 127.1 mg L^{-1}), consistent with alkalinity changes. The drainage is sulphate- and calcium-rich as seen from the stiff diagram (Figure 2-3b). Using the stiff diagram classification, this wastewater can be classified as $\text{Ca}^{2+}\text{-SO}_4^{2-}$ type of wastewater, whose Ca^{2+} and SO_4^{2-} concentrations are about 16 meqL^{-1} each. The dissolved oxygen (DO) varies from 6.54 to 9.37 mgL^{-1} in July, not too different from October when the DO rises to 11.53 mgL^{-1} . Electric conductivity (EC) remains nearly stable throughout the drainage with values ranging from 124.30 to 273 msm^{-1} . ORP values increase from the upper to lower drain (127 to 209 mV), possibly due to increasing pH (Wiley, 2006). Most properties exhibit negligible variation between July and October. However, the flow rate, turbidity, and Fe^{2+} concentrations display notable variations between the two months. The calculated charge imbalance for all water samples was within $\pm 15\%$.

Table 2-1. Data summary of on-site parameters of Ainai mine drainage measured during field work.

Site	pH		DO (mg L ⁻¹)		EC (ms m ⁻¹)		Eh (V)		Turbidity (FTU)		Fe ²⁺ (ppm)		Alkalinity (mg L ⁻¹)		Flow rate (L s ⁻¹)	
	Jul	Oct	Jul	Oct	Jul	Oct	Jul	Oct	Jul	Oct	Jul	Oct	Jul	Oct	Jul	Oct
S1	6.20	6.24	6.54	7.97	145.75	150.0	0.2	0.2	7.16	5.11	8.00	14.00	246.2	242.7	26.1	21.1
S2	6.43	6.55	7.79	11.28	135.50	137.0	0.1	0.1	28.77	20.90	7.50	12.00	221.9	147.5	-	-
S3	6.95	7.01	8.37	12.55	134.80	136.0	0.3	0.3	57.00	34.90	7.30	10.00	215.7	147.2	43.4	31.7
S4	7.38	7.42	9.23	11.94	131.93	137.0	0.3	0.3	68.00	50.67	1.50	5.00	221.3	156.9	-	-
S5	7.39	7.53	8.71	11.56	124.30	137.0	0.3	0.3	79.67	52.00	0.15	1.00	209.7	142.5	28.9	16.1
S6	7.34	7.52	9.23	11.46	131.96	136.0	0.4	0.4	89.66	38.50	0.05	0.10	199.1	156.8	-	-
P1	7.57	7.59	8.93	11.35	133.33	135.0	0.4	0.4	72.33	48.35	0.5	0.10	169.7	128.1	-	-
P2	7.82	7.91	9.37	11.63	273.0	148.64	0.4	0.4	19.11	2.32	0.5	0.20	169.2	127.1	-	-

- indicates locations where parameter was not measured.

The average flow rates in July and October were 32.80 and 22.96 Ls⁻¹, respectively, which is attributed to heavier precipitation in July (Figure 2-4a). As shown in Figure 2-4a, amount of precipitation varies through these months, and although the difference in the actual amount of precipitation seems minimal, some studies have reported such minor differences playing significant roles as they may affect the amount of ground water and the flowrate as we see in this case, therefore, warranting study. The average Fe²⁺ concentrations measured using the pack test decreased in both months.

An average of the Fe²⁺ measured in both months is plotted in Figure 2-4b. The concentrations were from 8.00 to 0.50 in July while they were 14.00 to 0.20 mg L⁻¹, displaying higher concentrations in October. Finally, the turbidity in July ranged from 7.16 FTU, increased to 89.66 in the lower mid-stream and drastically decreases to 19.11 FTU. In October, the turbidity is 5.11 FTU then increases only to 52.00 FTU in the midstream and decreases to 2.33 FTU in the downstream. Therefore, the turbidity decreases more in October when the precipitation is lower. The inverse relationship of turbidity and Fe²⁺ concentration is shown in Figure 2-4b.

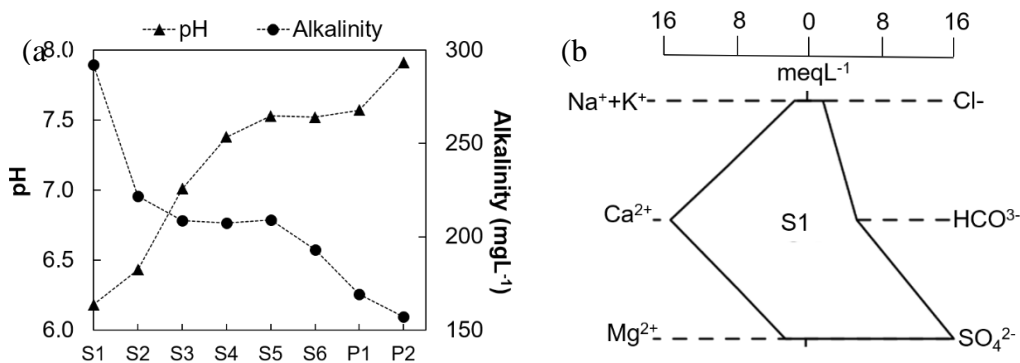


Figure 2-3. Average fluid compositions for July and October. (a) Down-drain pH and alkalinity trends and (b) stiff diagram.

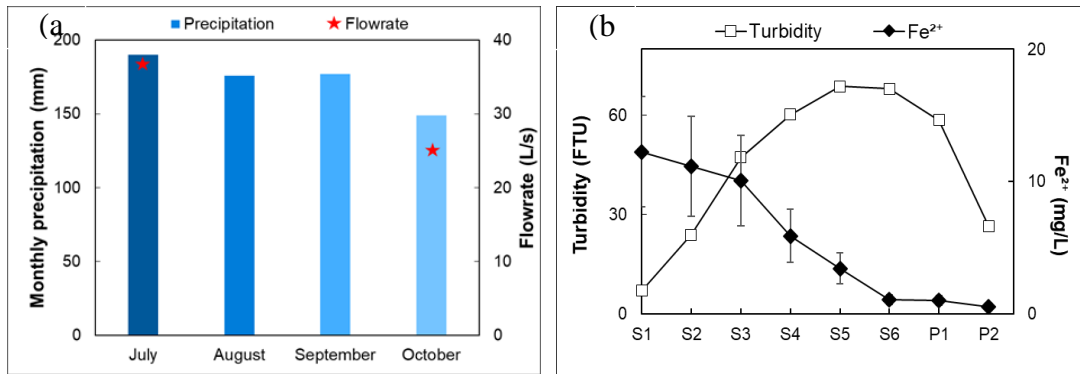


Figure 2-4. Average trends of the (a) Precipitation and flow rates at Ainai mine; (b) Fe²⁺ concentration (pack test) and turbidity in July 2016 and October 2018

In Figure 2-5a and b, a more specific variation in turbidity and Fe²⁺ is shown. The general trends are similar to those displayed by the average trends above, however, variations with season are also observed and worth noting. Turbidity in July, when the precipitation is higher is generally higher and quickly rises in the mid to downstream, but sharply decreases towards the pond. The trend slightly differs in October, when there is less precipitation. The turbidity increases, although not as much as in July, then stays slightly high, before decreasing minimally towards the pond. The turbidity in July decreases much more than it does in October. On the other hand, Fe²⁺ is generally high in October, when the precipitation is lower and decreases steadily towards the downstream, while in July, the Fe²⁺ concentration is lower and sharply decreases in the midstream (at S3), the point at which turbidity also shows significant increase. Finally, both Fe²⁺ concentrations are completely decreased in the downstream.

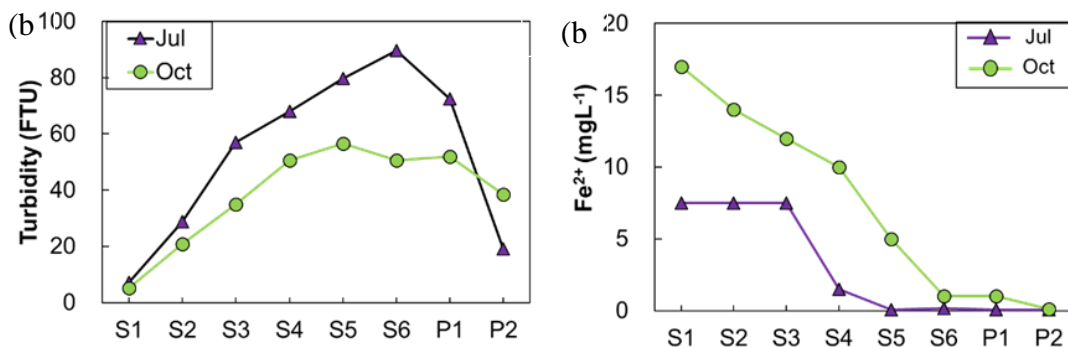


Figure 2-5. Trend displayed by (a) turbidity and (b) Fe²⁺ concentrations from pack test in July and October.

Along with the decrease in ferrous Fe concentrations, a decrease in the total organic carbon, which represents the total organic carbon (TOC) was also observed (Figure 2-6). As shown in the below figure, TOC decrease towards the downstream, with a sharp decrease observed at S3. This correlates strongly with the trend in ferrous Fe decrease in the drainage.

Sample	Total organic carbon (mgL ⁻¹)	SD
T1	13.5	0.17
S1	12.1	0.02
S2	11.7	0.01
S3	6.45	0.09
S4	5.00	0.07
S5	5.13	0.01
S6	5.15	0.03
P1'	4.84	0.1
P1	2.92	0.04

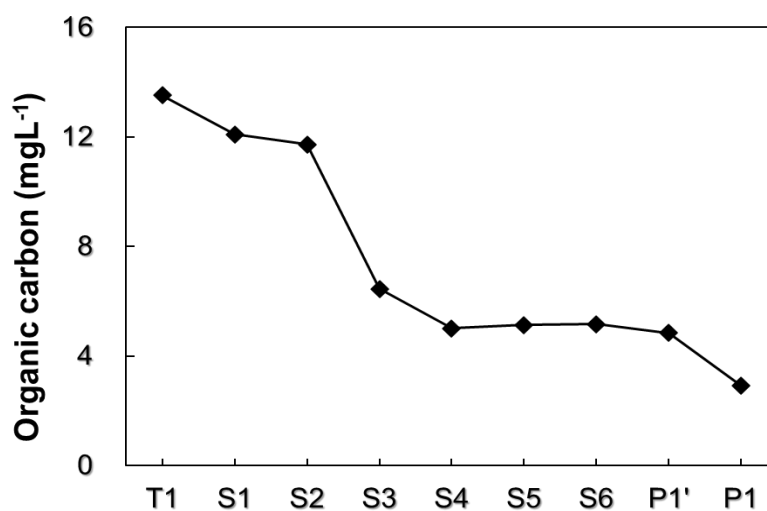


Figure 2-6. Amount of organic carbon in the Ainai wastewater samples

2.4.2 Dissolved and colloidal fractions of the toxic elements in the drainage

The fractions of the metals according to dissolved and colloid fractions from upstream to downstream are displayed in Table 2-2. The concentrations are also plotted for the different months i.e. July and October, when sampling was carried out. Analysis was

carried out for a variety of elements, however, apart from those plotted in the table, the other elements did not display observable fraction patterns. And besides these toxic elements, other element that were in considerable concentrations were within the WHO standard and mostly non-toxic. This correlated with the information that the main target elements for treatment at the site are Fe, As and Zn.

The trends of Fe, As, Zn and Si are plotted in Figure 2-7. All elements show a decreasing trend towards the downstream, to levels below the stipulated WHO standard. From the upstream and towards the downstream, as the decrease occurs, an increase in the colloidal fraction, with a decrease in dissolved fraction is observed, although the patterns may differ from element to element.

Fe concentration decreases towards the downstream (12.1 mg L^{-1} at S1 to 0.015 mg L^{-1} at P2), and a significant decrease in the dissolved fraction is observed. With the decrease in dissolved fraction, comes an increase in the colloidal fraction, which as an overall also decreases. The Fe concentration decrease is consistent with the decrease observed in the pack test. Between the months, Fe concentration is higher in July than October. At all of the sites, the decrease of dissolved and increase in colloidal fraction is similar, but after S4, the colloidal fraction in July is very low compared to that of October, despite October starting with a low overall Fe concentration. An inverse relationship is seen in the As concentrations. As concentration, which was mainly Arsenite, as seen following the analysis of As-column filtered sample, is higher in July than in October. At S4, all the colloids are not present, leaving all the remaining As in dissolved state. A constant dissolved As concentration is maintained towards the downstream in both months. However, in October, a small fraction of colloidal As is present up until S6, where we also see the last colloidal Fe. Similarities in the trends of Fe and As are prominent.

Table 2-2. Fe, As and Zn concentrations in dissolved and colloidal fractions in July and October.

Site	Fe concentration (mg L ⁻¹)				As concentration (µg L ⁻¹)				Zn concentration (µg L ⁻¹)			
	Dissolved		Colloidal		Dissolved		Colloidal		Dissolved		Colloidal	
	Jul	Oct	Jul	Oct	Jul	Oct	Jul	Oct	Jul	Oct	Jul	Oct
S1	12.1	10.16	1.39	0.52	13.0	30.76	3.08	1.27	452	247	0.15	b.d.
S2	2.51	2.14	8.79	6.12	4.43	11.07	7.28	12.57	316	281	3.07	23.1
S3	0.067	b.d.	8.65	5.13	3.68	9.27	6.23	12.57	208	214	10.6	34.2
S4	0.017	b.d.	2.86	1.95	3.84	9.26	1.67	10.09	115	187	60.9	54.4
S5	0.019	b.d.	0.066	1.04	3.80	7.99	0.069	2.56	111	123	0.02	50.1
S6	0.016	b.d.	0.175	0.41	3.76	8.44	0.028	1.10	147	138	0.01	76.7
P1	0.015	b.d.	0.009	0.10	3.53	8.06	0.029	1.00	104	116	0.01	b.d.
P2	0.015	b.d.	0.004	0.05	2.43	7.73	0.000	b.d.	60.1	105	0.01	20.1

-b.d. stands for below detection limit

Zn on the other hand displays a different pattern from Fe and As. At S1, Zn is present in the dissolved fraction, and colloid formation is observed from S2. The colloidal fraction is observed up until the downstream in October, similar to the As colloidal fraction, whereas the colloidal fraction ends at S4. The Zn concentration does not decrease as drastically as Fe and As but shows a steady decrease towards the downstream. Finally, Si concentrations show a minor decrease although some fractions of dissolved and colloid are present. The colloids are present until S4 and the concentrations do not differ significantly in July and October. Similar to Fe, the Si concentration is higher in July than in October, but concentrations remain higher in October until the pond. Overall, the element concentrations are observable in the dissolved and colloidal fractions and the total concentrations decrease and are within the accepted standard.

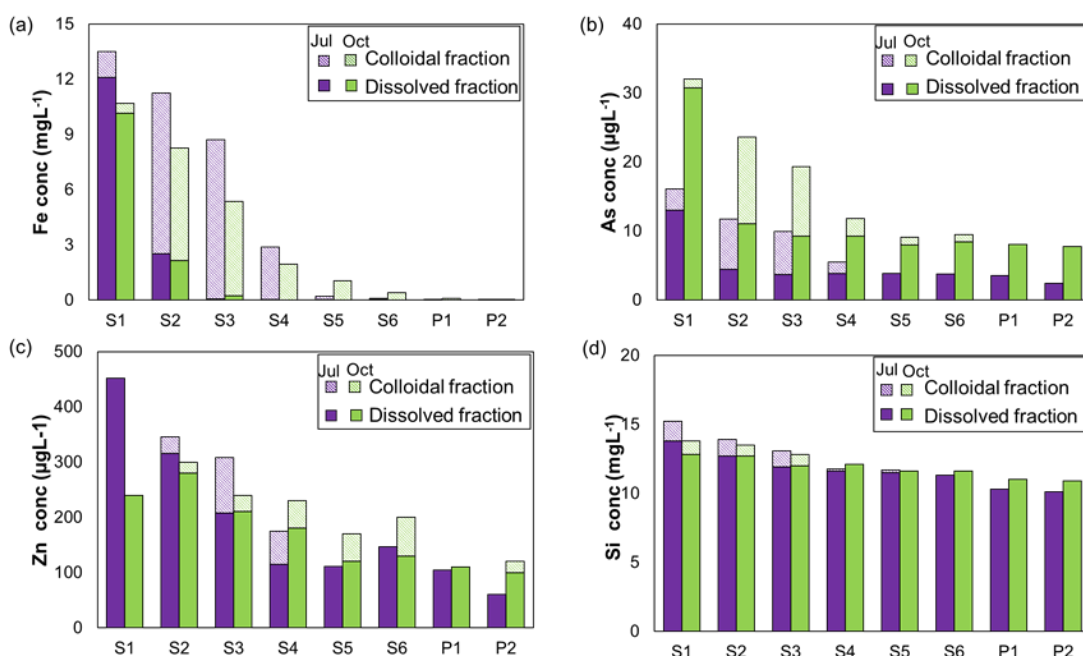


Figure 2-7. Distribution of (a) Fe, (b) As, (c) Zn and (d) Si concentrations in dissolved and colloidal fractions as a function of distance from the mine.

2.4.3 Characterization of the Fe colloids

Sediments and suspended particles: The sediments, suspended particles and colloid materials collected in the drainage were characterized to identify the dominant mineralogy present in the drainage. XRD was carried out on the sediment and suspended particles (Figure 2-8). The drainage samples, from S1 to S4 had similar profiles, hence only S1 is shown to represent all of them, in comparison to S5. In the upstream sediments,

the spectra are dominated by majorly 2-line ferrihydrite ($\text{Fe}_2\text{O}_3 \cdot 2\text{FeOOH} \cdot 2.6\text{H}_2\text{O}$ and/or $5\text{Fe}_2\text{O}_3 \cdot 9\text{H}_2\text{O}$). However, towards the downstream, the mineralogy of the sediments begins to vary, and calcite (CaCO_3) spectra were also observed. In the suspended particles from P1 (collected by filtration to under $0.2 \mu\text{m}$, a prominent gypsum peak ($\text{CaSO}_4 \cdot \text{H}_2\text{O}$), besides the 2-line ferrihydrite peaks similar to those observed in the upstream and sediment samples was observed. The precipitates were majorly yellowish brown and correlated with the XRD spectra and expected mineralogy.

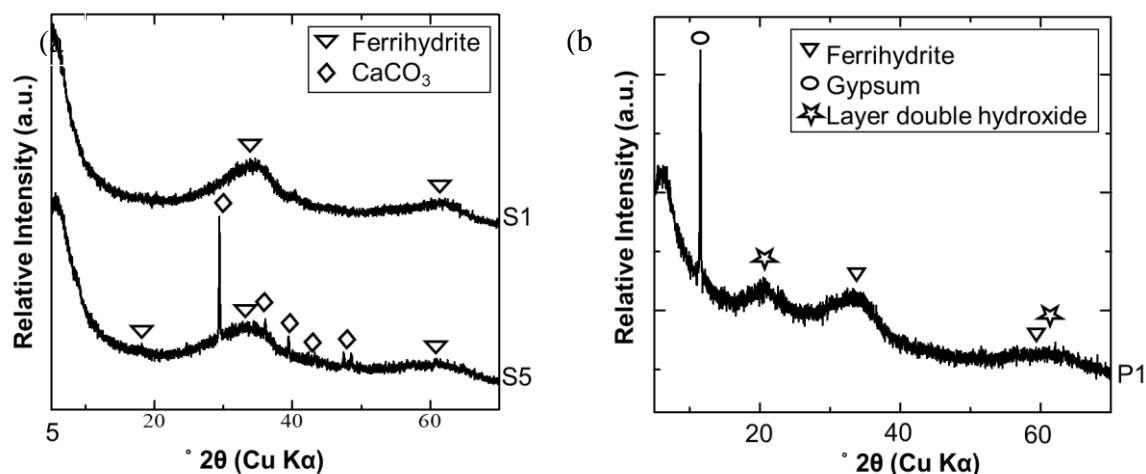


Figure 2-8. XRD profiles of (a) sediment samples from S1 and S5 and (b) suspended solids from P1.

from the water chemistry. In addition to these minerals, a peak that is suggestive of layered double hydroxides was observed in the suspended particles from P1.

Ultra-filtered material (Fe colloids): Following ultrafiltration, the particles collected on the ultra-filters were dried for observation under microscope (their volume was too small for an XRD analysis). The particles on the ultrafilter increases from visual observation from upstream to downstream (Figure 2-9). An observation at a larger scale was carried out on the ultrafilters and the number of colloids were indeed increasing from S1 to S6 (Figure 2-10).

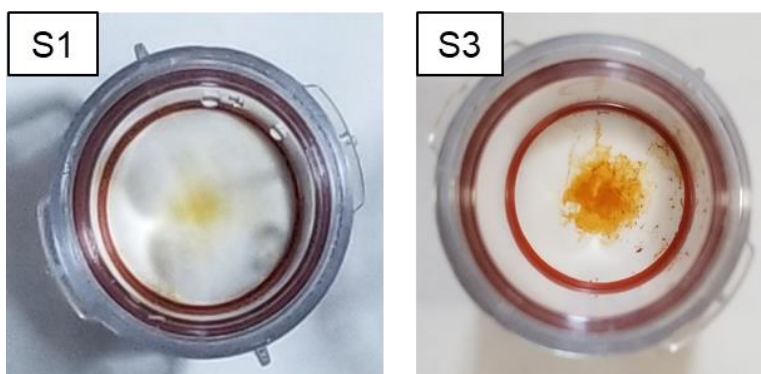


Figure 2-9. Fe colloids on a 200kDa ultrafilter

The average size of the colloids also increased towards the downstream. In addition to the increase in abundance, the following increase in colloid sizes was observed; S1, S2 and S3 have a distribution of 80 to 300 nm colloid aggregates which increase in abundance from S1 to S3. On the other hand, S4 was dominated by highly aggregated colloids of 300 – 400 nm.

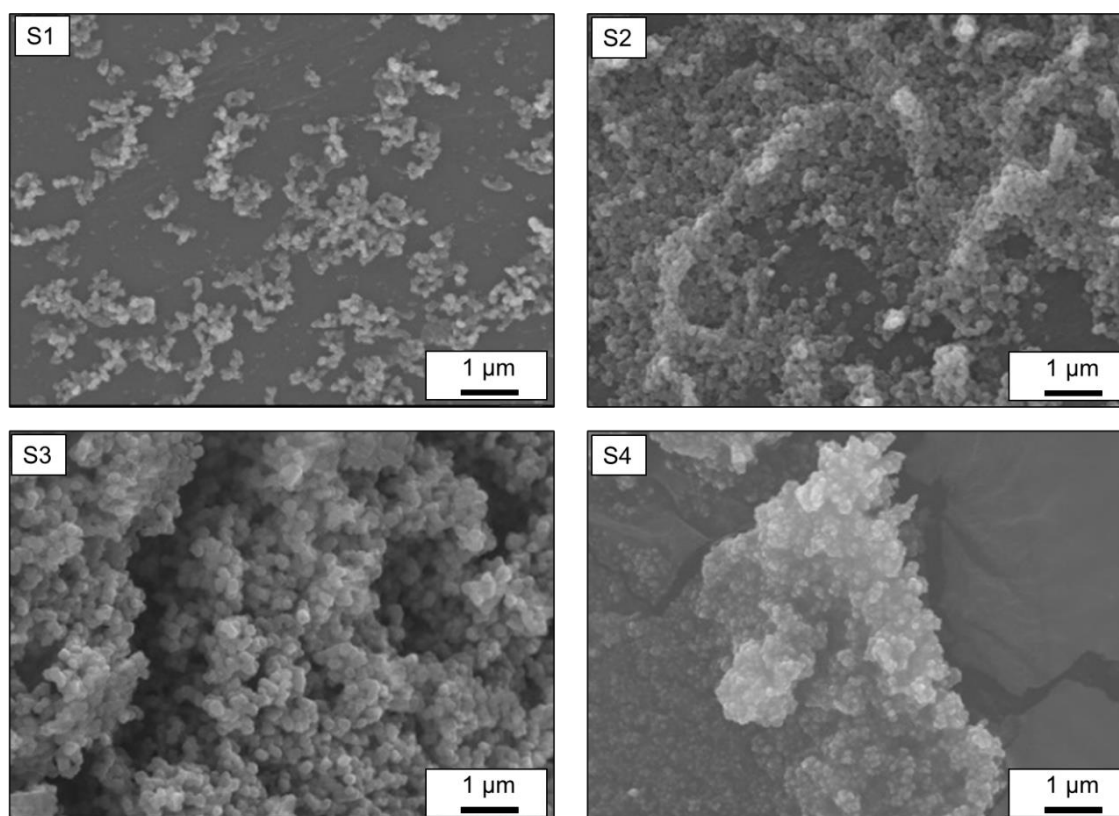


Figure 2-10. Size and aggregation variations of Fe colloids in the Ainai mine drainage.

The microscopic images obtained from FE-SEM are shown in Figure 2-11. An observation at a larger spectrum does not clearly show the orientation of the colloids, but at a larger magnification, the colloid aggregates were clearly observed. Homogenous spherical structures cover the ultrafilters and form these spherical aggregates that are homogenous from upstream to downstream. The aggregates were made of 100 nm structures, whose composition is shown in the EDS spectra. Main components of the colloids are Fe, Si, S, C and O (Pt is from the platinum coating used for sample preparation). This composition is consistent with the XRD peaks that were mainly for ferrihydrite, therefore, the drainage is dominated by Si-bearing ferrihydrite colloids.

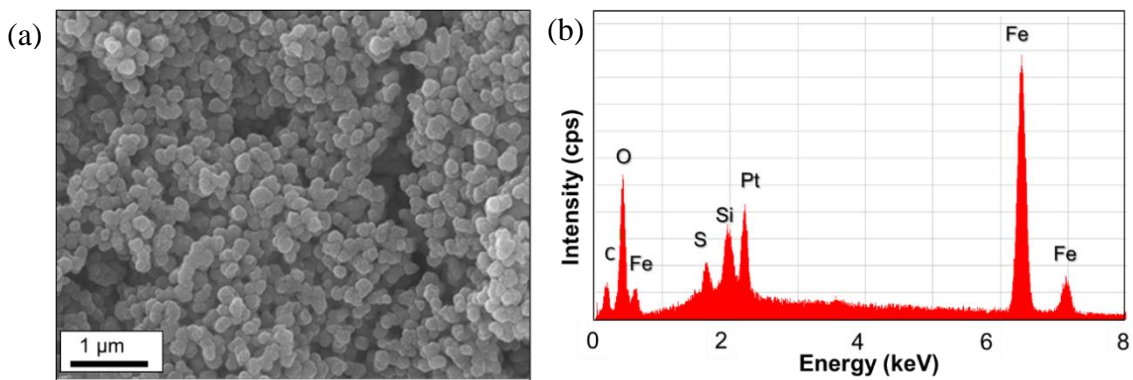


Figure 2-11. (a) An FE-SEM (secondary electron) image of colloid aggregates collected on ultrafilters and (b) the electron dispersive spectra of the colloids.

Since Fe colloids have been reported to evolve from smaller structures, TEM observation was carried out to further observe the colloids at a larger magnification than that made possible by FE-SEM. The TEM images (Figure 2-12. TEM images of the ferrihydrite colloids. (a) Colloid aggregate and (b) magnified colloid aggregate showing the 3 to 5 nm colloids that compose the larger 100 nm colloids.) revealed small spherical, 3 to 5 nm colloids that make up the 100 nm aggregates observed in Figure 2-11.

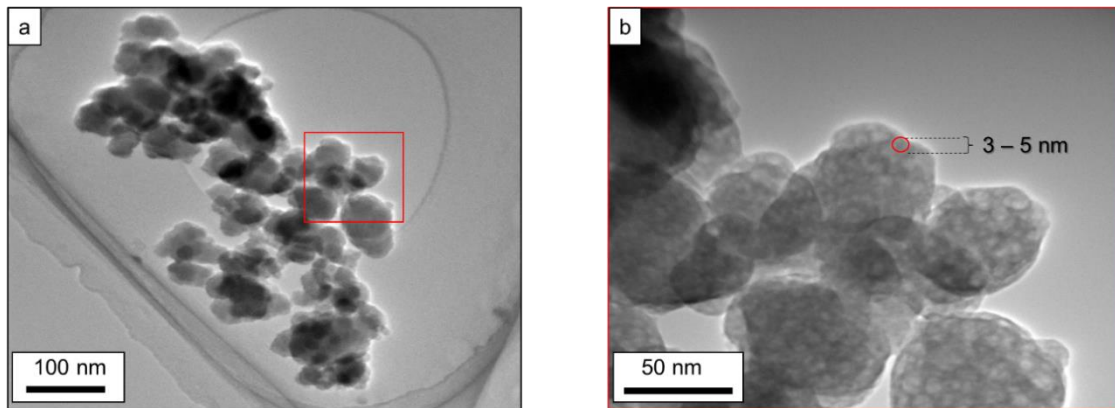


Figure 2-12. TEM images of the ferrihydrite colloids. (a) Colloid aggregate and (b) magnified colloid aggregate showing the 3 to 5 nm colloids that compose the larger 100 nm colloids.

Below is a histogram (Figure 2-13) showing the size distribution of the colloids, as summarized from the FE-SEM and TEM images. Since the precise colloids, at their smallest observable size, were better observed under TEM, besides morphological observations, the sizes of the colloids were also estimated using TEM. Following the measurements by TEM, the micrographs obtained were processed by ImageJ software, which was also used to obtain the size readings of the colloids and construct the below histogram. The size distribution plot shows that the colloids occur predominantly within the 100 to 250 nm window.

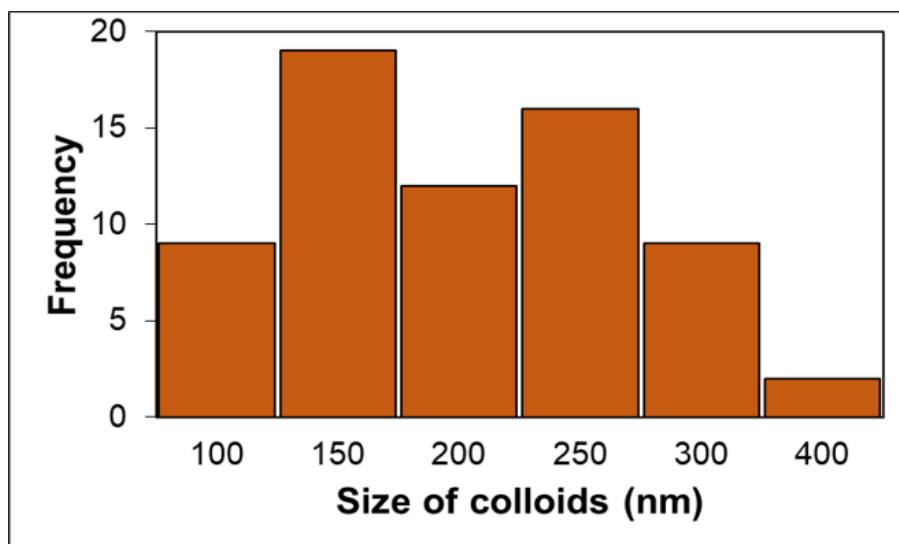


Figure 2-13. Size distribution of the colloids in Ainai mine drainage observed in FE-SEM and TEM images

2.4.4 Characterization of Zn colloids

Zn-containing layered minerals were also identified on the suspended particles. The mineralogical characteristics of solid samples were studied to constrain sequestration mechanisms for toxic elements. Zinc concentrations in the aqueous solutions from the drain may have been too low to produce observable amounts of Zn-bearing colloids in the sediments by the above methods. Therefore, $\text{ZnSO}_4 \cdot 7\text{H}_2\text{O}$ was added to wastewater collected in 2 L bottles to induce the synthesis of Zn-bearing minerals. With reference to previous studies (Morimoto *et al.*, 2015b; Parida and Mohapatra, 2012) and based on Aina mine water chemistry, synthesis was done using unfiltered water sample from S1 to act as a supply of Fe, and addition of $\text{ZnSO}_4 \cdot 7\text{H}_2\text{O}$ to increase the Zn concentration. The Zn reagent (249.5 mg) was added to 2 L of sample to provide a Zn:Fe molar ratio of 2:1. The samples were stirred and allowed to settle for 24 h at room temperature, after which precipitates were collected on 0.2 μm filters for XRD and SEM analysis. The Zn and Fe concentrations (by ICP–AES) and pH were recorded immediately after mixing and again after the 24 h. Solids collected from the synthesis were observed along with natural samples.

When closely observed, unlike the Fe colloids, the Zn particles were plate-like with layered structures. These particles would highlight the remediation pathway of the Zn from the drainage; however, they were scarce, therefore, using the wastewater, Zn reagent was added to synthesize more Zn containing minerals. In Figure 2-14, a comparison of the natural and synthesized material is displayed. Both minerals contained Zn, Fe, Si, Ca, C and O according to the EDS. A major difference was that the natural Zn mineral, was smaller in size compared to the synthesized mineral.

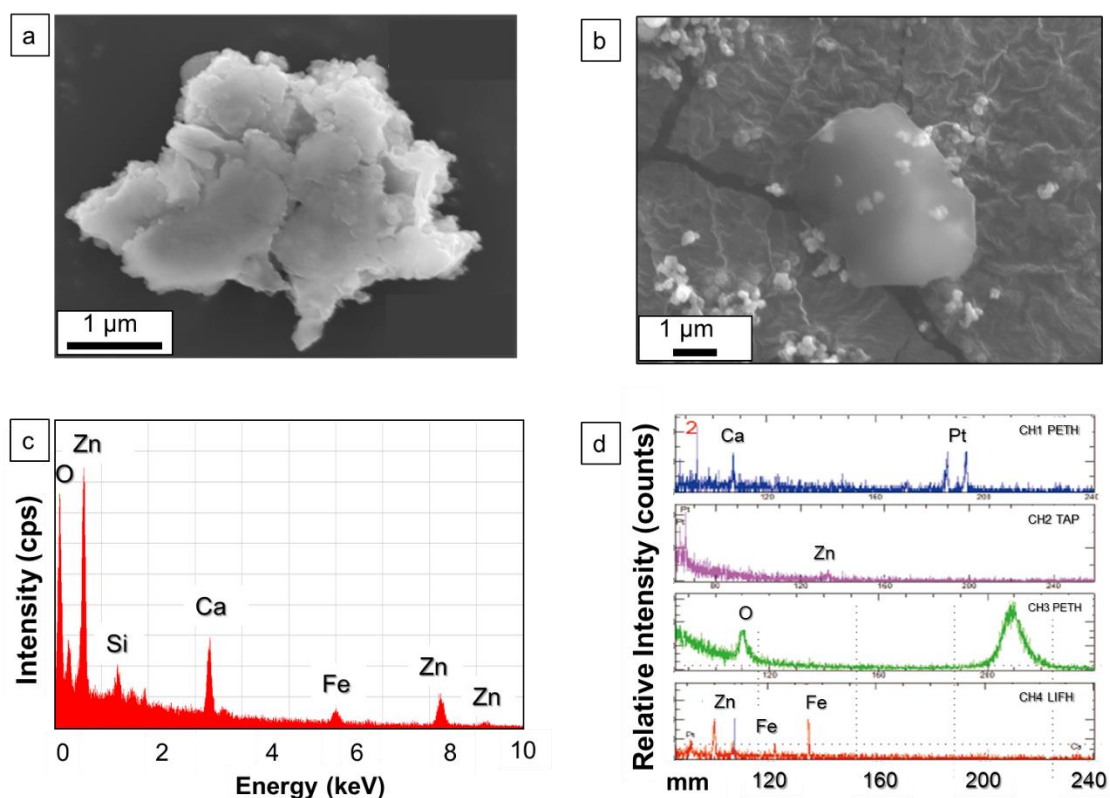


Figure 2-14. Field emission–SEM images of Zn LDH in (a) a natural sample from S3 suspended solids; and (b) a synthetic sample (c) EDS spectrum of the Zn-Fe LDH from synthesized sample and (d) EPMA peaks of the synthesized sample in (c).

2.5 Discussion

2.5.1 General characteristics of water samples

Ainai mine drainage is a circum-neutral mine drainage utilizing aeration for treatment. The wastewater is a Ca^{2+} - SO_4^{2-} type water, which is highly suggestive of mixing of the mine drainage with underground water rich in Ca and HCO_3^- before outflow from the mine head (Nakashima et al., 2012). Despite being unusual for mine drainage, this classification was observed from the upper to the lower drain with negligible variations, implying that external factors have no significant effect on the drainage system. Furthermore, the relatively high HCO_3^- concentrations indicate a strong buffering capacity and decreases towards the downstream with increasing pH. This inverse relationship reflects CO_2 degassing by aeration (Kirby et al., 2007), that results in the dissociation of HCO_3^- to CO_2 and OH^- (Langmuir, 1997). Unlike most mine drainages, which are actually acidic, Ainai mine drainage is circumneutral despite an abundance of SO_4^{2-} in the system and this is also attributed to the mixing of the drainage in the

underground. Ainaï mine drainage is generally an oxidative system, with oversaturation of DO (6.54–12.55 mg L⁻¹), possibly due to microbial photosynthesis (Wiley, 2006) and this supports the aeration that is implemented for the effective passive treatment.

2.5.2 Formation of the Fe colloids in the drainage and removal of As

The formation of Fe colloids was elucidated by the geochemical characteristics from the water samples, in addition to the on-site characteristics. To begin with, in the Ainaï drainage, the abundance of Fe and trend of decreasing Fe²⁺ suggests the formation of nanoparticles of Fe colloid (oxy)hydroxides, whose mobility and perhaps aggregation behavior might be reflected by the turbidity. There is an inverse relationship between turbidity and Fe²⁺ concentrations (Figure 2-5); turbidity increases and Fe²⁺ concentrations decrease down-drain. The turbidity is generally higher in July, when rainfall and flow rates are higher than in October, while Fe²⁺ concentrations are lower in July than October, as a result of dilution by higher precipitation rates. Turbidity is commonly higher in rainy seasons mainly due to the re-suspension of sediments (Rezaei et al., 2013; Zay Ya et al., 2020). Regarding the Fe²⁺ concentration, the oxidative nature of the drainage wastewater may have contributed to the inverse relationship between turbidity and Fe²⁺ concentration by initiating the oxidation of Fe²⁺ to Fe³⁺ (Nairn et al., 2002), thereby facilitating formation of nanoparticles (Buffle and Leppard, 1995) with increasing turbidity (Tikhonova et al., 2016; Yao et al., 2014). This process typically occurs in circumneutral pH systems, as in this case.

The turbidity continues to increase further down-drain in July, in contrast to the decrease observed in October when the flow rate is lower, indicating more rapid formation and/or aggregation of precipitates in the rainy season (July). The increasing turbidity supports the notion that the precipitates were mobilized over greater distances during the rainy season, indicating that flow rate should be a significant factor for consideration in the design of passive treatment systems. Turbidity increases with particle size (Tikhonova et al., 2016), implying more aggregation of Fe colloids in the rainy season, such that increased interaction among the colloids overcomes repulsive forces between them (Petosa et al., 2010; Baalousha, 2009a), leading to more aggregation. At reservoir pond (P1) and sedimentation pond (P2; Figure 2-1), turbidity decreases markedly, because of the longer residence time and sedimentation in the ponds; the larger particles in July settled more quickly with a greater drop in turbidity than in October.

Fe, As, Si, and Zn concentrations in the dissolved and colloidal fractions of water samples are reported in Table 2-2 and plotted in Figure 2-7. The dissolved Fe concentration decreases down-drain most notably between S1 and S3 where it is almost completely replaced by colloidal Fe, which forms increasingly as flow proceeds downstream. The concentration of dissolved Fe fraction is similar to the Fe²⁺

concentration (Figure 2-5) obtained by on-site pack tests, therefore implying that the dissolved Fe fraction (Figure 2-7) is predominantly Fe^{2+} . Subsequently, colloidal Fe forms in the upper drain, initiated by the oxidation of Fe^{2+} to Fe^{3+} and allowing the formation of the Fe hydroxide nanoparticles (Pokrovsky and Schott, 2002). The nanoparticles are prone to aggregating (Kellner and Köhler, 2005) with increasing particle size, and the turbidity increase (Figure 2-5) is attributed to the formation and aggregation of Fe colloids (Liao et al., 2017). Despite the increase in the colloidal Fe fraction (1.39 mg L⁻¹ at S1 to 8.79 mg L⁻¹ at S2), at the expense of dissolved Fe, the total Fe concentration decreases down-drain (Figure 2-7) due to the aggregation of colloids to a size that is removed efficiently by gravitational settling, thereby removing the particles effectively from the drainage.

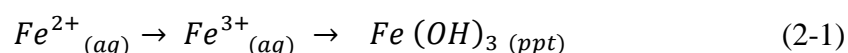
Arsenic, which is mainly Arsenite, As (III), throughout the drainage, shows a similar trend to Fe, most noticeably in the distribution between dissolved and colloidal fractions in the drain (Figure 2-7). Colloid formation is inferred at S2 and S3 (where Fe colloids also dominate) and total As continues to decrease down-drain, reflecting the impact of Fe colloids on As mobility. Conclusively, Fe colloids behave as the primary colloids, whereas As exists as pseudo-colloids, hence the fate of As being mainly determined by Fe colloids in the drainage (Fritzsche et al., 2011). The impact of Fe nanoparticles on As in aquatic systems has been widely studied previously (e.g. Zhao et al., 2011; Leupin and Hug, 2005), with several removal mechanisms being proposed, including co-precipitation of Fe hydroxides with As (Crawford et al., 1993; Yokoyama et al., 1999) and adsorption of As by Fe hydroxides (Khamphila et al., 2017). Considering the similar trends in Fe and As observed here, we suggest that As may be incorporated into the Fe colloids and removed from the mine drainage by co-precipitation and aggregation of the As containing Fe colloids. On the other hand, an inverse relationship where Fe concentrations in July are higher, while As concentrations are lower is observed. Higher Fe concentrations are most likely from the underground source, but the low As concentrations are associated with the increased Fe, which allows for more sorption of As, hence the inverse relationship also displayed in October when precipitation of As is lower due to higher Fe. However, further downstream, As remains in the drainage as the dissolved phase. Zeng (Zeng, 2003) reported a decreased affinity of iron oxides to adsorb As when the Fe oxides are associated with Si.

On the contrary, Zn and Si (Figure 2-7 c and d) display different trends from Fe and As in the drainage. They (Zn and Si) mainly exist as dissolved fractions and minimally removed from the drainage. There may be various constraining factors that resist the colloid formation and removal of the elements in the drainage, and since the metal concentration patterns may be difficult to utilize as clarification tools, therefore, mineralogy and modelling was utilized to clarify the behaviors of these elements.

2.5.3 Colloid mineralogy responsible for sequestration of toxic elements

The water chemistry and on-site data show the formation of Fe colloids in the Ainai mine drainage. Microscopic observations as shown in the results section also support the presence of the Fe minerals. The XRD peaks of the sediments and suspended particles showed peaks of 2-Line ferrihydrite, as the main Fe hydroxide mineral (Figure 2-8), making it the major mineral responsible for the remediation of the other elements in the drainage. These XRD patterns in support with EDS from the microscopy also support that the colloids at Ainai mine drainage are the 2-line ferrihydrite colloids. At circumneutral pH, ferrihydrite is reported to be a major Fe hydroxide mineral (Legg et al., 2014) and has been reported to have high sequestration mechanisms for other toxic elements (Webster et al., 1998).

The formation of the ferrihydrite may follow various pathways. In this case, the ferrihydrite is formed from the oxidation of ferrous Fe thereby allowing the precipitation of ferrihydrite particles as shown by the oxidation precipitation path in the equation below:



However, before the formation of the actual minerals of sizes large enough to be removed by gravity, the Fe colloids precede. The TEM images show that the ferrihydrite colloids before reaching a size of 100 nm are also preceded by the core-shell ferrihydrite. Core-shell ferrihydrite is a preceding member that is formed from Fe₁₃ Keggin clusters, which is basically a polymerization of Fe³⁺ monomers (Weatherill et al., 2016). This core-shell ferrihydrite is typically 3 nm in size and the Fe₁₃ Keggin structure is preserved during the evolution of the colloids. The resulting structures, i.e. spherical colloids in Ainai mine drainage are also a result of this preservation ability of the nanostructures. Unlike expanding the monomers, the abundance of hydroxyl groups in the waste water may have contributed to rather forming nanostructures that are stable (Legg et al., 2014; Gilbert et al., 2007), unlike endlessly growing into large size ferrihydrite minerals. A combination of the microscopic observations that were carried out highlight the evolution of the Fe colloids that are generated in the Ainai mine drainage. These colloids will then aggregate to the larger sized particles that will settle to the bottom of the drainage, forming the sediments that were scooped for analysis.

2.5.4 Aggregation and deposition of the Fe colloids

Observation of the colloids at different points of the drainage displayed variations in size and aggregation (Figure 2-10). An increase in size from S1 to S4 in particular, was measured following microscopic observations. The gradual increase in size and colloidal aggregates that was observed from S1, S2 and S3 evidently showed an evolutionary size increase of the colloids which correlates to the water chemistry, that shows a gradual increase in the colloid fraction. On the other hand, S4 was highly dominated by aggregated colloids of 300 – 400 nm. Particle aggregates larger than 400 nm were not observed on the ultrafilters, implying that colloid aggregates of > 400 nm were deposited to the bottom of the drainage. Subsequently, deposition of the colloids in the drainage occurs at ~300 to ~400 nm particle size indicating that the colloids are efficiently removed by gravitational settling when they reach a certain size.

The rate of aggregation in the drainage, as indicated by the turbidity, warrants study. The colloids in this system do not disintegrate after formation and are mobilized over considerable distances before deposition in the reservoir and sedimentation ponds. Colloid stability may be associated with Si (Vempati, Loeppert and Cocker, 1990), which allows formation of stable ferrihydrite. However, the aggregation rate may be explained by the DLVO theory, which highlights electrostatic factors affecting aggregation behavior. Given the high pH of the system and the presence of the organic matter measured from the TOC, which results in the system being near the point of zero charge, aggregation of the particles is quite significant. As seen in Figure 2-15, colloid deposition begins to be observed at about 500 m from their formation. According to the DLVO theory, repulsive forces limit aggregation, and this limitation is not so significant at Aina mine drainage and aggregation is achieved to remove colloids from the drainage.

A variation in the aggregation rate in July and October exists. In July, the turbidity quickly increases, and also quickly decreases towards the downstream, whereas, in October, the turbidity slowly increases and remains at values lower than July for longer distances (Figure 2-15). This indicates that in July, the colloids aggregate faster than in October and are deposited faster than in October. According to previous research, increased Van der Waals forces (Hiemenz, 1972; Hunter, 1963) may be responsible for this phenomenon, seeing as in July, more Fe is released from the source, implying more colloid formation, the interactions among colloids are also increased, and result in higher aggregation than October. Consequently, physical mixing of the wastewater assists in increased aggregation and hence the deposition of the As-bearing Fe colloids.

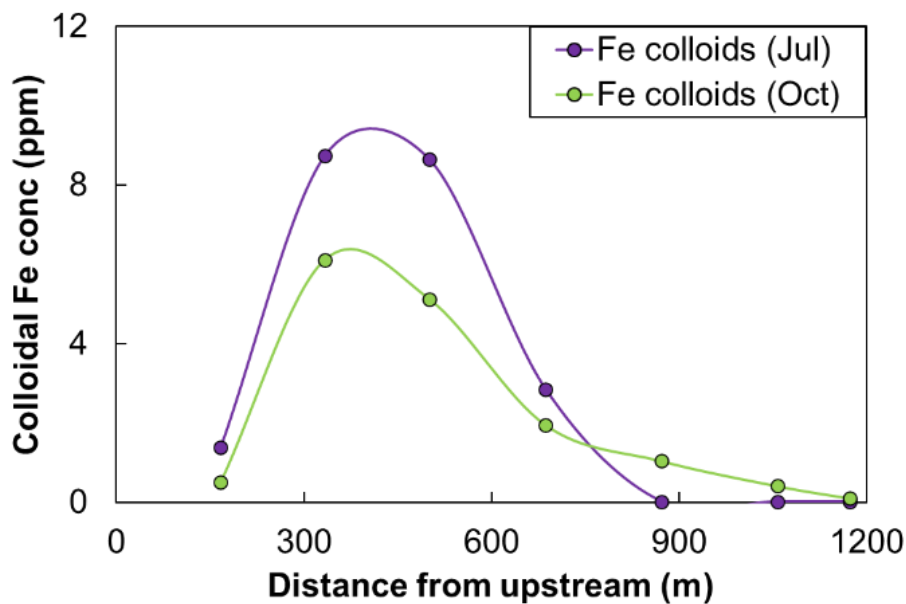


Figure 2-15. Colloidal concentrations of Fe in July and October as a function of distance from the mine.

2.5.5 Removal of Zn by Zn-Fe Layered Double Hydroxides

Fe and As concentrations decrease steadily in response to colloid formation but Zn concentrations decrease in an irregular pattern. (Figure 2-7). Formation of Zn colloids is observed downstream from S2 as pH increases slightly, most likely because Zn colloid formation is highly pH-dependent (Roberts et al., 2002). A colloidal fraction is also observed at sites S3 and S4, but the total Zn concentration does not reduce significantly at these sites. Considering that the Fe concentration in the drainage is significantly higher than that of As, and the high adsorption efficiency of ferrihydrite at circumneutral pH (Hao et al., 2018), the Fe in the drainage should be sufficient to remove the Zn. It follows that there must be other factors inhibiting Zn removal by colloids, possibly involving a different removal mechanism.

An FE-SEM examination of natural suspended particles (Figure 2-14a) and synthesized particles (Figure 2-14c) besides minor calcite and gypsum, revealed what seem to be LDHs containing Zn, Fe, Ca, Si, C, and O (Figure 2-14). Furthermore, XRD peaks similar to those of LDHs (Figure 2-8). The presence of Zn in these natural and synthetic samples strongly suggests that an LDH is responsible for the removal of Zn from the mine drainage. However, considering the small size of natural LDHs, as well as their rarity in the drainage as colloids or suspended solids and precipitates, the concentration of Zn may have limited their formation in the drainage, with the larger and more abundant particles

in the synthetic experiment being due to the addition of Zn. Furthermore, following the synthesis, more Zn particles were collected following filtration of the sample and an increase in pH was observed. This suggests that Zn concentration is a critical factor in Zn sequestration from mine drainage.

Layered double hydroxides comprising trivalent and divalent cations and anions (Hase et al., 2017) remove toxic elements effectively from a variety of systems (Hase et al., 2017; Hao et al., 2018). Heavy-metal ions can be removed from water by LDHs via: (i) precipitation of metal hydroxides onto their surface; (ii) adsorption through bonding with LDH surface hydroxyls; (iii) isomorphous substitution; and (iv) chelation with the functional ligands in the interlayers (Xu et al., 2013). The chemistry of Ainaí mine drainage includes Fe^{3+} and Fe^{2+} cations and HCO_3^- and SO_4^{2-} anions. Coexisting Fe^{3+} and Fe^{2+} might have supported LDH formation, along with HCO_3^- , as the major anion in this drainage system, thereby making an ideal candidate for LDH formation, unlike SO_4^{2-} because the abundance of HCO_3^- makes it more feasible than SO_4^{2-} . Therefore, we suggest the formation of an $\text{Fe}^{2+}\text{-Fe}^{3+}\text{-CO}_3^{2-}$ LDH, in which Zn may be isomorphically substituted, as a remediation mechanism for the Ainaí mine drainage, which quickly transforms to a stable phase composed of Zn, Fe, Ca, C and O i.e., Zn-Fe LDH.

2.6 Summary

This chapter provides insights into the importance of nanomaterials such as Fe colloids and LDHs for sequestration of toxic elements in circumneutral mine drainage. A graphical summary is provided in Figure 2-16. A graphical summary of the Ainaí mine drainage Our understanding of the formation of these nanomaterials highlights the geochemical properties and processes that play important roles in mine drainage and might be applicable to the treatment of drainage from other mines. A supply of Fe^{2+} from underground wastewater promotes the formation of spherical, homogenous ~100 nm Fe colloids that are micro-aggregates of core-shell ferrihydrite, which co-precipitate with As thereby facilitating the removal of As. Minor Fe concentration variations significantly affect the inverse relationship between Fe and As, especially in terms of colloid size, with a minimal decrease in Fe concentration in October significantly increasing the As concentration. We have established that the mobility of elements depends highly on the size of colloids, which is significantly affected by the aggregation rate. Fe colloids are mobilized for longer in the drainage until aggregating to about 300 nm in size, when they are gravitationally separated. Precipitation and flow rate affect colloid interaction and thereby provide first-order controls on aggregation and deposition, so these parameters should be closely monitored in passive treatment systems.

The application of LDHs as sequestration agents has been explored previously (Wang et al., 2016). Zn is reportedly a challenging element to remediate in natural systems due

to its high solubility and poor adsorption onto minerals such as hydroxides and carbonates. Here a novel approach involving isomorphous incorporation of Zn onto an existing Fe^{2+} – Fe^{3+} – CO_3^{2-} LDH to form a Zn–Fe LDH is demonstrated using geochemical modelling, synthetic samples, and observations of natural samples. A combination of high Zn and Fe concentrations and $\text{pH} > 7.5$ is ideal for efficient removal of Zn in passive treatment systems, with Zn–Fe LDH nanoparticles predominating in naturally treated mine drainage.

Critical geochemical factors for heavy-metal removal include wastewater chemistry and composition, pH, flow rate, and aggregation rate. Understanding of these factors enables the role of turbidity and sequestration mechanisms to be clarified. Our findings imply that quantitative prediction of the behavior of nanoparticles such as colloids and LDHs might facilitate optimal design of highly efficient treatment systems, have general applications to mine drainage and other aquatic systems, and improve our understanding of the interaction between toxic elements and colloids that form in these systems.

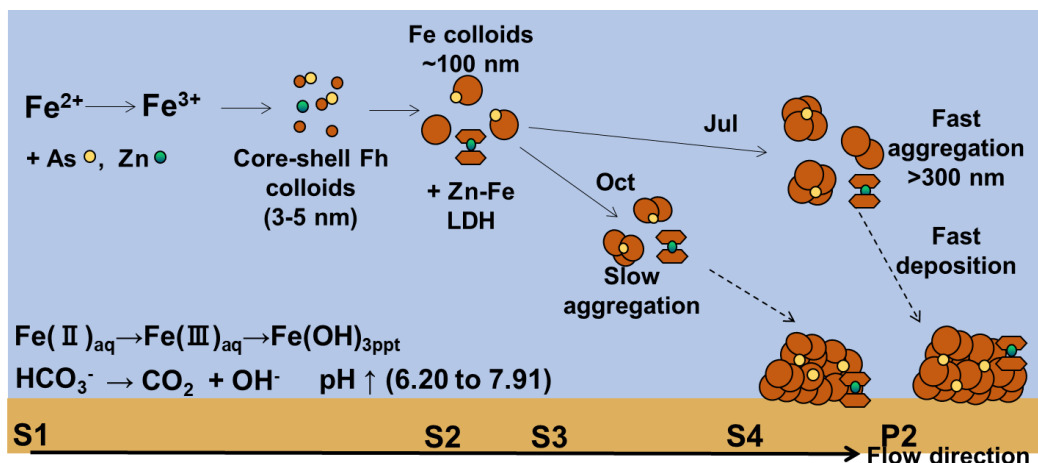


Figure 2-16. A graphical summary of the Ainaí mine drainage

3 Chapter 3: Formation of Schwertmannite colloids in the acidic Shojin river and their impact on metal sequestration

3.1 Introduction

Mine drainages draw wide attention in terms of their contribution to water contamination. Despite the wide studies conducted, their significant variety in geochemical properties still warrants further research. To cover a wide scope, we carried out our work at two study sites, namely Aina mine drainage and Shojin river, which were selected due to their contrasting characteristics. Aina systematics are explained in the Chapter 2, while the latter, Shojin, is mainly described in this chapter.

Shojin river flows through Shojingawa mine, an abandoned iron sulphide mine (Watanabe et al., 1997) Its water mixes with sulfur rich wastewater, and flows for about 2 km before being discharged to a nearby river. In this drainage system, the presence of Fe has also been reported, and warrants a study to highlight the role of the Fe in the drainage. Shojin river system is marked by its low pH (avg 3.1) and high Fe concentration, besides other metals/metalloids. At this pH, natural remediation of mine drainages has been proven challenging or hardly possible due to the difficulty in precipitating stable (Fe) minerals that assist in the remediation process. In this study, an investigation was carried out to elucidate the remediation process at the mine drainage.

The Shojin river system is a 2 km stretch, that has yellowish-brown precipitates at the shallow river's bed, that become more prominent towards the downstream. A report by the Hokkaido Geological survey (Geological Survey of Japan, 2019) states that elements of focus for treatment i.e. are initially in concentrations above the WHO are mainly Fe, As, Pb, and Cd . The presence of Fe in mine drainage systems has for a long time been utilized as a remediation pathway, that allows Fe to precipitate and incorporate other elements, thereby aiding in the removal of other elements from the drainage. A similar concept is applied at Shojin river, where a limestone bed was constructed to raise the pH and aid the precipitation of Fe and remove the other elements. In this study, a focus is mainly given on the formation of minerals at a nanoscale, i.e. on Fe colloids. Fe colloids are known for their large surface areas and hence increased reactivity with other elements. This is of utter importance as these colloids, when present in the drainages will determine the behavior and fate of the co-existing elements.

Despite the crucial role that colloids have been reported to play in controlling other element behaviors, few studies have carried out field investigations to highlight the role of these colloids in mine drainages. The colloid formation is affected by various factors, which also require highlighting, in the case where an efficient mine drainage is to be constructed. Besides the colloid formations, the aggregation and transportation behavior

of the colloids was also studied to highlight the impact of the colloids on the remediation of other elements in the drainage.

Based on this background, the objectives of this chapter are to (i) highlight the formation process of Fe colloids at acidic pH (ii) clarify the underlying factors that affect the behavior of the colloids in the drainage and (iii) understand the impact of the colloids on the other elements in the drainage. This was done using interpretation of on-site measurements, geochemical trends and microscopic observations of the solid particles collected from the drainage.

3.2 Description of study area: Location, geology, and drainage system

Shojin river flows in Nanae town, southern Hokkaido, Japan (Figure 3-1). Mining activities were carried out at Shojin mine for a period of 21 years (1937 to 1958). Elemental sulphur, iron sulphide ores and limonite were mined for S and Fe. Extracted ores were transported to a nearby site for beneficiation. However, since ores were extracted from an underground mine, wastewater continues to flow to the surface, thereby requiring treatment. Underground water interacts with the exposed sulphide ores before being released to the surface resulting in the typical acidic mine drainage. Management of the wastewater is undertaken by Hokkaido Geological Survey in which an open limestone channel (OLC) was constructed to allow the wastewater to flow through before joining the river after which, the Shojin river merges with Amemasu river, before emptying into the Japan sea. Various industrial activities such as concrete manufacturing, fish and rice farming are carried out mainly towards the downstream of the rivers. Particularly, the farming activities demand the water to be within environmental standards, thereby calling for more need for study. Given the previous reports by the company, Fe concentrations in the drainage and hence the possibility of colloid formation in the drainage was investigated.

Shojin river is about 2 km, and flows through thick forest, making some points hardly accessible, however, for this research investigation, sampling points that are representative of the behavior of the toxic elements in the drainage (Figure 3-1) were identified. Sampling was carried out from SW1, 2, 3 and 4, which are representative of the wastewater that flows to the surface from the underground abandoned mines. However, input from SW3 is very minimal and was therefore removed from most of the data reporting. SR1 is the Shojin river water before mixing with the wastewater. SR2 to SR9 are the river and wastewater after mixing, from the upstream to downstream. The complementary remediation applied is the limestone bed that is between SW1 and SW2 (Figure 3-2a). The large area in SW1 is the limestone bed (Figure 3-2 top), and most of it is currently covered in brownish precipitates. Wastewater flows through the limestone bed and some from underground, is released at SW2. SR1 is the background water (Figure

3-2 bottom left), which is basically the natural river water. SR2 (Figure 3-2 second from the left) is the mixing point at which wastewater (SW1 and SW2) meet the natural river water (SR1). The various waters have relatively clear water, whereas reddish precipitates begin to appear prominently from SR2 all the way to SR9 (Figure 3-2 bottom right). The flow rate of Shojin is relatively high. Multiple inputs, mainly negligible were observed during the field sampling, which are seepage from the tailings but are in very small volumes, hence do not significantly alter the system's geochemistry. The mixing ratio of the wastewater to river water is about 4:1.

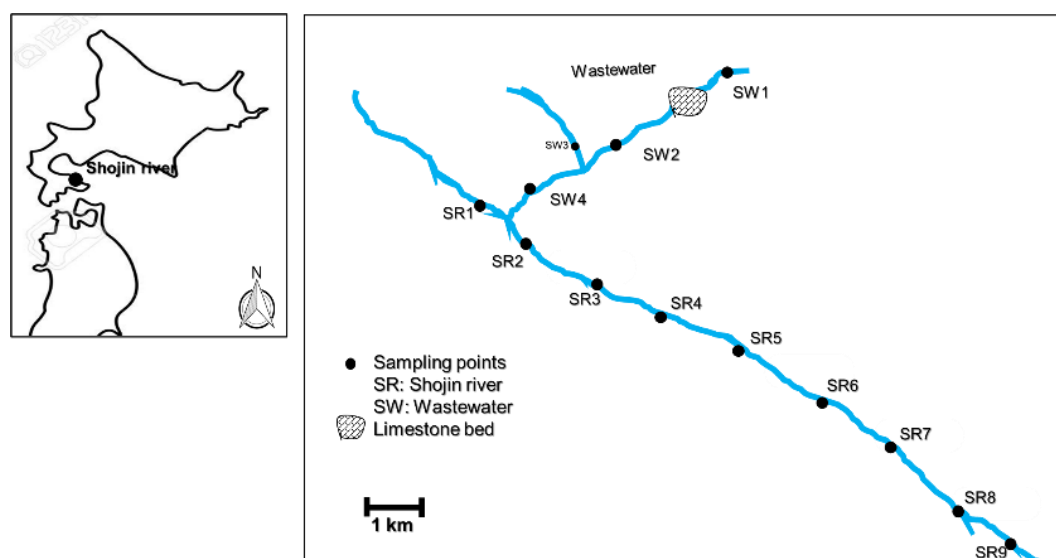


Figure 3-1. Schematic of the Shojin river drainage, showing the sampling points. Insert map is the location of Shojin river in Hakodate area.



Figure 3-2. Pictures of the Shojin drainage. SW1 shows the SW1 sampling point and the limestone bed, SR1 is the river water before mixing, SW2 is the second source of wastewater, SR2 is after mixing of the waste and river waters and SR7 is further downstream of the drainage.

3.3 Materials and methods

3.3.1 Field sampling: Water and solid samples

Field surveys at Shojin were conducted in July 2019 and August 2020. Samples of water, suspended solids, and sediments were collected from the upstream to downstream to represent the processes occurring in the drainages. Water was sampled through three types of filters, 0.2 μm PTFE membrane filter (Advantec 25HP020AN), 200 kDa ultrafilter (Advantec USY-20) and As filters (Sep-Pack cartridge: As exchange column), to provide four types of samples: 0.2 μm membrane-filtered, non-acidified sample for anion analyses; acidified 0.2 μm membrane-filtered sample; and 200 kDa ultra-filtered sample and samples to be analyzed for As speciation, with the latter three being acidified by 1 vol.% HNO_3 (ultrapure grade, Kanto chemicals) for cation analyses. Here, we define the dissolved and colloidal fractions as follows: (1) ultra-filtered (200 kDa) water samples contain the dissolved fraction; (2) membrane-filtered (0.2 μm) samples contain the colloidal and dissolved fractions; (3) the difference between (1) and (2) provides the colloidal fraction. Samples were collected in 50 mL polypropylene bottles, pre-rinsed with 6 vol.% HNO_3 overnight, and stored at $\sim 4^\circ\text{C}$ pending analysis.

On-site measurements were undertaken for Fe^{2+} concentrations, dissolved oxygen (DO), pH, electrical conductivity (EC), turbidity, temperature, oxidation-reduction potential (ORP), and alkalinity of water samples. A pack test was used for Fe^{2+} concentrations; Eh (Redox potential of the normal hydrogen electrode) was calculated as $Eh = E + 206 - 0.7 \times (T - 25)$ (E: oxidation - reduction potential (mV), T: temperature ($^\circ\text{C}$)). Alkalinity was determined by HNO_3 titration of water samples filtered through a 0.45 μm PTFE membrane filter. A Gran-function plot was applied to obtain HCO_3^- concentrations from alkalinity. Distances from each sampling site and flowrates were measured on site. Sediments samples were also collected at most sampling points using a shovel while suspended particles were collected by pumping 0.5 L to 1 L of water through 0.2 μm mixed-cellulose-ester filters (Advantec A020A047A).

3.3.2 Analytical methods

Anion and cation analyses: Non-acidified water samples were diluted 10 times and analyzed by ion chromatography (IC; Metrohm IC861) using Multi-anion Standard Solution 1 (Wako Pure Chemical Corporation) for calibration. Acidified samples were diluted 40 times and analyzed for major and trace elements by inductively coupled plasma-atomic emission spectroscopy (ICP-AES; Shimadzu ICPE-9000) and ICP-mass spectrometry (ICP-MS; Thermo Scientific iCap Qc). Standards were prepared from a

multi-standard solution (Wako). In, Ru and Rh and were used as internal standards for ICP–MS analysis. Oxide formation during analysis was monitored by the CeO/Ce ratio and maintained at <0.5% and He collision mode was utilized to avoid molecular interference from $^{40}\text{Ar}^{35}\text{Cl}^+$ on $^{75}\text{As}^+$.

Microscopic observations: Sediment and suspended particulate samples were dried using two methods for comparison's sake. All samples that were analyzed were dried at room temperature by being placed in balance trays, that were carefully stored in secured cabinets for about 1 week. The replicate of these samples was dried using the freeze—drying method, with the target of preserving the minerals in their initial state and avoid any transformations that may occur during drying. The minerals present in the sediment and suspended particulates were determined by X-ray diffraction (XRD; Rigaku XRD Multi-Flex) using Cu K α radiation ($\lambda = 0.15406$ nm) with an accelerating voltage of 30 kV and beam current of 20 mA, in the 5°–70° range, scanned at 2.0° min $^{-1}$. The morphology and chemical composition of the suspended particulates were analyzed by field-emission scanning electron microscopy with an energy-dispersive X-ray spectrometer (FE–SEM–EDS; JEOL JSM-6500F). Samples were prepared for transmission electron microscopy (TEM; JEOL JEM-2010) by dispersion in ethanol (with ultrasonication) and placed on a Cu grid with a film. Minerals were identified using Crystal Structures Libraries (HULINKS). Samples that were dried using different methods gave similar data and no significant difference was noticed between the two.

3.4 Results

3.4.1 On-site and general water characteristics

The data obtained from on-site measurements are reported in Table 3-1. Results of on-site measurements from the Shojin river and are plotted in Figure 3-3. Shojin river drainage is an acidic, oxidative and Fe abundant mine drainage system. The wastewater pH ranges from 2.6 in the wastewater (SW1) to 3.4 in the downstream (SR9) which is over 2 km away. The background river, before mixing with the wastewater has a pH of 6.9, which then decreases drastically to 3.5 after mixing with the wastewater (Fig. 3-3a). Overall, the pH slightly increases towards the downstream. The pH in the two sampling times was not too different hence most of the data is reported in average. The dissolved oxygen concentrations are from 7.6 mgL $^{-1}$ to 11.1 mgL $^{-1}$ and remains relatively stable throughout the drainage. The DO is within the recommended standard for water quality. EC ranged from 6.5 in the background river and increases significantly in the wastewater (~129.5 mS m $^{-1}$) and then decreases to about 55 ms m $^{-1}$ after mixing. ORP is relatively stable, (495.7 to 616.8 mV) throughout the drainage. Turbidity on the other hand, is very low with most values being under 5 NTU, irrespective of the point in the drainage (Fig.

3-3b). Ferrous Fe measured by the pack test was also very low throughout the drainage, with a high of ~ 2 ppm (Fig. 3-3a). These on-site parameters did not show significant variations within the two sampling seasons, therefore seasonal variations are not discussed in this chapter.

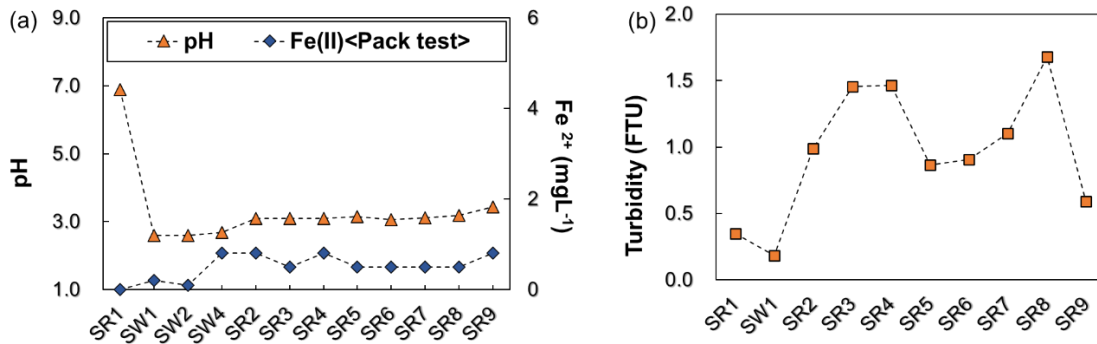


Figure 3-3. Trends of (a) pH, Fe²⁺ and (b) turbidity from upstream to downstream

Major anion chemistry was also investigated from the samples brought back to the laboratory. The wastewater was mainly sulphate-rich according to the anion chemistry and this is highly attributed to the ore that was extracted from this drainage, therefore making SO₄²⁻ the dominant anion in the drainage. The major anion in the drainage and the stiff diagram is shown to have an imbalance due to this abundance which is complemented by H⁺ ions supplied by the high pH. Charge balance of the wastewater was calculated as better than 16% for all the samples.

In Table 3-2 and Figure 3-4, the major anion chemistry is summarized to give a picture of the nature of the drainage. In contrast to Ainaí mine drainage (Chapter 2), SO₄²⁻ is dominant and followed by Cl⁻. Comparatively, the other anions exist in negligible concentrations. A trend in the SO₄²⁻ concentrations is also observed. In the background river (SR1), the sulphate concentration is 82 ppm, while it is over 10 times higher in the wastewater (SW1,2 and 4). A sharp decrease is observed after the mixing at SR2 and fluctuates from there, slightly increasing towards SR6 and decreasing again towards SR8. A slight increase is also observed at SR9.

Table 3-1. Results of on-site measurements from the Shojin river

Site	pH		DO (mg/L)		EC (ms/m)		ORP (mV)		Turb (NTU)		Fe ²⁺ (ppm)		Eh (mV)	
	Jul	Aug	Jul	Aug	Jul	Aug	Jul	Aug	Jul	Aug	Jul	Aug	Jul	Aug
SR1	6.9	5.9	9.9	10.3	6.5	12.7	308.3	-	0.4	1.7	0.0	0.1	520.6	189.7
SW1	2.6	2.7	7.8	7.6	129.5	112.0	606.3	-	0.2	1.7	0.2	0.3	819.8	235.2
SW2	2.6	2.8	8.2	9.7	127.3	106.3	616.3	-	0.6	0.4	0.1	0.1	830.5	193.7
SW4	2.7	2.8	10.4	10.5	114.8	105.3	588.0	-	0.4	0.3	0.8	0.3	799.6	192.9
SR2	3.1	3.5	10.1	10.2	48.7	24.6	561.0	-	1.0	0.7	0.8	0.3	773.0	267.7
SR3	3.1	3.2	10.3	-	49.8	27.2	585.0	-	1.5	2.6	0.5	0.8	798.4	-
SR4	3.1	3.2	10.3	10.6	50.2	27.2	558.3	-	1.5	1.5	1.0	0.7	770.6	154.8
SR5	3.2	3.2	10.1	-	50.7	27.3	559.7	-	0.9	1.7	0.5	0.8	771.3	-
SR6	3.1	3.1	10.0	10.1	63.6	35.3	545.0	-	0.9	2.3	0.5	1.0	756.0	298.6
SR7	3.1	3.1	9.9	11.1	55.5	33.4	529.3	-	1.1	1.1	0.5	0.7	739.9	295.2
SR8	3.2	3.1	10.2	11.2	51.1	34.0	522.7	-	1.7	2.1	0.5	0.3	733.1	287.3
SR9	3.4	3.4	9.5	10.6	41.7	34.8	495.7	-	0.6	1.8	0.8	0.5	707.4	269.1

- Indicates sites at which data was not collected.

Table 3-2. Main anion chemistry of the Shojin river mine drainage.

	SO ₄ ²⁻ (ppm)	Cl (ppm)
SR1	82.8	10.5
SW1	1275.7	10.5
SW2	939.7	10.5
SW4	980.3	10.5
SR2	408.9	14.3
SR3	131.4	10.5
SR4	384.4	13.3
SR5	412.1	14.0
SR6	559.0	14.1
SR7	486.6	13.0
SR8	342.6	10.5
SR9	594.6	14.1

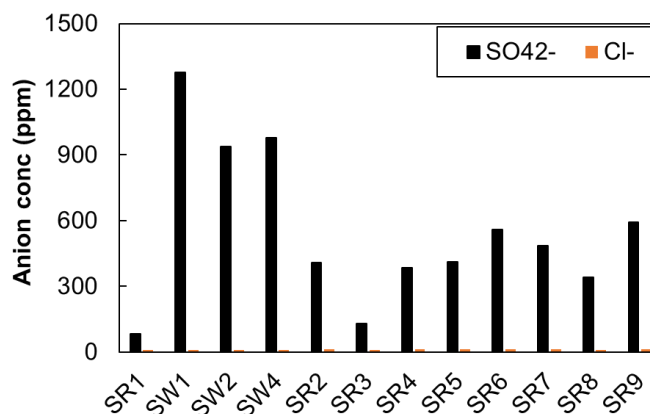


Figure 3-4. Anion concentrations of the Shojin river drainage.

3.4.2 Colloidal and dissolved fractions of Fe, As and Pb

At Shojin river, the main elements that are focused on for treatment are Fe, As Cd and Pb. A detailed table for other element concentrations is provided in the appendix. Here, focus is given to Fe, As and Pb (

Table 3-3). In particular, Fe and As exhibit clear fractions of colloid and dissolved fractions, thereby allowing the understanding of colloid behavior in the drainage. Overall, despite starting at relatively high concentration Fe: 44 ppm and As: 110 ppb, the Fe and As concentrations decrease (3.37 ppm and 1.2 ppb respectively) to concentrations that are below the WHO recommended guidelines (Fe: 10 ppm and As: 10 ppb) (Fig. 3-5a and b). Pb concentrations are 9.41 ppb (Fig. 3-5c). 4 wastewater sources were identified at Shojin river, namely SW1, SW2, SW3 and SW4, and these occur in between SR1 and SR2. The concentrations of Fe among the wastewater are about 43 ppm (Table 3-3), except at SW3, which seems to contribute minor Fe concentrations comparatively. The Fe concentrations significantly decrease by about one third, after mixing with the background water whose pH is near neutral and has Fe concentrations that are below detection. From SR2 to SR9, a steady decrease in the total Fe is observed, until the Fe concentrations reach below 10 ppm. A very similar trend is seen in the As concentrations, which are very high, i.e. over

100 ppm in the wastewater, except SW3, then significantly decrease by about a fourth at SR2 after mixing. From SR2 to SR5 a steady decrease is observed, followed by a sharp decrease in the Fe and As concentration at SR6 to SR9.

Table 3-3. Fe, As and Zn concentrations in dissolved and colloidal fractions in July and October.

	Fe		As		Pb	
	Dissolved	Colloidal	Dissolved	Colloidal	Dissolved	Colloidal
SR1	b.d.	b.d.	0.18	b.d.	0.43	b.d.
SW1	43.62	b.d.	110.56	b.d.	30.86	b.d.
SW2	42.88	b.d.	103.23	b.d.	30.10	b.d.
SW4	38.17	b.d.	-	-	-	-
SR2	9.14	4.74	0.68	28.03	11.99	-1.77
SR3	11.10	2.39	1.73	23.10	10.56	-0.49
SR4	11.30	1.23	2.73	17.92	9.99	0.25
SR5	10.94	0.35	4.91	9.75	9.52	-0.37
SR6	6.32	b.d.	2.89	-0.06	17.14	-0.78
SR7	5.12	0.14	2.10	0.10	14.20	0.24
SR8	4.26	0.05	1.84	-0.04	12.46	0.02
SR9	3.36	0.01	1.16	0.04	9.01	0.40

- Indicates data that is unavailable.

In the fraction distribution plots, the wastewater sources (SW1 to 4) are eliminated because their concentrations are too high and hence decrease the visibility of the trends of colloid formation from SR2 onwards. No colloid formation was observed in the wastewater source (SW1 to 4) because the pH in the wastewaters is too low. From SR2, colloid formation is quickly observed in both Fe and As, with half of the Fe remaining in the dissolved fraction, while a very small amount of the As is dissolved fraction (Fig. 3-5d, e). At SR3, instead of the dissolved fraction continuously decreasing, while the colloids are increasing, a slight increase in the dissolved fraction is observed, in both element plots. The dissolved fraction at SR3, 4 and 5 remains almost stagnant in the Fe plot, while it slightly increases in the As plot. Worth noting is that the pH at SR2 is slightly above 3 and remains almost stable with minimal decrease towards SR4 then increases at SR5. From SR5 to SR6, the colloidal fraction quickly vanishes from the plot, as if none had formed, but a notable decrease in both Fe and As is evident. From SR6 onwards, the

pH increases and concurrently, the Fe and As dissolved concentrations also decrease. However, similar to the case in Aina mine drainage, the As concentration towards the downstream remains nearly constant in the dissolved fraction, despite the Fe concentration showing minor decreases. Irrespective of this, both concentrations are below the WHO recommendation at the downstream of Shojin river. The Pb concentrations on the other hand are dominantly in the dissolved fraction, with negligible colloidal concentrations. An increase in the Pb concentration is observed mid-stream, which is from an input that joins the river between SR5 and SR6. colloid formation is looked at from the perspective of Fe and As only.

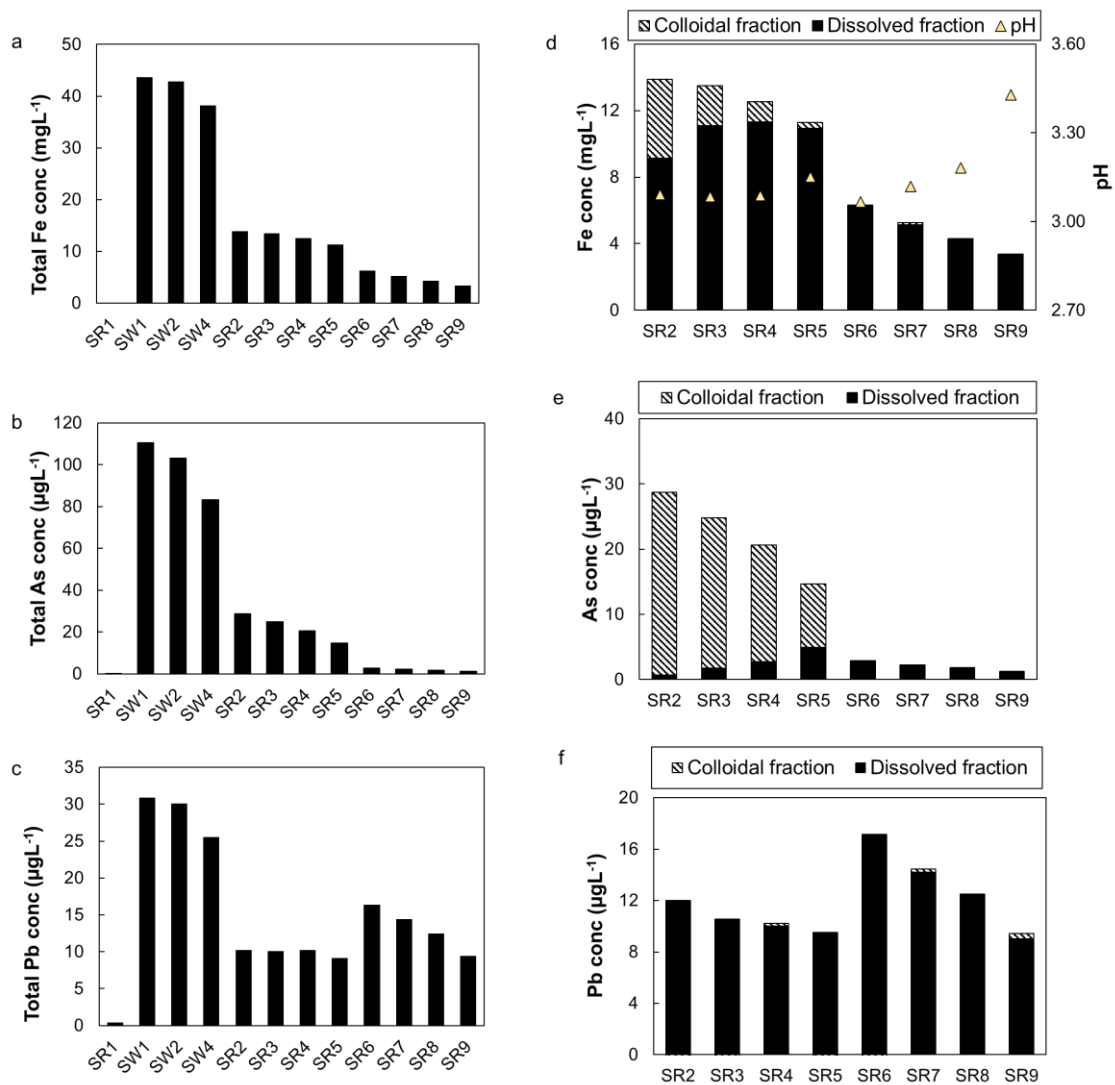


Figure 3-5. Concentrations of (a) total Fe, (b) total As, and (c) total Pb. Fe, As and Pb in dissolved and colloidal fractions are shown in (d), (e) and (f) respectively. pH is

shown as yellow triangles in the Fe plot. “Total” in all the element plots refers to concentrations obtained as the sum of the colloidal and dissolved fractions. In the fraction distribution plots, the wastewater sources (SW1 to 4) are eliminated because their concentrations are too high and hence decrease the visibility of the trends of colloid formation from SR2 onwards.

3.4.3 Characterization of Schwertmannite colloids and other mineralogy in the drainage

Characterization of Schwertmannite has for a long time been challenging due to its weak crystallinity. Fortunately, various studies have successfully characterized the mineral using XRD and infrared spectroscopy among other approaches (e.g. Bigham et al., 1996). The crystal structure of schwertmannite was also reported by Bigham et al. (1996) to be isothermal to mineral akageneite (β -FeOOH), comprising of chains of iron (III) oxide- and hydroxide-octahedra that are connected in a style that forms the cavities in which anions are stored. With this regard, XRD was used to characterize the sediments collected from the drainage from the upstream to downstream. The major mineralogy in the drainage was observed to be schwertmannite with traces of goethite, which was derived from peaks at 2θ at around 20° 28° 35° 40° 45° 55° and 60° (Fig. 3-6). Most of the sediments are dominantly schwertmannite but due to aging, the presence of goethite, and some minor hematite was observed (Figure 3-7 e and f). However, despite wider mineralogy observed, the major mineral responsible for sequestration may be the schwertmannite and further characterization was also carried out on suspended particles and particularly on the ultrafilters to deduce the major colloidal mineral.

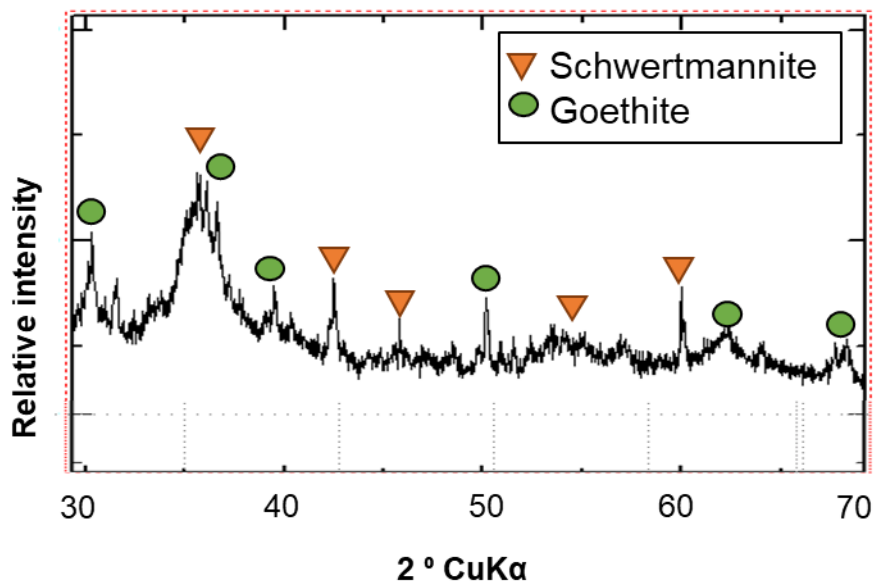


Figure 3-6. XRD profile of the sediments collected at SR2. Sh: Schwertmannite.

In Figure 3-7, the mineralogy observed in the drainage is summarized. An aggregated bed of aged spherical colloidal structures was observed (Fig. 3-7a). The structure presented by the aged material is bulbous and forms plate-like structures, most likely from impact of water flow. Irrespective of this, the bulbous structure is highly preserved even after the pressing. Figure 3-7 (b) is an up-close micrograph of the schwertmannite colloids, that are aggregated and preserve hedgehog-like structures on the outside of the mineral. The aggregates are spherical and have the fibrous surfaces. Figure 3-7 (c) shows the schwertmannite colloids together with other minerals. Figure 3-7 (d) is another up-close image of the schwertmannite aggregates observed in the sediment, along with other minerals. Figure 3-7 (f) shows an interaction of the schwertmannite colloids with goethite and other minerals in the sediments. Schwertmannite colloids in b, c, and d may be a different morphology of schwertmannite from the one displayed in (a) especially given the sea-urchin shape displayed by (b), (c), and (d), a typical and characteristic feature that is associated with schwertmannite. The length of the fibers or strips on the schwertmannite surfaces have been reported to vary because of differing concentrations of SO_4^{2-} , organic matter contents and hydrolysis temperature among others (Bigham et al., 1996; Bigham et al., 1994). Furthermore, well developed rod-like goethite crystals, sea-urchin-like schwertmannite aggregates and bulbous, aged schwertmannite with a smooth surface are observed in co-existence with each other (Fig. 3-7d, e). Some structures resembling bacteria mats were also observed in the sediments. They were abundant in C on the EDS analysis, which symbolizes organic matter. Overall, the mineralogy at Shojin river is within those expected for an Fe- and sulphate-rich acidic

mine drainage, with the presence of the various morphologies of schwertmannite, goethite and other minor minerals. This is also in correspondence with the XRD peaks that were described earlier.

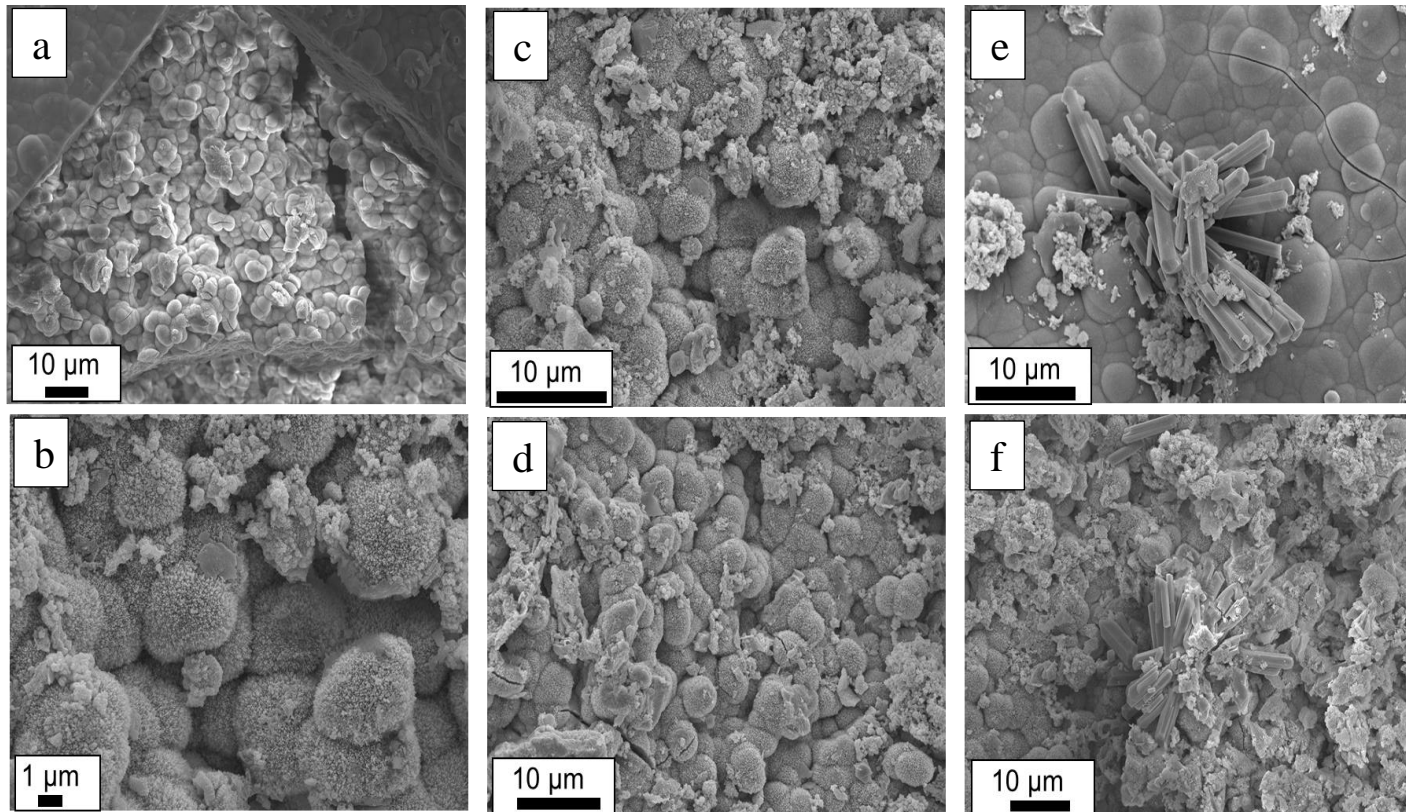


Figure 3-7. The mineralogy identified in the solid particle analyses carried out on Shojin river samples. (a) An aggregation of the Fe colloids, (b, c and d) up-close images of the bulbous, fibrous schwertmannite colloids (e) goethite occurring on an aged aggregate surface of the schwertmannite colloids, and (f) goethite crystals amongst colloid aggregates and other minerals.

Following the major mineralogy observation and characterization that was carried out on the sediment samples, an observation of the ultrafilters was also carried out to particularly characterize the colloid particles i.e. particles between 200 kDa and 0.2 μm (Figure 3-8). The colloid particles were most abundant on the ultrafilter of SR2 and decreased until almost disappearing at SR5 (Figure 3-8). These particles were collected on a sample holder taped with carbon tape and coated with platinum coating for microscopic observation.

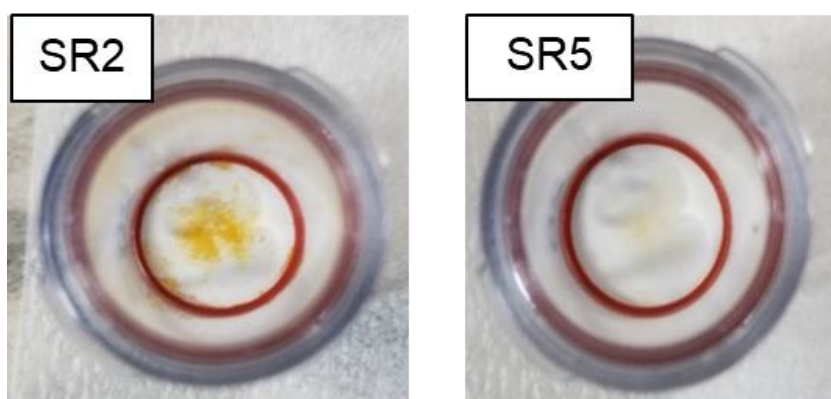


Figure 3-8. Colloids collected on the 200 kDa ultrafilters of SR2 and SR5.

Colloid aggregates were observed in abundance on the ultrafilters (Figure 3-9a), where clear fibrous structure aggregates of schwertmannite were collected on the ultrafilter. The colloids on the ultrafilters were mainly as aggregates, which would hardly be deduced whether they had formed on the filters or in the field. However, these clusters had passed through the 0.2 μm , therefore some of them must have come together after initial filtration. Nonetheless, the colloids were characterized to establish their composition. As seen in the EDS spectra (Figure 3-9b), the colloids were mainly composed of Fe, S, C, O and As (Pt was from the coating during sample preparation). The colloids were quite homogenous throughout the drainage, in terms of elemental compositions.

Given their size, a closer observation of the spherical, fibrous structures became unclear, therefore, TEM was used. Under TEM, the fibrous structures of schwertmannite became clearer (Figure 3-9b). The schwertmannite colloids had an average size of 80 to 100 nm including the fibers, and these fibers were present in almost all the colloids observed in the ultrafilter samples. The surface area of the schwertmannite colloids was also analyzed to be around 92.15 g/m^3 . Unlike the ferrihydrite colloids at Ainai (that were seen to be formed from core-shell ferrihydrite), the schwertmannite colloids seemed to appear as whole colloids, thereby making it difficult to deuce whether these are products of preceding smaller nanoparticles. Some studies have however reported spherical ferrihydrite colloids preceding the schwertmannite but with time, the fibers that surround

schwermannite are formed as goethite predevelopment as at the low pH, unlike forming as separate entities, result in the development of the fibrous structures as observed in these samples. The size of the needles were about 20 nm and this may be due to the formation process, since these may be shorter than others reported in previous studies (Hockridge et al., 2009). The detailed formation mechanisms are explained in the following sections and may highlight the traits of the schwermannite that are observed at Shojin river.

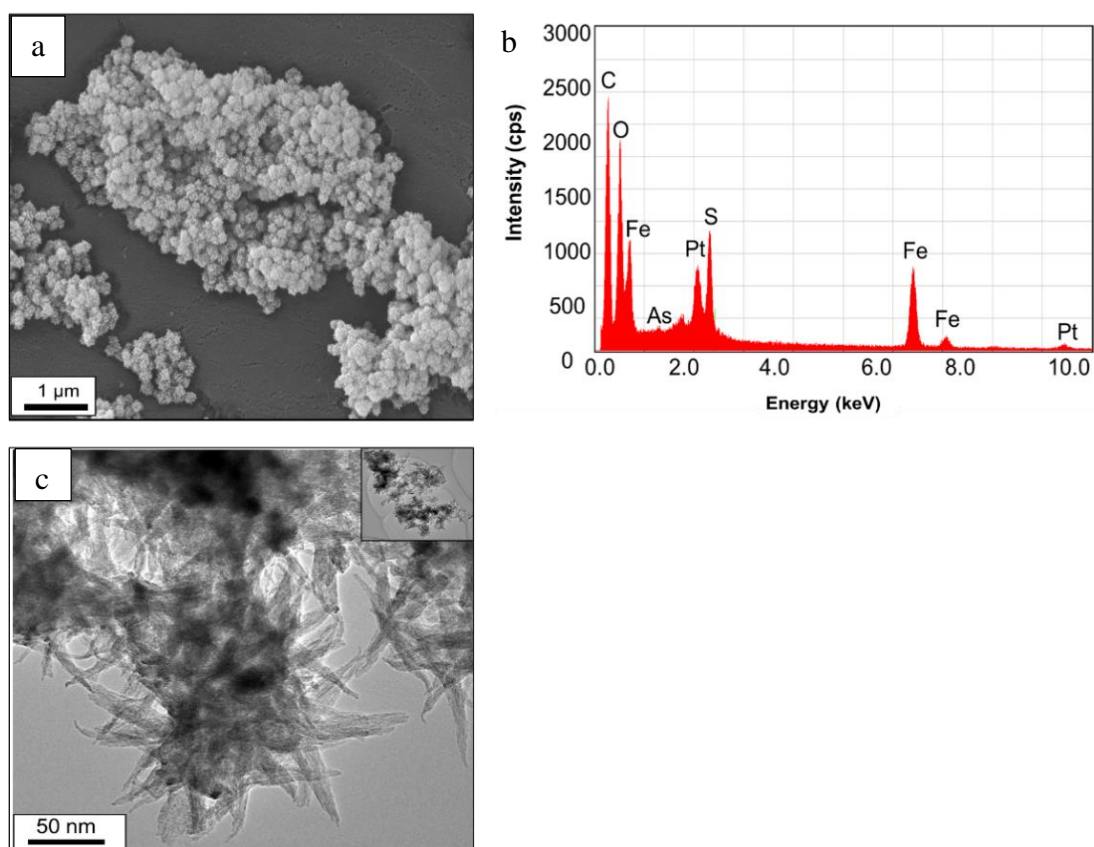


Figure 3-9. An up-close observation of the schwermannite colloids collected on the 200 kDa ultrafilter. (a) A secondary electron image of colloid aggregates, (b) the EDS spectra from SEM showing the elemental composition of the colloids and (c) a TEM image of the colloids.

3.5 Discussion

3.5.1 General water characteristics

Shojin river is an acidic mine drainage system, whose background river has a near-neutral pH (6.9), but the wastewater from the abandoned mine bears highly acidic waters (pH: 2.8). Upon mixing the pH rises to 3.1, because of dilution and an impact from the background river water. The drainage then remains within a pH range of about 3.1 to 3.9 implying that no processes naturally increase the pH of the drainage system significantly. Electric conductivity is about $112 \text{ mS}\cdot\text{m}^{-1}$ in the wastewater but quickly reduces to $24.6 \text{ mS}\cdot\text{m}^{-1}$, after mixing with the background water that has an EC of about $12.7 \text{ mS}\cdot\text{m}^{-1}$ showing the variation of the anions present in the wastewater, river water and water after mixing. Similar to pH, EC remains relatively stable after mixing. ORP remains average throughout the river with an average value 235.5 mV, besides the slightly elevated values in the wastewater.

The Fe^{2+} concentration, measured using pack test was very low in the drainage, less than 2 ppm throughout the drainage implying that any Fe present in the drainage was mainly in the ferric state. The major controlling factor for the oxidation state of the Fe in mine drainages is the source of the Fe, which in this case was limonite along with other Fe sulphides. Various reaction paths have been suggested to explain the resulting state of Fe, for instance, oxidation of the sulphides by O_2 or Fe^{3+} , as well as the primary effect of microbes in the pyrite oxidation which regenerates Fe^{3+} from Fe^{2+} (Williamson et al., 2006). These parameters are highly affected by pH, therefore, given the pH at Shojin, the oxidation of the sulphides by Fe^{3+} may have been the major controlling agent resulting in Fe^{3+} being released from the wastewater. Turbidity was also very low, with a high of 2.6 NTU. Despite these significantly low values, that may even be regarded as negligible, a noticeable trend was observed. The turbidity in the wastewater is very low, then after mixing, an increase is observed which stabilizes mid-drainage and later increases again. The behavior displayed by turbidity is highly suggestive of the occurrence of precipitates in the drainage, i.e. after mixing, an increase in precipitate formation, most likely colloidal particles prevail. Even though the turbidity continues to increase towards the downstream after mixing, Figure 3-3 shows that the number of colloidal particles in the drainage does not necessarily increase. Consequently, it can be deduced that the increase in turbidity is due to the aggregation of the particles formed at around SR2. From SR5, the pH slightly increased, and the turbidity slightly decreases although not as much. This may be interpreted as the result of very quick formation of the colloids followed by quick settling of the aggregates, which is consistent with the absence of the colloid fraction in the downstream of the drainage. Therefore, it can be said that, from the geochemical properties understood from on-site measurements, a rough picture of the formation, aggregation and deposition behavior can be understood, in that colloids are forming after

mixing, then aggregate towards SR5, before increasing the formation and aggregation rate in the river.

3.5.2 Formation of schwertmannite colloids in the drainage and their sequestration of toxic elements

The general trend of the Fe, As and Pb in the drainage shows that the Fe and As concentrations, despite being very high in the upstream, decrease significantly towards the downstream, while Pb on the other hand behaves differently by decreasing towards mid-stream, but slightly increasing towards the downstream (Fig. 3-5). The trends displayed by the 3 elements are key to understanding the processes that govern the remediation in the Shojin river.

At SW4 going to SR2, mixing of the wastewater and river water occurs, and concurrently, the Fe, As and Pb concentrations all show a decrease in concentrations (Fig. 3-5). Given that two major processes are occurring at this point, i.e. dilution of the wastewater by river water, and change in the geochemical properties of the resulting (mixed) water from the differing geochemical properties in the different waters (waste and neutral river water), it is suggestive that the decrease of the element concentrations is triggered by two things: (i) the dilution of the wastewater by background river water and (ii) the increase in pH after the mixing. The mixing ration of the waste to river water was estimated to be about 1:4, which majorly explains the nearly 4 times decrease of the Fe, As and Pb concentrations from the SW4 to SR2. Dilution is an important factor for mine drainage treatment as evident from this decrease and is highly applied for mine treatment systems, however, the efficiency of dilution highly depends on the pH and buffering capacity of the neutral river water. In most cases of mine drainage systems, since the river is flowing through similar geology as the mine wastewater, its buffering capacity may be decreased and result in reduced efficiency of the wastewater to remediate the wastewater only by dilution. In this case, further intervention, such as a modification of the geochemical parameters, specifically pH, comes into play. At Shojin, dilution efficiently reduces the heavy metal concentrations by about a fourth, however, an increase in the pH is also observed, which further supports the remediation process, by initializing the precipitation of Fe minerals that play a part in the removal of the toxic elements towards the downstream.

Having highlighted the significance of dilution in the mixing of the drainages, a geochemical perspective is not highlighted from SR2 to SR9, mainly because the element concentrations continue to decrease, which is evident of further geochemical processes occurring in the drainage. A dissection of these processes is done, with respect to the colloid formation. An analysis of the metal fractions in their dissolved and colloidal fractions shows that an occurrence of the colloidal fraction dominates from SR2 (Figure

3-5 d and e), particularly for Fe and As. The presence of the colloidal fraction, which indicates the formation of colloids from SR2, suggests that in the drainage, once mixing occurs, dilution of the wastewater by river water occurs, but in addition, colloid formation, i.e. precipitation of the Fe colloids is initiated. Since an increase in pH is observed from SW4 to SR2, the formation of the colloids was likely initiated by the slight increase in pH, that was reached after the mixing. This can easily be seen from the trends displayed by the Fe and As, where colloid formation was only observed in the drainage from SR2. In support, the turbidity also begins to rise at SR2, confirming the presence of the colloids. Prior to mixing, the pH in the wastewater was too low, such that no colloid fraction was detected, implying no colloid formation or colloid formation that was barely noticeable and below our measurement detection limits. This therefore shows that the colloids in the drainage required a pH of 3.1 or over for the colloids to form in the drainage.

The correspondence in the Fe and As concentration trends, is suggestive of sorption processes that are occurring, thereby As being removed during Fe colloid formation in the drainage. At pH 3.1, considered acidic pH, but common in mine drainages, schwertmannite precipitation has been widely reported (Webster, Swedlund and Webster, 1998; Dold and Fontboté, 2002). At this pH, schwertmannite has shown the ability to efficiently remove As from water by surface complexation. The chemical and channel structure of schwertmannite (Figure 3-10), which is described in detail by Zhang et al., 2018, has surface OH groups, which allow for the surface complexation with metals or metalloids. Further to that, a novel channel structure is characteristic of the mineral, Figure 3-10, that favors adsorption of other elements in addition to the surface complexation, thereby increasing the efficiency of the removal of other elements by schwertmannite. Evidently, we see that the colloid formation is dominantly of schwertmannite colloids, that are formed from SR2 after the mixing of the two waters and a triggered increase in pH. These colloids are then responsible for the removal of As from the drainage, i.e. the schwertmannite colloids are the primary colloids, while the As colloidal fraction represents the pseudo colloids.

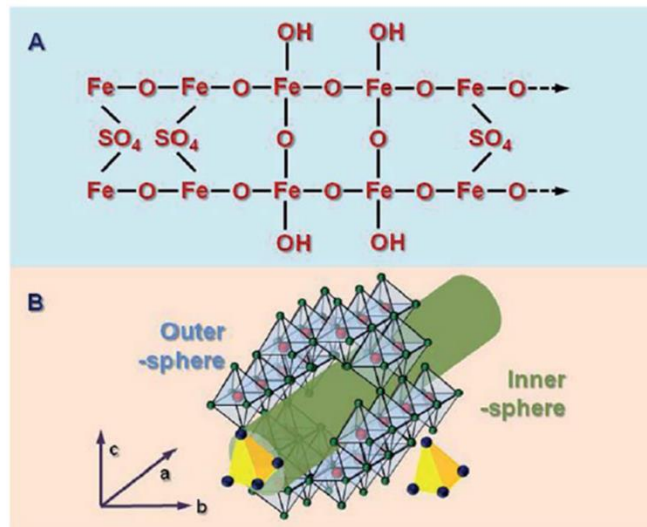


Figure 3-10. (a) Chemical and (b) channel structures of schwertmannite (Zhang et al., 2018).

The remediation process seen above, i.e. formation of primary Fe colloids that remove the As from the drainage, is highly pH dependent (Fukushi et al., 2003). As seen in the trend of Pb (Figure 3-5), after mixing, the concentration of Pb only decreases a slight minimal compared to As. The behavior of Pb was modelled using GWB (Figure 3-11), to elucidate its possible removal mechanism. It was established that Pb requires a pH of about 5.5 and above to reduce to the recommended WHO standard. Although As does not immediately reach the stipulated standard of under 5 µg/L, further towards the downstream, that concentration is reached efficiently without significant increase in pH. On the other hand, the concentration of Pb, displays an increasing trend from SR6, contrary to the quick decrease reached by Fe and As. In this part of the drainage, competitive sorption is playing a significant role in controlling the behavior of the elements. Since the pH increases slightly, schwertmannite colloid formation is sped up, and quickly removes the As, in both cases leaving no trace of the colloids, due to quick precipitation, however in the case of Pb, the Pb that was sorbed by the schwertmannite is released due to the preferential incorporation of As by schwertmannite than Pb (Crawford et al., 1993).

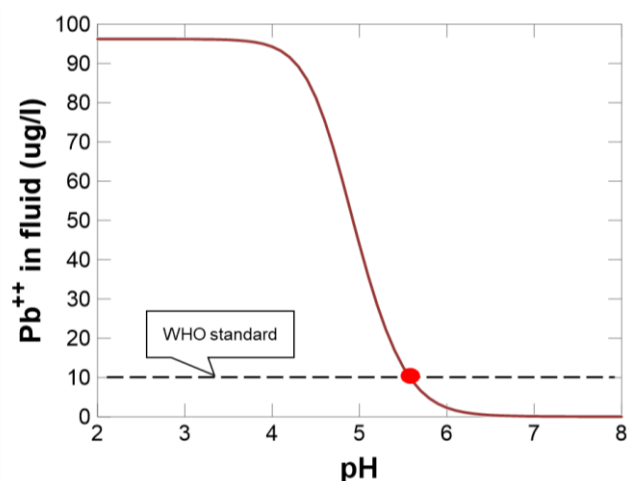


Figure 3-11. Removal of Pb as a function of pH calculated by a surface complexation model (GWB)

Another spectacular trend in the metals is observed between SR2 and SR3 to SR5. Following the initial formation of the colloids, a minor dissolution behavior of the colloids is observed from SR2 to SR3, that is understood from the slight increase in the dissolved fraction of both the Fe and As (Figure 3-5 b and d). At this low pH, such a behavior is expected, as studies have shown that colloids may be unstable at such low pH. The pH decreases appears to be 3.09 at both, a difference that may seem minimal, but regarding that pH is measured and reported at a log scale, this difference justifies the dissolution that occurs from SR2 to SR3. From SR3 to SR5, the total Fe hardly decreases but a decrease in the colloidal fraction is observed (Figure 3-5), implying a possible aggregation of the colloids that formed at SR2. This is also supported by the continued increase in turbidity at the said locations (Figure 3-3b). Although compared to Aina's aggregation behavior, the aggregation at Shojin seems slower, probably because at this low pH not many colloids formed, and some were lost to dissolution. However, from SR6, an increase in the pH is observed, probably because some H⁺ ions are lost during the formation of the colloids. In addition, minor seepage is observed around SR5, which may have also contributed to the increase in pH at around SR6. From the dissolved and colloidal trends, the overall Fe concentration drastically decreases, without a clear record of colloid formation, however, the turbidity increases at these locations (Figure 3-3b). Evidently, colloid formation is occurring, just that the colloids form and aggregate very quickly, due to the drastic increase in pH that is observed towards the downstream i.e. (SR6 to SR9). The trends of dissolved and colloidal As are very similar to those of Fe (Figure 3-5 d and e), therefore, we describe the Fe colloids as the primary colloids, while the As colloids are pseudo colloids, whose behavior is determined by the primary Fe colloids. Conclusively, colloid formation is evident at Shojin and is a relevant stage that the Fe and As undergo, to initiate the removal of the elements from the drainage.

3.5.3 Dominant mineralogy for sequestration of toxic elements

Following the confirmation of the formation of the colloids, a characterization of the colloids was necessary. Previous studies regarding Fe mineral formation have highlighted the dominance of schwertmannite in such acidic conditions (Webster et al., 1998). In line with our microscopic observations, schwertmannite is the dominant form of the colloids in the drainage. The general mineralogy showed the presence of schwertmannite in the colloids as well as the sediments, in addition to the other minerals such as goethite and minor hematite and ferrihydrite, that were observed in the sediments. The schwertmannite displayed a characteristic morphology in the crystals of both sediments and the colloids. The schwertmannite has clear, spherical structure surrounded by needle-like, fibrous structures, that are grouped into spheroidal hedgehog aggregates. Considering that the dominant Fe species is the ferric state of Fe, oxidation stage, i.e. from ferrous to ferric Fe, is most likely absent in this drainage. However, the Fe^{3+} in the drainage undergoes hydrolysis process, which is a well reported pathway for the formation of Schwertmannite in acidic mine drainages. A simplified equation that summarizes the hydrolysis process is;



where Fe^{3+} represents the precipitates from ferric species. A detailed account and investigation has been done by (Fu et al., 2011), highlighting the significant factors that come into play during formation of Fe oxides by hydrolysis. Although our study does not dissect these phenomena in detail, an analysis of the schwertmannite colloids formed at Shojin river had an average size of 80 nm (from TEM analysis) and surface area estimated to about 92.15 m²/g. The colloid particles analyzed were those obtained on the ultrafilters for the particle sizes and sediments for the surface area (colloid sample was too little for the surface area analysis). Our analyses were most likely performed on the minerals after multiple primary nucleation stages, and this was beyond the scope of this work. These values, correspond to others investigated in previous studies and although slightly low surface area was recorded, the general characteristics of the precipitates in this study are certainly in line with those of schwertmannite,

Once aged, the schwertmannite may be transforming to other minerals, particularly goethite (Cruz-Hernández et al., 2017), but also various morphologies of the schwertmannite may have formed in the drainage. A variation in formation pathways may also be a controlling factor for the variation in mineralogy of the drainage. Processes such as dehydration, phase restructuring or solid-state growth of minerals into specific oxyhydroxides may have resulted in the spherical and rod-like mineral structures observed in the drainage (Figure 3-9). The presence of minor ferrihydrite was also a

possible reason for the varied schwertmannite structures in the drainage, resulting in other spherical aggregated sediments. Schwertmannite forms through various pathways but given that the Fe from the source is majorly Fe^{3+} , we suggest that the schwertmannite formed through hydrolysis of the ferric Fe as represented in the simplified equation.

3.6 Summary

This chapter summarizes the formation of schwertmannite colloids, that act as scavengers of As in an acidic mine drainage. Shojin river is a mine drainage that is highly acidic and has an input of ferric Fe that is hydrolyzed to form schwertmannite colloids that aid in the removal of Fe and As from the drainage. Most mine drainages increase the pH to (near)-neutral pH as a prerequisite for removal of toxic elements. Here, we, not only show that it is possible to scavenge the toxic elements, particularly As at low pH, but we also show that colloids do form and can become stable at pH as low as 3.1. We see minor pH changes having drastic impacts, and at such low pH, the colloids form and aggregate, although slower than in neutral conditions. Overall, the toxic element concentrations are significantly reduced to below the recommended standard by WHO, signifying an efficiency of the colloid scavenging As at the low pH.

Furthermore, the application of turbidity to understand colloid behavior is highlighted and acts as an easily accessible tool to unfold the behavior of the colloids. From this, the formation and aggregation behavior can be understood qualitatively, thereby allowing an assessment of the need for a quantitative assessment. Finally, the transportation behavior shows that the colloids formed at Shojin are slowly transported from the upstream towards further downstream, before completely settling to the bed of the drainage. This is attributed to the rate of aggregation which is slow at Shojin compared to that at Ainai. Nonetheless, this gives insight on the distance that the colloids are transported, which is highly dependent on the size of the colloids i.e. connecting to aggregation.

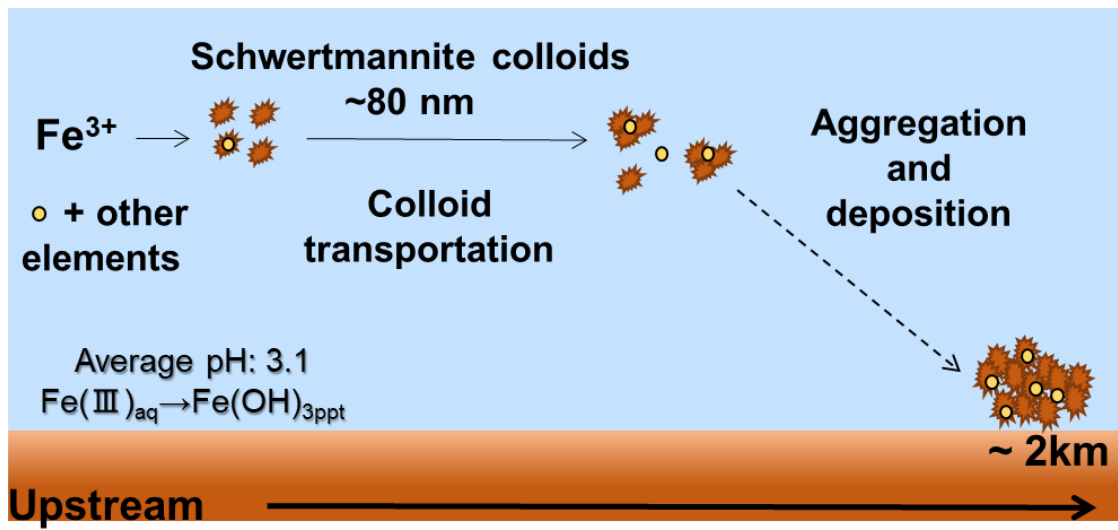


Figure 3-12. A graphical summary of the remediation process at Shojin river

4 Chapter 4: A comparison of colloid behavior in the Ainai and Shojin river drainages

4.1 Introduction

The significance of colloids in the remediation of mine drainages has been well explained in the previous chapters, i.e., 2 and 3. It has been reported that colloid formation occurs in both the drainages under study, that is, in both acidic and circumneutral conditions. In this chapter a detailed comparison is done to highlight the variations that exist in the remediation approaches when geochemical properties such as pH, element concentrations and others differ, with the two study sites named above as case studies.

In the mine drainages studied, variations exist, as is the case with other mine drainages. This makes understanding and highlighting their variations significant. The characteristics of mine drainages vary vastly, as a result of geology, weather and other factors, which consequently result in different remediation processes dominating at different sites. With regards to this study, colloid formation also depends greatly on the nature of the drainage. The colloids formed in the drainages vary, and because the colloids are investigated as sequestration media for toxic elements, the remediation efficiency is also compared at the two study sites. Finally, given the nature of colloids to resist settling by gravity, their mobility poses as a significant characteristic to be investigated.

It is based on these factors, that the objectives of this chapter are to; (i) compare the formation processes and its impact on the behavior of colloids in the circumneutral and acidic mine drainages, (ii) compare the sorption capacity of the colloids and (ii) compare the transportation behavior of the colloids in the drainages. The chapter summarizes the field observations as case studies that are compared for Ainai mine drainage and Shojin river.

4.2 Methodology

Samples used for the comparison of the colloid behavior on this chapter are those reported in chapters 2 and 3 and hence sampling methods and analyses are primarily those reported in chapters 2 and 3.

Investigation of colloid mobility in the field was investigated as follows; during field sampling, distances from each point were measured. The flowrates, times and distance were all estimated using a balance tray that was let to freely flow from one point to the next. This data was merged with the water chemistry data to compare the behaviors with distance. Similar approaches were done at both Ainai drainage and Shojin river, and a comparison of the same is reported.

4.3 Results

4.3.1 A comparison in the colloid formation from field observations

To begin with, a summary in the characteristics of Ainai and Shojin are displayed in Table 4-1. The distinct characteristics that the mine drainages bear, may be playing roles in controlling the colloid that form in the drainages and their transportation behavior. The table below summarizes the major differences that exist at Ainai and Shojin. Despite other variations that might be existent, the pH, Fe^{2+} concentration, the mineralogy and formation pathways are highlighted in the study until this point. Ainai has pH ranges within the circum-neutral ranges and an abundant supply of Fe^{2+} , while Shojin is acidic, with a supply of Fe^{3+} . These characteristics are determinant factors of the formation processes that dominate each system i.e., oxidative precipitation and hydrolysis at Ainai and Shojin respectively, which, with respect to the solution chemistry, result in the dominant mineralogy of the Fe colloids, i.e. ferrihydrite for Ainai and schwertmannite for Shojin. These colloids and processes in turn, are the cause for the varied R^2 values, that show how correlated the Fe colloids are, to As colloids in each system respectively.

Table 4-1. A comparison of geochemical characteristics of Ainai and Shojin

	Ainai	Shojin
pH	6.20 to 7.91	2.6 to 3.1
Fe^{2+} (mg/L)	14 to 0.05	< 1
$R^2_{(\text{Fe:As})_Dissolved}$	0.970	0.647
$R^2_{(\text{Fe:As})_Colloidal}$	0.928	0.829
Dominant colloid mineral	Ferrihydrite	Schwertmannite
Formation pathway	Oxidative precipitation	Hydrolysis

In Figure 4-1 a and b, a correlation of the primary and pseudo colloids is shown. At Ainai a significant correlation in Fe and As, both colloidal and dissolved fractions is seen. R^2 values of the elements in both fractions are over 0.9 (Figure 4-1a). On the other hand, a strong correlation in the colloidal fraction is observed at Shojin, but a weak, although existent relationship exists in the dissolved fraction of the dissolved fraction (Figure 4-1b). The colloids at Shojin are absent in the wastewater and towards the downstream, therefore their dataset is smaller than that of the dissolved fraction. Nonetheless, correlations are existent in both fractions at the two study sites, however, the correlation in the colloidal

fractions is stronger in both cases. This highlights the need to understand in depth, the transportation behavior of the Fe colloids, as this will reflect the number of other colloids that are being transported in the mine drainage.

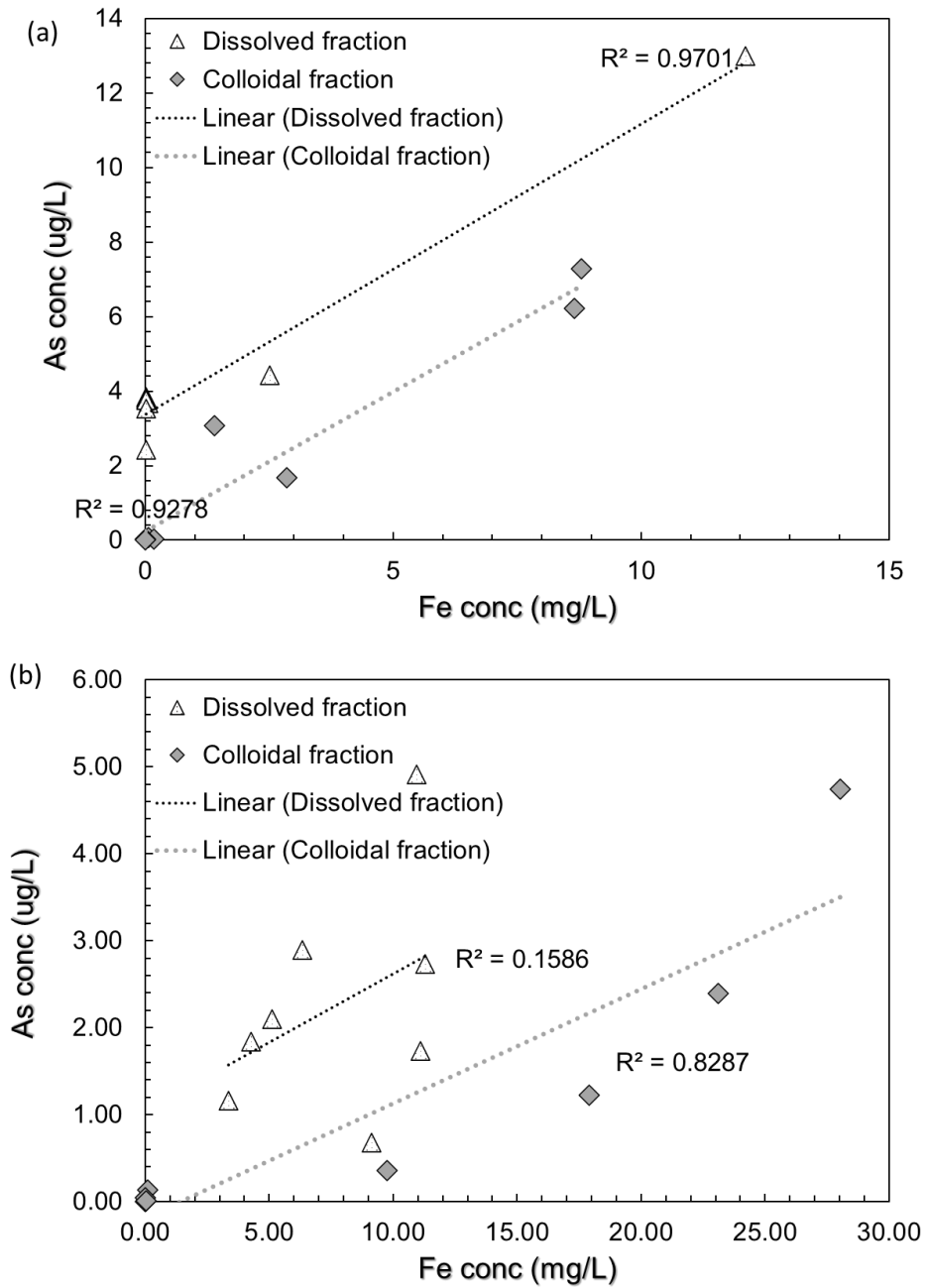


Figure 4-1. A comparison in correlation of the Fe and As in dissolved and colloidal fractions at (a) Ainaï mine drainage and (b) Shojin river.

4.3.2 Colloid mobility at Ainaï and Shojin drainages

The number of colloids transported, presented as their concentrations, from the upstream to the downstream was estimated from the field observations (Figure 4-2). The behavior displayed by the colloids reflects at what distance from the upstream the colloids are formed, and how much of them are transported towards the downstream. The plot is presented for the Fe colloids formed at Ainai mine drainage in comparison with Shojin river. At Ainai, the colloids are formed a bit later in the drainage, are transported a short distance, before drastically decreasing before 1000 m. On the other hand, at Shojin, the colloids form early in the drainage, although in much lower concentrations than at Ainai. Their concentration slowly decreases, and colloids remain in the drainage until about 2000 m from the upstream. The decrease in colloid concentration is slow and steady. Evidently, the rate at which the colloids are settled from the system differs between Ainai and Shojin, which lead towards the following calculation of the settling rate.

The variation in the settling rate was quantitatively estimated to clarify if it is a significant factor, that controls how far the colloids travel and at what rate they settle, using the below equation.

$$V_s = \frac{g}{18} \frac{\rho_s - \rho}{\eta} d^2 \quad (4-4)$$

Where η is the Absolute viscosity (kg/m/s), g is the gravity (m/s²), ρ_s is the particle mass density (kg/m³), " ρ " is the water mass density (kg/m³) and d is Particle diameter (m). The settling rate is shown in Figure 4-2, where Ainai has a settling rate of 1.76×10^{-7} m/s while Shojin has a slower settling rate of 1.23×10^{-8} m/s. The settling rate is one order faster at Ainai, than at Shojin, and given that the other parameters are (nearly) constant, this leaves the particle size as a peculiar characteristic controlling the settling rate.

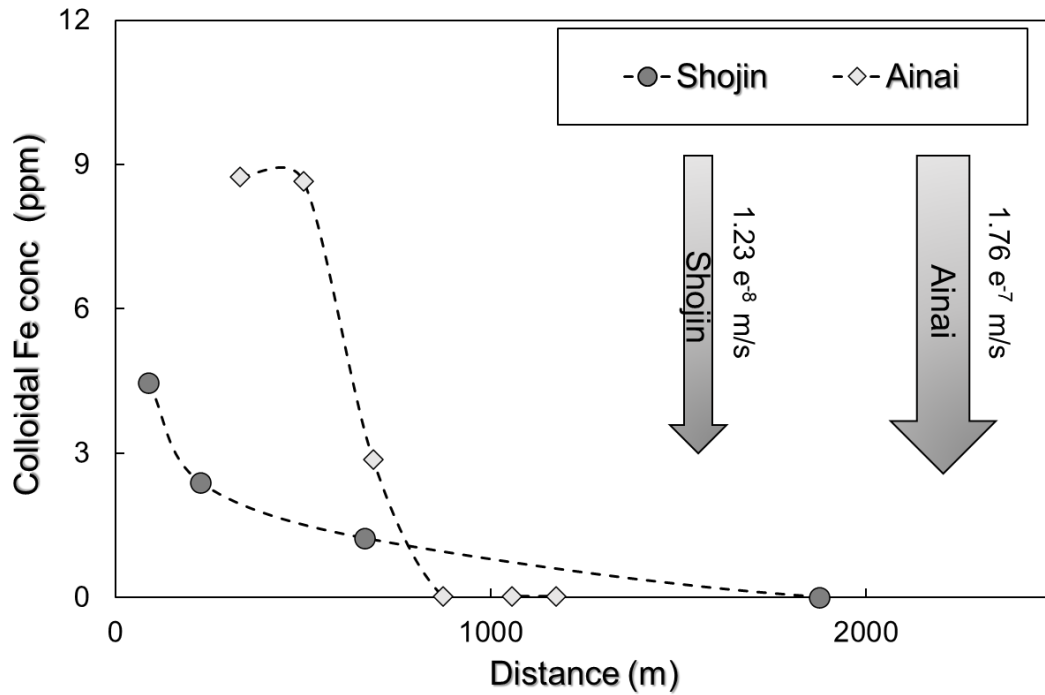


Figure 4-2. Colloids transported from the upstream as a function of distance. The arrows represent the settling rate at the two study sites.

The particle sizes that were obtained from microscopic observations with respect to the colloid formation trend are displayed in Figure 4-3. At Ainai the dominant particle size that was observed was about 100 nm on average while 80 nm particles dominated the colloids at Shojin river.

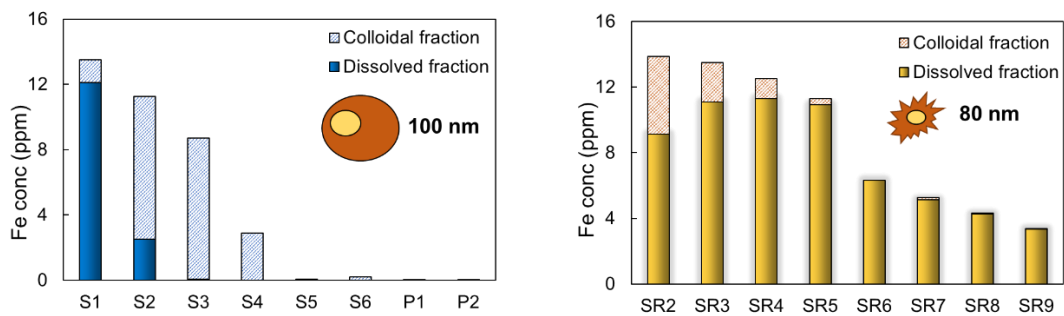


Figure 4-3. Fe colloid concentrations and size variations at Ainai and Shojin. Brown structures are the Fe colloids, while the yellow circles represent the incorporated As.

4.4 Discussion

4.4.1 Key variations in the geochemical characteristics of Ainai and Shojin rivers.

Colloid mobility in the mine drainages along with the significant factors affecting them are reported. As reported in the results section, the colloids at Ainai emerge in high concentration in the upstream since the oxidation of ferrous Fe, which is the rate determining process proceeds quickly in the upstream, unlike the hydrolysis of the ferric Fe which is highly limited by low pH at Shojin. This is irrespective of the fact that the Fe concentration at Shojin is higher than that at Ainai. Once colloids form in both drainages, some of the colloids are mobilized towards the downstream, Shojin colloids seemingly travelling longer distances than Ainai colloids. The colloids at Ainai from and quickly deposit to the bed of the drainage, unlike Shojin colloids that continue to be transported downstream. This phenomenon is highly related to the rate of aggregation, that we earlier observed was slower at Shojin. Therefore, seeing that aggregation rate is a significant factor for the mobility of the colloids, it is further looked at quantitatively in chapter 5.

Significant parameters are important to pick out, to know the point of focus when designing mine drainages. Besides those mention above, settling velocity was also quantitatively looked at. In the calculation carried out above, since most parameters are either constant or do not vary significantly, the particle diameter stood out as the major controlling factor that determines the settling rate. The average size of the colloids taken from the microscopic observations was 100 nm and 80 nm for the Ainai colloids and Shojin colloids, respectively. Although significantly slow, the settling rate at Ainai was 1.76×10^{-7} ms⁻¹, while Shojin colloids settled at 1.23×10^{-8} ms⁻¹, signifying an order difference in the rate of settling, which explains the difference in the colloid transport trends in (Figure 4-2). The size observed on the ultrafilters was used as the determinant since that is where the stability may have been gained for colloids at both sites. Evidently, the rate at which the particle aggregate determines this size, which in turn affects the settling rate as well as the rate at which the colloids are transported.

To address the issue of particle size and settling rate, the formation pathways for the colloids at the two sites were compared (Figure 4-3). As pointed out in the previous chapters 2 and 3, at Ainai, the colloids were formed as a result of oxidative precipitation, while at Shojin, the dominant process for colloid formation was the hydrolysis of ferric Fe, resulting in the schwertmannite colloids. Despite this, the pH of the two sites played a large role in controlling their mobility, since pH along with the bulk water, subsequently control the ionic strength and hence rate of aggregation and particle size.

Similarly, the mobility of the colloids is affected by the pH. The colloids formed at circumneutral pH are more abundant in concentration compared to those at low pH, as

seen in Figure 4-2. The precipitation pathway at near neutral pH, which is oxidative precipitation in this case, enhances the formation of the colloids, allowing for a saturation of the colloids in the water, an opposite of the low pH system, which has lower concentrations of colloids, and hence undersaturated. The saturated colloids become unstable, and therefore aggregate to form larger particles, thereby initiating the abrupt deposition that is observed at the circumneutral pH. This explains the faster settling rate and therefore, efficient deposition of the colloids by the time the wastewater reaches the downstream of the drainage. The varying natures of the two systems, thereby determine the mobility and deposition behaviors of the colloids in the drainage.

4.5 Summary

A comparison of the two mine drainages investigated in this research are reported. Colloid formation, particularly in mine drainages, still requires a detailed understanding and this research makes a significant contribution to understanding colloid behavior in mine drainages. In the initial chapters of this study, colloid formation in the respective drainages was confirmed, however, their variations, which highlight the significant factors that play key roles in determining colloid behaviors are explained. Colloid mobility, which is a characteristic behavior of the particles, determines the fate of other toxic elements, and in this chapter, we conclude that particle size, which is affected by the formation and aggregation are important factors for colloid transport.

The ferrihydrite colloids at Ainai mine drainage were formed by oxidative precipitation and resulted in colloids of 100 nm and over, while the schwertmannite colloids at Shojin river, were formed by hydrolysis of ferric Fe and resulted in 80 nm particles. This difference resulted in the colloids at Shojin river being transported a longer distance due to their smaller size and hence lighter weight. The acidic condition at Shojin may have played a larger role in keeping the colloids smaller and undersaturated, than those at Ainai, which quickly aggregated to larger sizes, large enough to settle quickly by gravity.

5 Chapter 5: Fe isotope systematics associated with the formation and transportation of Fe colloids in Ainai and Shojin river mine drainages

5.1 Introduction

Fe behavior is affected by various processes but most importantly, size, speciation and mineralogy (Raiswell et al., 2018). Fe supplied to rivers varies in these properties and should therefore be understood in order to clearly constrain the circulation of Fe. In the mine drainages, characteristics such as pH, Fe speciation from the source, organic matter content and others may vary, thereby affecting the behavior of the Fe. Approaches have been applied to constrain the Fe fluxes in various aquatic systems, but minimal studies have applied, particularly Fe isotopic fractions to highlight the contribution from mine drainages using the iron isotopes. Therefore, an investigation was carried out at two mine drainages of varying characteristics to fingerprint the sources, phases and behavior of Fe from the mine drainages to the rivers.

Fe has four stable isotopes, ^{54}Fe (5.8 %), ^{56}Fe (91.8 %), ^{57}Fe (2.1 %) and ^{58}Fe (0.3 %) (Federation, 2011). These isotopes fractionate because of various processes such as redox state and therefore their variations, that are usually reported in parts per thousand or in delta notation, can be applied to understand the behavior of Fe. The Fe isotopes are expressed as $\delta^{56}\text{Fe}$, defined relative to the international reference material IRMM-014. In this study, besides understanding the source of the Fe, seeing as Fe exists in different phases, the isotopic fractionations were also investigated in the dissolved (< 200 kDa) and colloidal fractions (200 kDa to 0.2 μm) to understand the fractionation in the different fractions. Studies have been carried out for bulk Fe in riverine systems and among them, Ito et al, 2017, for instance, reported that possible discrepancies might exist when the Fe isotopic fractionations are studied in bulk, unlike in their respective fractions, i.e. dissolved and colloidal. Samples collected for this analysis require to be ultra-filtered, a mechanism that has been suspected to cause some fractionations. However, on the brighter side, recent studies have proven that this sampling mechanism does not result in Fe isotopic fractionations (Lotfi-Kalahroodi et al., 2021) and can therefore be used to collect the samples accordingly.

The continental crust has $\delta^{56}\text{Fe}$ values of 0.06 ± 0.03 ‰, which has been reported to represent the isotopic values of Fe containing unweathered minerals (Poitrasson, 2006). It is worth noting however, that this value varies depending on publication, but majority are within the stated values. Therefore, weathering and any form of alteration of the minerals may be a potential trigger to a variation in Fe isotopic fractionations. Highlighting this phenomenon is becoming widespread and therefore our study poses as one that contributes to this emerging development and can assist in understanding Fe

circulation from the perspective of mine drainages and their contribution to the global Fe cycle.

Based on this background, the objectives of this chapter were to (i) identify the sources and pathways of Fe utilizing its isotopes from the mine discharge to the down streams of the drainages; (ii) highlight the dominant processes that control the Fe isotopic fractionations in the mine drainages and (iii) quantitatively estimate colloid formation and transportation from the isotopic fractionation values in the drainages.

5.2 Materials and methods

5.2.1 Purification of Fe solution

Significant developments have been made with regards to non-traditional isotopes in the recent years. Consequently, analyses can be carried out with a precision of 0.03‰, which is a strong point for such an analysis that requires high precision and reliability due to the small range in which Fe isotope values in natural systems occur; -4.0‰ to +2.0‰ (Dauphas and Rouxel, 2006) or -5.5‰ to +3.0‰ (Wu et al., 2019). Methodologies for the analyses of Fe isotopes in various aquatic systems are also outlined in previous studies (e.g. Conway and John, 2014). In this PhD thesis, the detailed methodology utilized, that applies to analyses in aquatic systems of similar nature is outlined below. All processes were carried out in the clean room and analysis room at the Research Institute for Humanity and Nature, Kyoto, Japan.

The pre-filtered solution samples collected during field work were weighed in unspiked Teflon containers to a volume that allowed collection of 50 µg Fe from the sample. The samples were then dried at ~140°C and then redissolved by adding 0.05 mL HNO₃ to convert all of the iron to ferric state. The ferric iron was then converted to a chloride complex by the addition of 0.1 mL of 8 M HCl. Samples were then purified by passing through columns compacted with anion exchange resin (Figure 5-1a) and the matrix was removed by 5 mL of 8 M and 3 M HCl. To improve the purity of the Fe solution, the purification process was repeated twice for each sample. Samples were then stored in tubes awaiting analysis (Figure 5-1b).

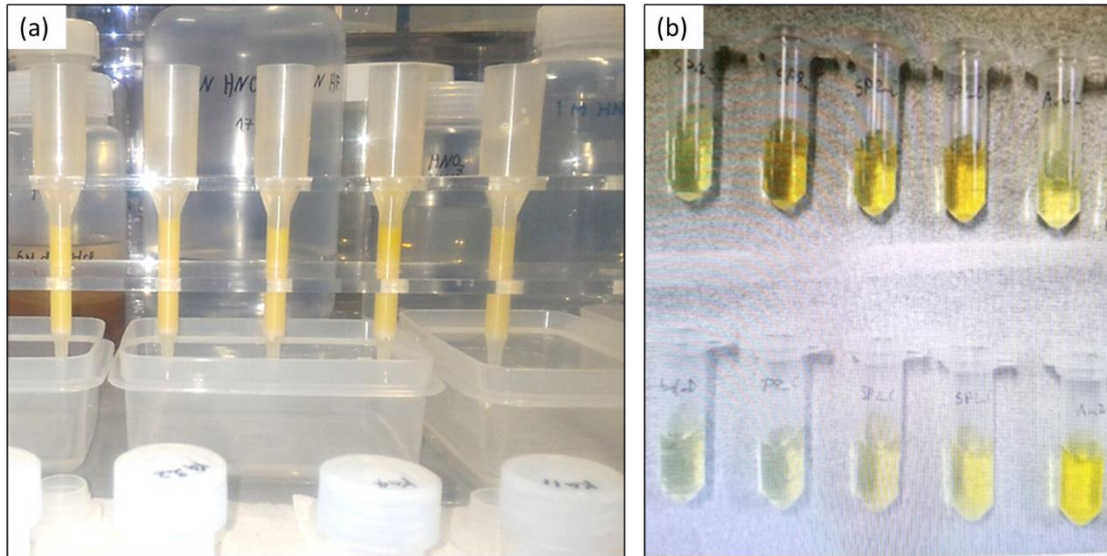


Figure 5-1. Photographic images showing (a) separation of Fe solution through resin and (b) final solution collected in micro vials for analysis

5.2.2 Analytical methods

The Fe isotopic compositions were obtained by Neptune plus, Thermo Scientific multi-collector ICP-MS (MC-ICP-MS). Instrumental mass bias was corrected using the standard-sample-standard approach adopted from Weyer and Schwieters (2003). The reproducibility of the standard measured as 2σ during analysis was 0.01‰. The isotopic compositions are reported using the delta notation:

$$\delta^{56}\text{Fe} (\text{‰}) = [({}^{56}\text{Fe}/{}^{54}\text{Fe})_{\text{sample}}/({}^{56}\text{Fe}/{}^{54}\text{Fe})_{\text{IRMM-014b-1}} - 1] \times 10^3 \quad (5-1)$$

5.3 Results

5.3.1 Isotopic fractionations in the dissolved and colloidal fractions of Ainai mine drainage and Shojin river

Isotopic fractionations of the dissolved and colloidal fractions of Fe at Ainai and Shojin were analyzed, and the data obtained from the analyses are summarized in Table 5-1. Samples were analyzed in two seasons, i.e. rainy and dry seasons and one sample set was obtained from Shojin river. Total fraction represents samples that contain both dissolved and colloidal fraction, while dissolved fraction is from samples that were ultra-filtered and contained only the truly dissolved fraction of Fe from the system. Finally, the colloidal fraction was calculated as a difference of the two (total and dissolved). For Ainai,

data was obtained in two seasons, from S1 to S5 as these contained Fe concentrations enough to be analyzed unlike S6, P1 and P2. On the other hand, Shojin data was obtained from SW1 and SW3 to account for any processes that may be occurring in the wastewater, and then SR2 to SR4, while other data plots are expected to be added with time. Nonetheless, the isotopic behavior at Shojin is also explained from the current data set.

The Fe isotopic fractionations were investigated in three fractions and are represented using these abbreviations: the total fraction as $\delta^{56}\text{TFe}$, the colloidal fraction as $\delta^{56}\text{CFe}$ and the dissolved fraction as $\delta^{56}\text{DFe}$. The abbreviations are used from now on for easy reference. Table 5-1 summarizes, the Fe concentrations along with the isotopic fractionations in the three fractions for both Ainai and Shojin river. The data for Ainai is then plotted in Figure 5-3. The isotopic fractionation pattern of Fe in Ainai mine drainage in the (a) rainy and (b) dry seasons. The two plots represent two data sets that were collected in different seasons. Figure 5-3 a was sampled in a rainy season while Figure 5-3 b was sampled during dry season.

The $\delta^{56}\text{TFe}$ values for Ainai in the rainy season range from -0.49 ‰ to $-4.06 \text{ ‰} \pm 0.07 \text{ ‰}$. In the dry season the $\delta^{56}\text{TFe}$ values reported a smaller range of -0.41 ‰ to $-3.44 \text{ ‰} \pm 0.08 \text{ ‰}$. The isotopic values of the dissolved fraction, $\delta^{56}\text{DFe}$ in the rainy season are -0.71 ‰ to $-3.46 \text{ ‰} \pm 0.20 \text{ ‰}$, while in the dry season, the $\delta^{56}\text{DFe}$ are -0.73 ‰ to $-4.19 \text{ ‰} \pm 0.31 \text{ ‰}$, displaying a larger range than that of rainy season. Finally, the colloidal fraction, whose values were calculated as a difference of the total and colloidal fractions, has $\delta^{56}\text{CFe}$ values ranging from $+0.82 \text{ ‰}$ to $-4.06 \text{ ‰} \pm 0.39 \text{ ‰}$ in the rainy season. In the dry season the isotopic values range from $+2.35 \text{ ‰}$ to $-3.44 \text{ ‰} \pm 0.17 \text{ ‰}$.

All the data was plotted against the remaining Fe concentration at each point respectively, when being compared to the Rayleigh fractionation model. The remaining Fe fraction was calculated as the ratio of the total Fe released to the drainage, to the dissolved Fe concentration at each point. This assumed that the remaining Fe is in dissolved phase at each point. The remaining fractions of Fe concentrations ranged from 0.801 to 0.001.

At Shojin, a dataset for the dissolved fraction in one season is reported. The $\delta^{56}\text{DFe}$ values range from -0.12 ‰ to $-0.54 \text{ ‰} \pm 0.09 \text{ ‰}$. The data is compared to continental crust and Fe-sulphide minerals, especially for the dissolved fraction, to highlight the source of the Fe in the analyzed fractions.

Table 5-1. Summary of the Fe isotopic fractionation values in the different fractions of total, dissolved and colloidal fractions at Ainai drainage and Shojin river.

Site	Sample location	Total		Dissolved		Colloid		Remaining fraction of Fe
		$\delta^{56}\text{Fe}$	2σ	$\delta^{56}\text{Fe}$	2σ	$\delta^{56}\text{Fe}$	2σ	
Ainai (Rainy)	S1	-0.49	0.18	-0.71	0.05	0.82	0.83	0.801
	S2	-0.45	0.05	-1.05	0.42	0.56	0.70	0.559
	S3	-0.80	0.04	-3.46	0.20	0.32	0.37	0.220
	S4	-1.65	0.05	-	-	-1.65	0.05	0.001
	S5	-4.06	0.03	-	-	-4.06	0.03	0.001

Site	Sample location	Total		Dissolved		Colloid		Remaining fraction of Fe
		$\delta^{56}\text{Fe}$	2σ	$\delta^{56}\text{Fe}$	2σ	$\delta^{56}\text{Fe}$	2σ	
Ainai (Dry)	S1	-0.41	0.19	-0.73	0.21	2.35	0.28	0.84
	S2	-	-	-	-	-	-	-
	S3	-0.84	0.06	-4.19	0.41	0.13	0.11	0.17
	S4	-1.24	0.04	-	-	-1.24	0.18	0.005
	S5	-3.44	0.03	-	-	-3.44	0.12	0.001

Site	Sample location	Total		Dissolved		Colloid		Fe conc (ppm)
		$\delta^{56}\text{Fe}$	2σ	$\delta^{56}\text{Fe}$	2σ	$\delta^{56}\text{Fe}$ (‰)	2σ (‰)	
Shojin	SW1	-	-	-0.12	0.14	-	-	48.18
	SW3	-	-	-0.07	0.11	-	-	48.18
	SR2	-	-	-0.58	0.03	-	-	44.86
	SR3	-	-	-0.03	0.10	-	-	13.88
	SR4	-	-	-0.54	0.10	-	-	2.02

5.4 Discussion

5.4.1 Relationship between the colloid formation and isotopic fractionations of the dissolved and colloidal fractions.

The amount of Fe in the different fractions was investigated prior to the isotopic fractionations. A trend of the Fe in both of the drainages showed a general decrease in the Fe concentration from upstream to downstream.

The details in the mechanisms and behavior of the Fe are explained in chapters 2 and 3. However, at Ainai, Fe is input as ferrous Fe, which oxidizes to ferric Fe and, given the pH of the drainage water, forms ferrihydrite colloids. The colloids are transported towards the downstream while others aggregate and settle from the wastewater. On the other hand, Fe at Shojin is released as ferric Fe, and at the low pH that the drainage is, the ferric Fe simply hydrolyses to form schwertmannite colloids. Similar to Ainai colloids, the colloids are transported towards the downstream, while some are settled to the bottom of the drainage. A particular phenomenon that exists in the Shojin system, that is absent at Ainai is the dissolution of the colloids within the drainage.

To begin with, data trends of Fe isotopic fractionations at Shojin river are reported in Figure 5-2. Despite the limited data set, which is mainly only for the dissolved fraction, with one sample of the colloidal fraction, some variations were observed. Before mixing, the $\delta^{56}\text{DFe}$ values were about 0.12 to 0.07 ‰ in the wastewater, and values begin to fluctuate after mixing of the waste and river water. At SR2, mixing of the river and colloid formation occurs. At this point, the dissolved fraction has the heaviest isotopic value of +0.57 ‰, followed by the total fraction, then the colloidal fraction with the lightest isotopic value. The formation process of the colloids governs this process. The absence of the oxidation stage, at least within the scope of our analysis, leaves the precipitation stage, that is majorly hydrolysis of the colloids as the controlling stage for the isotopic values. The precipitation stage involves a kinetic isotopic effect which gives an overall negative value, that is borne by the colloids. The precipitation of these colloids and the negative shift, leaves the dissolved fraction with a positive value, and the total fraction giving values that are within the initial isotopic values. Towards the downstream, aggregation and quick removal of the colloids also leaves an elevated isotopic signature in the dissolved fraction, as a result of the kinetic effect. waste water occurs, along with colloid formation. An important characteristic of the Shojin is that the colloid formation is a non-redox dependent process, thereby explaining the minimal fractionations and highly in agreement with previous studies (Henkel *et al.*, 2016). Since the river water had Fe concentrations below detection limits, the control of these fractionations was evidently the colloid precipitation that occurs following dilution and mixing of the two waters.

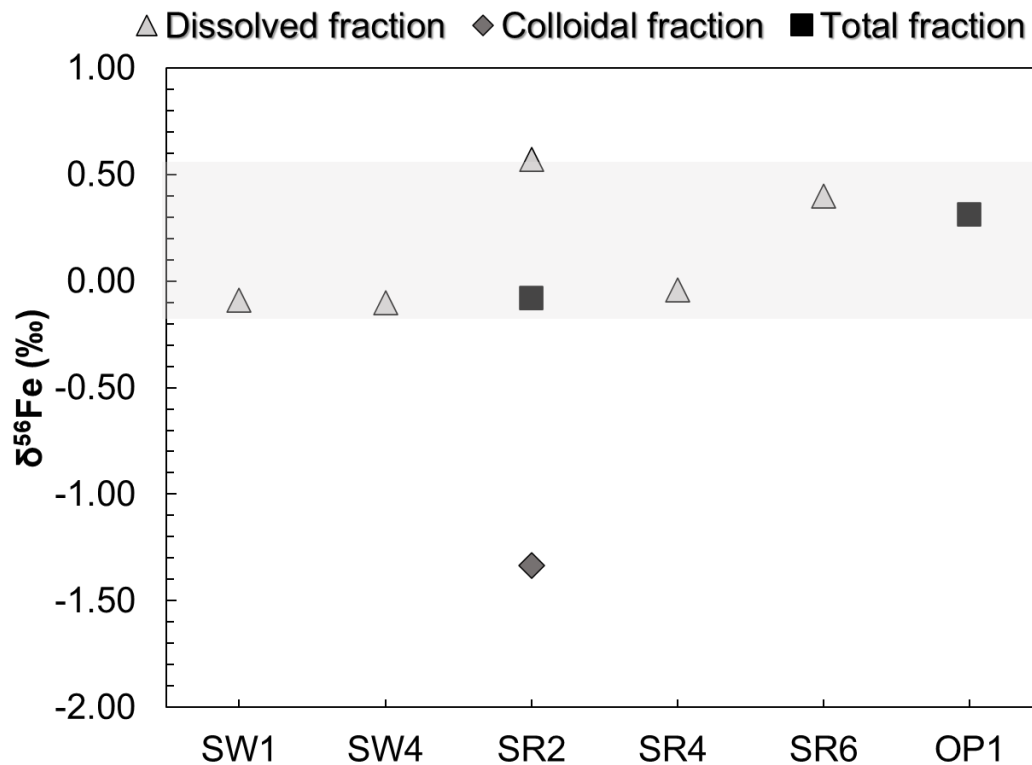


Figure 5-2. Fe isotope variation of total, dissolved and colloidal Fe of Shojin river drainage. The light gray shade shows the region for $\delta^{56}\text{Fe}$ of Fe sulphides (Sharma et al., 2001).

Despite the minimal fractionations, we see that following the precipitation, the $\delta^{56}\text{DFe}$ values display a negative shift, a phenomenon similar to that at Aina, in which the heavier Fe is up taken by the colloids, leaving the lighter Fe in the dissolved state. The dissolution that occurs at SR3 may have resulted in the slight positive shift, which is due to the release of the Fe from the colloidal fraction thereby increasing the isotopic values. Further onwards, the Fe concentration in the dissolved fraction remains stable while the $\delta^{56}\text{DFe}$ values negatively shift, possibly due to the aggregation and deposition process which removes the colloids that were earlier formed. Overall, the formation and dissolution behavior are evident from the fractionation patterns displayed.

Hereafter, the data compilation of Aina mine drainage is reported and discussed. The data is reported for three sample types: the total fraction, shown as $\delta^{56}\text{TFe}$, the dissolved fraction as $\delta^{56}\text{DFe}$, and the colloidal fraction as $\delta^{56}\text{CFe}$. Direct analyses were done on the samples that included total and dissolved to represent the total fraction ($\delta^{56}\text{TFe}$) and the dissolved fraction ($\delta^{56}\text{DFe}$), and then the colloidal fraction was calculated as their

difference ($\delta^{56}\text{TFe} - \delta^{56}\text{DFe}$). Since the concentrations were also to be considered, the following formula was used to calculate the $\delta^{56}\text{CFe}$ from the $\delta^{56}\text{TFe}$ and $\delta^{56}\text{DFe}$.

$$\frac{(\delta^{56}\text{Fe}_{total} \times \text{Fe conc.}_{total}) - (\delta^{56}\text{Fe}_{dissolved} \times \text{Fe conc.}_{dissolved})}{\text{Fe conc.}_{colloid}} \quad (5-2)$$

In the sample set for the rainy season, in the upstream (S1 to S3), the $\delta^{56}\text{TFe}$ of the Ainai samples were all near 0, and ranged from -0.49 to -0.80 ‰, thereafter more negative values are observed from S4 to S5. The $\delta^{56}\text{DFe}$ values displayed a more negative shift compared to the $\delta^{56}\text{TFe}$ within the same upstream (S1 to S3), ranging from -0.71 to -3.46 ‰. However, the Fe concentrations in the dissolved fractions at S4 and S5 were about zero, therefore, the $\delta^{56}\text{TFe}$ values were considered as the colloidal fraction values. Finally, the $\delta^{56}\text{CFe}$ values were the highest and most positive of the three fractions analyzed and ranged from 0.82 to -0.46 ‰. Contrary to the $\delta^{56}\text{TFe}$ values, that displayed minimal fractionation in the upstream, a strong negative shift was observed, particularly in the dissolved fraction, whose shift is prominent right from S2. The $\delta^{56}\text{TFe}$ values were the nearest to those of continental crust (-0.06 ± 0.02 ‰), while the dissolved and colloidal fractions display significant variations in their $\delta^{56}\text{Fe}$ values.

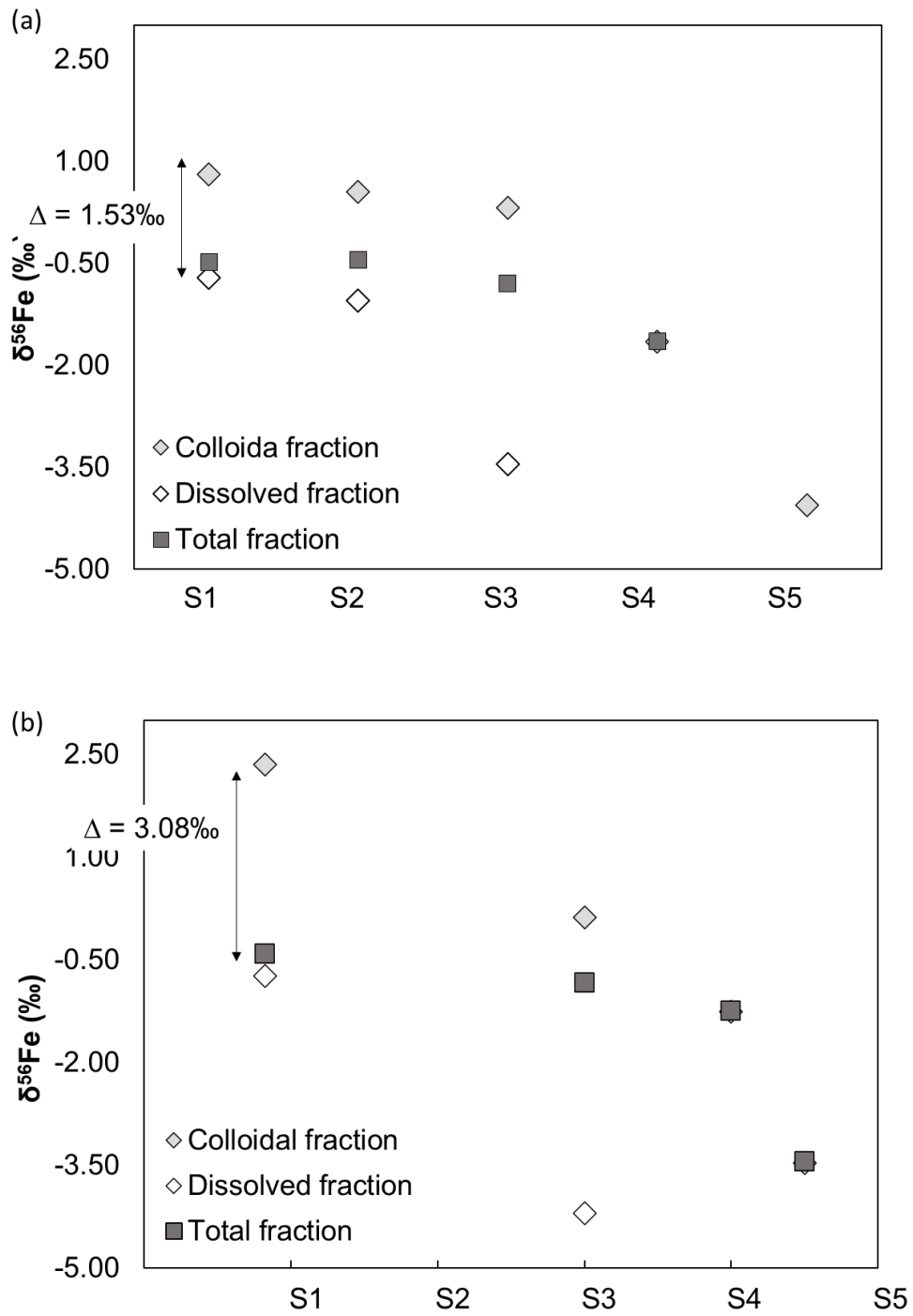


Figure 5-3. The isotopic fractionation pattern of Fe in Ainaí mine drainage in the (a) rainy and (b) dry seasons.

Seasonal variations in the data trends at Ainaí produced varying findings. The general trends of the $\delta^{56}\text{CFe}$, $\delta^{56}\text{TFe}$ and $\delta^{56}\text{DFe}$ are similar. The main difference is the increased

variation in the values between the colloidal and dissolved fractionation values. When the two datasets were compared, the samples that were collected in the dry season displayed a larger variation in the colloidal and dissolved fractions, despite the total fraction of both samplings being within a quite similar range with each other. In the dry season, the variation between the dissolved and colloidal fraction was about 3.08 ‰ while in the rainy season the variation was about 1.53 ‰ (Figure 5-3. The isotopic fractionation pattern of Fe in Ainai mine drainage in the (a) rainy and (b) dry seasons. Previous studies have reported a wide range of $\Delta^{56}\text{Fe}_{\text{Fe}(\text{OH})_3 - \text{Fe}^{2+}}$ variations from 1.5 ‰ to 2 ‰ (Kappler et al., 2010), 1.5 ‰ to 3 ‰ (Swanner et al., 2017; Wu et al., 2017; Swanner et al., 2015) depending on among, the many factors, primarily oxidation rate. These previous studies have highlighted the fractionation that results from oxidation of Fe^{2+} and may therefore be applied to understand the variations in our study. A compilation describing the $\delta^{56}\text{Fe}$ variations that exist due to Fe^{3+} precipitate formation from Fe^{2+} in previous studies is summarized in the previous studies. The compilation is made based on the Rayleigh fractionation model. According to the rate of oxidation, whether slow, intermediate or fast, the $\Delta^{56}\text{Fe}_{\text{Fe}(\text{III}) - \text{Fe}(\text{II})}$ difference also varied. In the Rayleigh fractionation model, re-equilibration of the Fe^{3+} precipitate with aqueous Fe^{2+} is assumed to not occur, i.e. the precipitates are removed from the system once the isotopic fractionation occurs. At Ainai mine drainage, a redox relationship is existent between the ferrous and ferric Fe, and this presence of Fe^{3+} and Fe^{2+} , allows comparison of the data with the Rayleigh fractionation model, as the model better predicts Fe fractionation among the Fe species.

At Ainai mine drainage, the Fe^{2+} estimated in the dry season from the source was higher than that in the rainy season, however, the total Fe displayed an inverse relationship. Given this observation and with reference to the above studies, it is safe to conclude that oxidative precipitation of the colloids plays a role in determining the $\delta^{56}\text{Fe}$ variation in the data obtained from Fe^{2+} and Fe^{3+} , which in our study are represented as the dissolved and colloidal fractions. In particular, the oxidation behavior in the different seasons is highlighted. At Ainai, oxidation rate is higher in the dry season which is reflected by the $\Delta^{56}\text{Fe}_{\text{Fe}(\text{OH})_3 - \text{Fe}^{2+}}$ of about 3.08 ‰, while comparatively slower oxidation occurs in the rainy season, leaving a signature difference in the ferric and ferrous Fe of 1.53 ‰. Furthermore, though more complex and highly dependent on the Fe mineralogy, the precipitation rate may also impact these differences as reported by Johnson et al. (2020). This may be seen in a smaller kinetic isotopic effect in the rapid Fe oxidizing experiments, unlike the larger kinetic effect in the slower oxidation. Although slightly different from the observation in our data set, we see that isotopic re-equilibrium in these systems strive to attain an equilibrium of -3 ‰, a process that is common when ferrihydrite is the main precipitate (Wu et al., 2011) .

On the other hand, a variation of 1.5 to 1.8 ‰ fractionations was reported to result from oxidative precipitation of the colloids (Oleinikova et al., 2019). This has been explained to result from the preferential selection of heavier Fe during colloid formation in order to

form stronger bonds with the hydroxyl groups. The presence or absence of organic matter may also play a role in these behaviors in that organic matter containing complexes also preferentially select the heavier Fe unlike the lighter Fe, thereby leaving the dissolved fraction with the depleted Fe resulting in lighter isotopic values. At Ainai, a difference of 1.53 ‰ was observed between the dissolved and colloidal fraction, which corresponds to the oxidative precipitation that occurred in formation of the ferrihydrite colloids. Following their formation, the variation in the fractions persist, but are relatively consistent towards the downstream. This continued negative shift implies that the processes that are occurring in the drainage are one way or reaching an equilibrium. This trend corresponds very well with the finding that the colloid formation at Ainai mine drainage was irreversible, meaning the Fe in the drainage, once oxidized and forms the colloids, remains as the colloidal form and does not dissolve or reverse to the dissolved phase. Consequently, the Fe in the drainage is therefore in the colloidal phase, allowing us to understand the major phase of Fe in the drainage. Towards the downstream, a kinetic effect is observed which results in a further negative shift in the isotopic values towards the downstream, that is indicative of the settling of the colloids especially from S3 further downwards.

The trends displayed by dissolved and colloidal fractions were further investigated with respect to the Rayleigh fractionation model (Figure 5-4. Fractionation pattern of Ainai Fe with respect to Rayleigh fractionation model) Parameters used to control the model were mainly the initial $\delta^{56}\text{Fe}$ value and the fractionation factor, Δ . Beard et al, 2010 reported that a fractionation factor of about 2 ‰ has usually been seen in such systems and was a candidate fractionation factor. The dissolved fraction was used to fit the model and determine an ideal fractionation factor for our system because the dissolved fraction represents the direct field analysis without calculations unlike the colloidal fraction. Consequently, fractionation factors of 1.5 to 2 ‰ were considered for the system. 0.0 ‰ was an initial $\delta^{56}\text{Fe}$ value for the dissolved fraction while 2.60 ‰ was the initial value for the colloidal fraction. The Rayleigh fractionation model was calculated by the following equation:

$$\delta_{\text{parent}(X)} = (\delta_{\text{parent}(\text{ini})} + 1000) * X^{(\alpha-1)} - 1000 \quad (5-3),$$

where $\delta_{\text{parent}(\text{ini})}$ is the initial isotope ratio value ($d^{56}\text{Fe}/d^{54}\text{Fe}$), X is the fraction of remaining substrate and α is the fractionation factor.

The Fe concentration in the dissolved fraction decreased drastically towards S2 and S3, accounting for the increased error range towards the downstream, which is the opposite for the colloidal fraction which has a wider error range in the upstream. When the model with a fractionation factor of 2 was fit to the $\delta^{56}\text{Fe}$ values, a misfit was particularly seen

in the downstream, with the model underestimating the colloidal values. Similar misfits were also observed by Ito et al. (2017), however, in their study, the cause for the misfit was attributed to the bulk analysis approach, which did not clearly account for colloids in their system. That was addressed in this study, however, at Ainai mine drainage, the possibility of colloids being transported from the upstream exists. These colloids may be transported from the S1 and/or S2, carrying with them Fe of heavier isotopic values. When these colloids interact with the colloids at S3 and onwards, they may have resulted in the colloids having higher values than what the model would estimate. Therefore, this misfit is interpreted to source from the colloids which the model could not account for, i.e. the colloids that were transported from the upstream to around S3, S4 and S5 respectively. Qualitatively, in addition to determining the phase of the Fe in the drainage, the transportation of the colloids from the upstream can also be unfolded from the Fe isotopes.

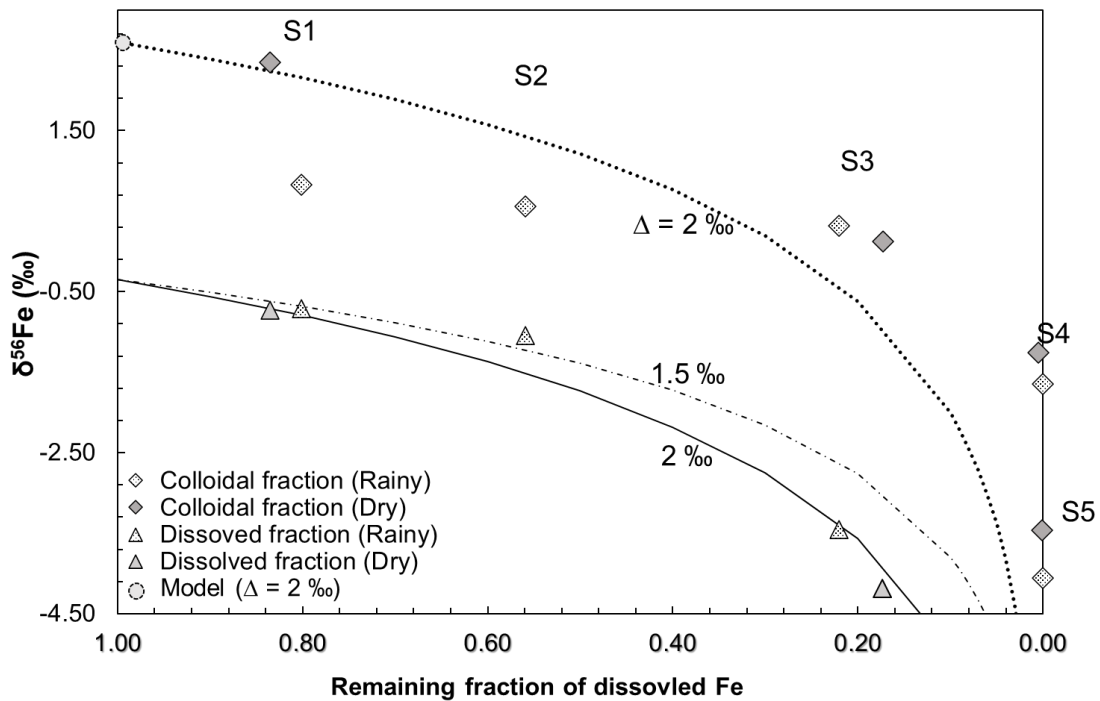


Figure 5-4. Fractionation pattern of Ainai Fe with respect to Rayleigh fractionation model at various fractionation factors ($\Delta=1.5$ and 2‰).

5.4.2 Flux of Fe inferred from Fe isotopes and colloid behavior

Fe isotopes have been studied further and widely to understand the global Fe budget. Rivers have been reported to supply way over 1.8×10^{16} g/year of Fe to oceans and a major part of this is contributed through runoff and suspended particulate matter (e.g.

Escoube et al., 2015; Milliman and Syvitski, 1992; Pokrovsky et al., 2010). Flux from river systems has been investigated in various regions and the Fe particulate matter have shown variations with regions. These variations may be in seasonal, bio-uptake, coagulation and deposition rates among others, which therefore cause significant variations in the flux, making a it difficult to generalize Fe flux supplied to oceans (dos Santos Pinheiro et al., 2013). Nonetheless, estimations have been made, which are shedding more light on the amount of Fe that is supplied from rivers and other sources as summarized in Figure 5-5. Fe isotopic values of various Fe sources including rivers. Since isotopic values vary with source, tracing Fe behaviour can be done using isotopic signatures from different sources. In Ainai's case, datasets that are well representative of a drainage system that has circumneutral pH.

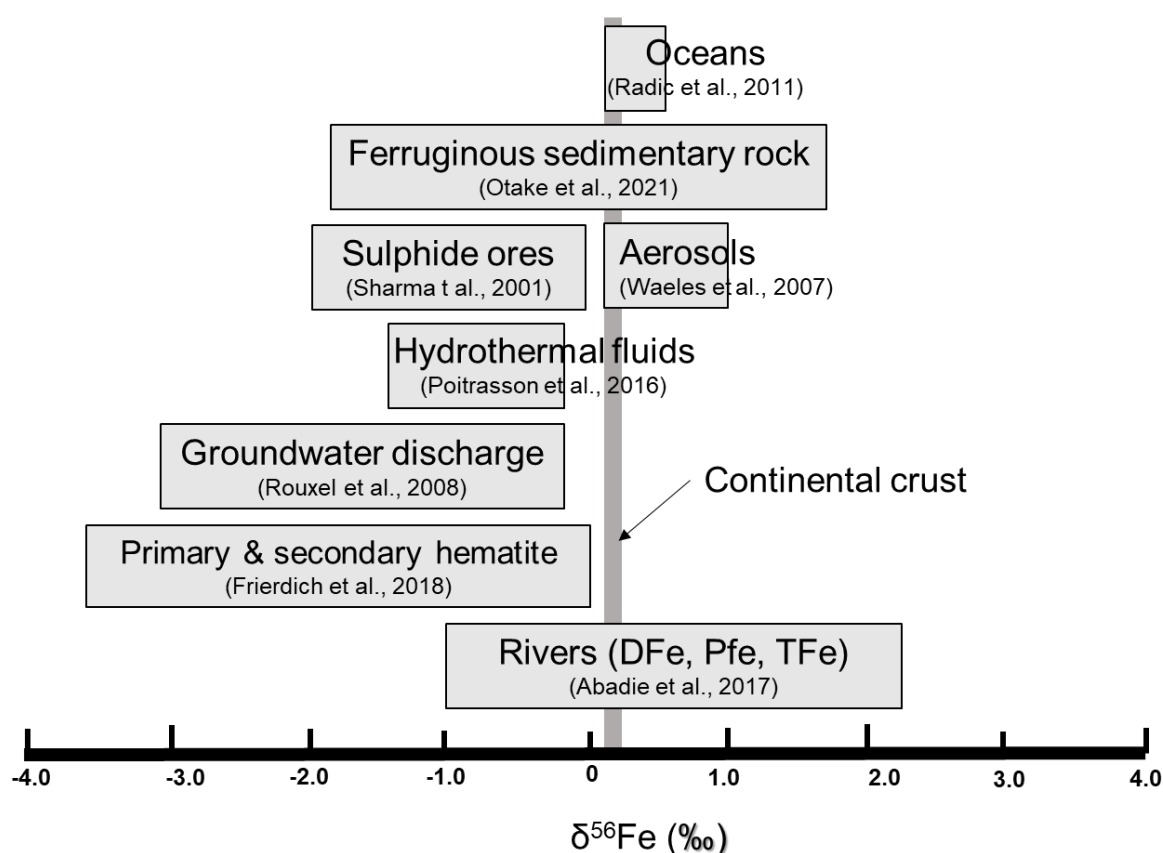


Figure 5-5. Fe isotopic values of various Fe sources including rivers.

Most of the values are below continental crust values in all fractions reported in these datasets with an inclination towards negative values. However, in cases where weathering persists, seasonal variations are highly pronounced, and anthropogenic effects were prominent, variations were observed in the isotopic values (Song et al., 2011). In addition, emphasis has been put on the size of the particles that are analyzed, to allow for

comprehensive understanding. Not only did these studies compile the Fe isotopic data, but many others have shown the variations that occur in different river systems (e.g. Escoubé et al., 2015; Ingri et al., 2006; Frierdich et al., 2014). Most of these studies investigated river particulate matter defining particles under 0.2 μm as dissolved fractions, and those over as particulate matters. However, the possibility of Fe being transported from drainages to river systems, and river systems to oceans, in the form of small sized i.e. between 200 kDa to 0.2 μm is high, because these particles are usually resistant to settling by gravity unless aggregated. In this section, the contribution of mine drainages to river Fe is explained with reference to the isotopic values obtained from the Ainaí mine drainage samples.

To begin with, the $\delta^{56}\text{TFe}$ data from Ainaí mine drainage, which included particles from the <200 kDa range to 0.2 μm , displayed minimal fractionation from the near continental value, which may have slightly been altered since the Fe in the water is a product of dissolution from Fe-sulphide minerals that were mined from the drainage. For instance, pyrite has been recorded to have isotopic ratios between -3.5 ‰ and +1.2 ‰ (Herbert and Schippers, 2008), leaving the values of the $\delta^{56}\text{TFe}_{\text{Ainaí}}$ within the reasonable window. But as explained earlier, within the total fraction, fractionation of the particles of different cut-offs are prominent. This has been explained to result from the oxidative precipitation of the colloids from ferrous Fe. However, important to note, is the presence of the colloids in the drainage, which are potential transport media for Fe from the drainages to rivers and oceans. The fractionation values observed in the drainage may be applied as tracers from Fe in the ocean systems. A major drawback in tracing Fe in these fractions is the possible loss of the Fe to flocculation, in which Fe may be lost and result in inconsistencies in the Fe estimated transported to the ocean systems. This is partly addressed by quantitative estimates of the rate of aggregation, to account for losses that may occur.

An analysis of the $\delta^{56}\text{Fe}$ of dFe and CFe provides insight on Fe flux from the mine drainage to river systems. An estimate of the number of colloids transported at a smaller scale are estimated from extrapolating the $\delta^{56}\text{Fe}$ values under the model from just before S3 (Figure 5-6a). The point from which the calculation is done is assumed to be a point at which new colloids form after S2. The misfit between the dataset and the Rayleigh fractionation model; $\Delta\delta^{56}\text{Fe}_{\text{measured}} - \Delta\delta^{56}\text{Fe}_{\text{Rayleigh fractionation}}$ represents the number of colloids unaccounted for by the model. This misfit was calculated with respect to the area under selection between S2 and S3 and S3 and S4 and S4 and S5. The regions were subdivided into small trapezoids to calculate the areas of interest. The areas of interest were calculated using the integration by trapezoidal rule which follows the below basic formula:

$$\text{Area of trapezoid} = ((a+b)/2) * h \quad (5-4),$$

Where a is the length, b is the height and h is the height of the trapezoid. All areas were taken from a bottom of zero, for simplicity. A summary of the calculations from one sampling point to the next are explained. Colloids transported to S3 are translated from the misfit between the modelled and measured data at S3. The difference in this data is minimal and hence the area under the region under which colloids are transported is small (Appendix), and calculated as; Area of the model = Σ all sub-trapezoids = +0.181 %.

Following a similar approach, the colloids transported to S4 are also calculated. The misfit of S4 modelled and measured data is larger than the data at S3, hence the area under the region that represents the number of colloids transported towards S4 is relatively larger than those of S3. This is analytically expressed through the increase in the area integrated to calculate the misfit in the two datasets, thereby presenting a larger misfit (Figure 5-6b). This was calculated as: Area of the model = Σ all sub-trapezoids = +1.294 %.

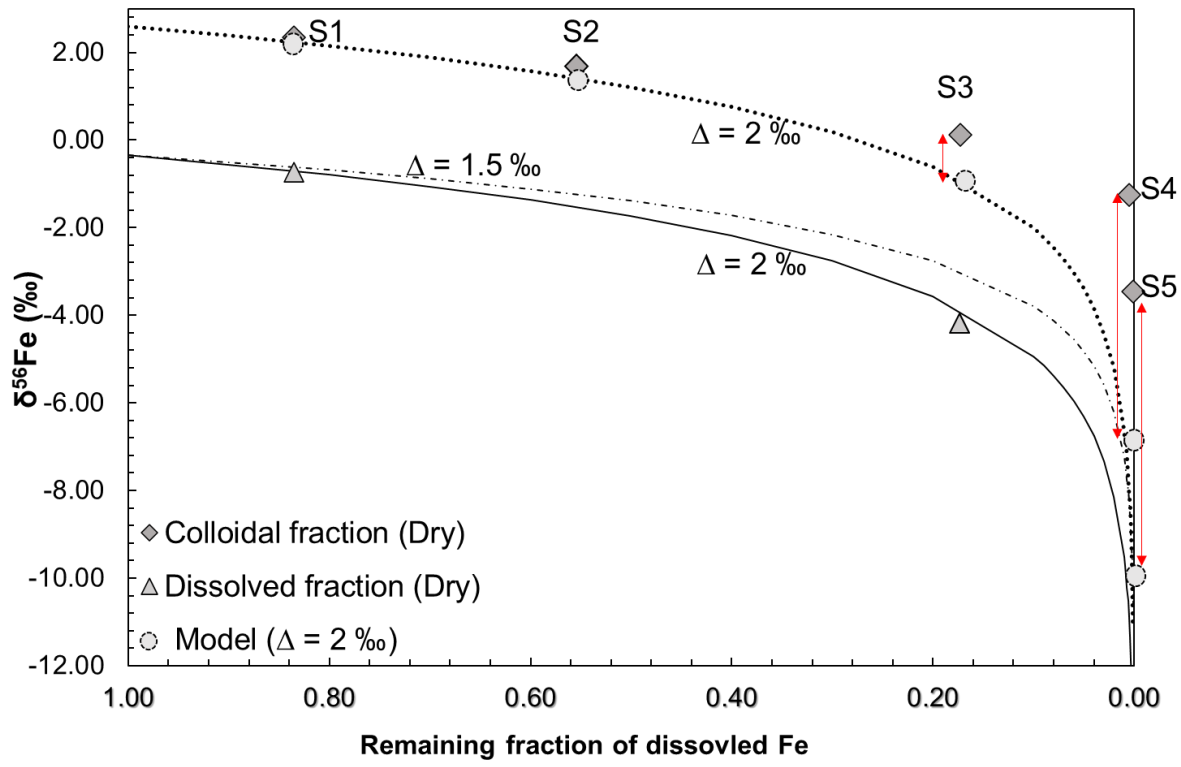
Finally, the colloids transported to S5, were also calculated from the misfit, which is seen to be larger than that portrayed at S3 and S4. The misfit was calculated as: Area of the model = Σ all sub-trapezoids = +1.598 %.

In all cases, the positive isotopic values of the colloids elevate the isotopic values of actual measured data. This elevation of data is not reflected in the modelled dataset, but represent the

Furthermore, the colloids transported are quantified by percentage using a combination of Fe isotopes and water chemistry, to show the number of colloids that are transported from upstream to a particular sampling site. The number of colloids transported to S3, S4 and S5 respectively are 30.80%, 76.65% and 90.37%. These colloids are responsible for the isotopic variations that are observed.

30.80 % of the colloids formed in Oct translates to 2.69 ppm of the colloidal fraction, 76.65% and 90.37% represent 6.63 ppm and 2.58 ppm showing that these colloids were the ones responsible for raising the isotopic fractionations at S3, S4 and S5 respectively. The simplified estimation highlights on the number of colloids transported the distance of about 100 to 300 m, confirming that indeed following their formation, some of the colloids undergo transportation from one point to the next.

This nature of estimation is one that can be applied in systems in which similar trends are observed. For instance, in a river system, fluctuations in isotopic values are an initial indicator of the presence of colloids, and if their formation was not in the river, but the river is receiving water from nearby sources, the sources may easily be traced by closely observing the trend displayed by the $\delta^{56}\text{Fe}$ values. Given that the Rayleigh fractionation model applies for the system, the quantitative estimation approach may easily be applied too in the case that misfits are present.



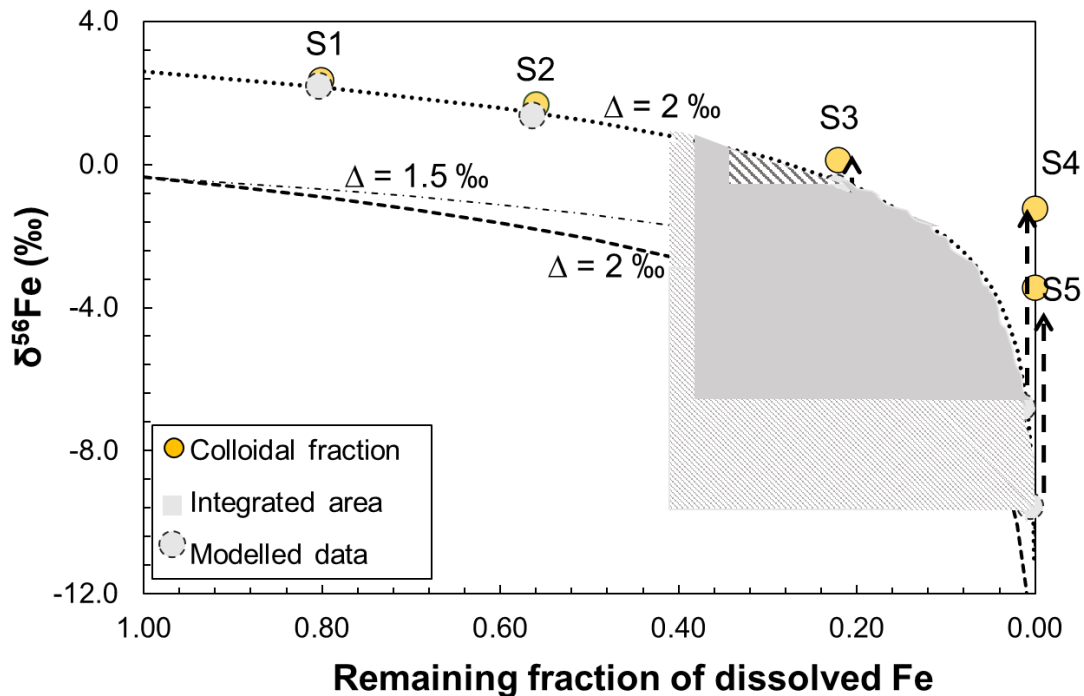


Figure 5-6. (top) A relationship of the measured vs modelled data of the Aina mine drainage. The arrows represent the misfits between the modelled and actual data. (bottom) The $\delta^{56}\text{Fe}$ plot displaying the area whose integration gives the $\delta^{56}\text{Fe}$ that is attained as a result of colloids transported from upstream to the particular site.

5.5 Summary

The Fe isotopic fractionations are increasing gaining fame with regards to understanding Fe behavior in various fields. In aquatic systems, the fractionation of the stable isotope has been used to unfold circulation of Fe from its various sources, or within oceans, and goes as far as assisting in addressing climate change problems that relate to global Fe and C cycle. In this study, a novel approach of highlighting Fe behavior in mine drainages is reported. Mine drainages are one of the highest suppliers of Fe (and other toxic elements) to rivers, which then provide the largest Fe supply to oceans. Fe highly determines the fate of other toxic elements and therefore understanding the circulation of Fe also highlights the behavior of toxic elements form mine drainages.

The observations from the two study sites highlight the following points.

(i) The oxidation process is a significant control on the Fe isotopic values. At Ainai, the oxidative precipitation resulted in a significant difference in the isotopic values of the dissolved and colloidal fractions. At Shojin, the values remain near continental values, without variations similar to those of Ainai, due to the absence of the redox stage in the formation of the colloids.

(ii) The dominant phase of Fe in the drainages is in colloidal form, particularly at Ainai. The Fe exists as colloidal Fe and is transported to the downstream of the drainage as the colloidal form. This confirms and highlights the need to always consider the Fe colloids in mine drainages, because if these colloids do not aggregate and settle, they will be transported to the rivers and hence oceans, together with the toxic elements that they sequester. Furthermore, the amount of Fe transported may be underestimated if colloids are neglected.

(iii) The amount of Fe transported in the drainage, a distance of about 75 m is approximated to be about 1.4 ppm of the colloidal fraction. In the event that aggregation does not occur, the estimated fraction may easily be transported all the way to rivers. Since the Fe has a distinct isotopic signature, the Fe supplied by rivers may be traced.

In conclusion, the Fe isotopes provide a platform for understanding the phase of Fe, the amount of Fe transported from mine drainages and gives insight on the significance of the contribution of mine drainages to Fe supply to rivers.

6 Chapter 6: Theoretical simulations of Ainai and Shojin mine drainages using geochemical modelling and thermodynamic calculations

6.1 Introduction

Geochemical modelling was carried out to simulate the environments in which the studies were carried out. The modelling carried out highlights the nature of the drainages under study, the expected behavior of the elements in the drainage, given the particular characteristics. Various studies have highlighted the significance of confirming research findings using experiments or through geochemical modelling. Complementing studies by these approaches is important especially when it comes to increasing the applicability and impact of a study. Through field observations and analysis, so much has been highlighted, however in this section, some gaps and confirmations for the studies are provided. This chapter will be subdivided into various sections to address the various aspects of interest.

6.2 Methodology

6.2.1 Thermodynamic modelling

Stability diagram for possible mineral forms expected in the Ainai mine drainage was constructed using the Geochemist's Workbench software (GWB model, Ver. 14) to evaluate their formation in the drainage at various pH values. Measured element concentrations, during field samplings were used as input parameters for modelling to account for the effects of coexisting cations and anions on solubility. The Eh values are given relative to the Standard Hydrogen Electrode (SHE) potential. Solubility diagrams were constructed using thermodynamic datasets generated from the thermodem, modified where necessary by additions from the literature, in particular, incorporating layered double hydroxides and other iron oxides (Bravo-Suárez et al., 2004), for the Ainai mine drainage system. Interlamellar anions, combinations of divalent and trivalent cations, and related species, cause wide variations in the chemical compositions of LDHs. Therefore, the solubility products of Zn-Fe LDHs were estimated using the chemical compositions and thermodynamic data of the end-member hydroxides, sulfates, and carbonates (Allada et al., 2006). Thermodynamic data for these compounds were referred from the enthalpies of formation measured by acid-solution calorimetry, and solubility products were based on solubility measurements (Bravo-Suárez et al., 2004; Hase et al., 2017).

Stability diagram was constructed for Shojin river to simulate the possible mineral formations and highlight the characteristics of the river. The diagram was plotted using the Act2 module on GWB ver 14. Plots were made for temperatures of 25°C and 1 bar. The database utilizing log K values of Sanchez were applied, as they have been reported to suit environmental samples. Input parameters for the samples were taken from those collected during field work.

6.2.2 Transport modelling

A simulation of the colloid transport was done using the Phreeqc software. Phreeqc coding provides a comprehensive approach that combines sorption of elements by oxyhydroxides (or other sorbents), with their rate kinetics as well as colloid transportation. The flexibility in the coding approach by Phreeqc, and ability to account for the processes of interest, particularly colloid transport, made this approach an ideal one to meet the chapters objectives. A further description of the model is outlined below.

PHREEQC was used as the modelling approach to clarify the sorption processes along with their transportation in the drainage. For easy following of the data, a brief description of the modelling code is broken down below. Surface complexation model on hydrous ferric oxide (HFO) was utilized for the simulation of the processes (Dzombak and Morel, 1993). The database wateq4f.dat was used to develop the model. Surface species depicting the strong and weak diffusion coefficients were defined based on the ferrihydrite data for Ferrihydrite_cdmusic, which also incorporates the intermediate diffusion coefficient, allowing for a better prediction of HFO as colloids (Appendix). Most species definition is adopted from the same database unless modification was required. Under surface species, log K values are given for reactions of the elements with HFO in the system.

Following the surface species, a definition of the colloid mobility by the diffusion coefficient is defined as DW. Solution 1 to 21 represents the mine drainage system, which has been subdivided into 21 cells. The number of moles, surface area and diffusion coefficients are defined to help simulate the behavior of the colloids in the drainage. Solution 0 represents the initial state of the solution before reaction begins to occur. Then the rate of reaction, which defines the rate of reaction depending on the properties of the site was defined. The rate was estimated based on other previous studies, since that was not calculated in our study. The distance is defined in the model through cell division, depicting the distance of the drainages. The distance aspect was fit in the model through incorporation of a one-direction advective transport model by the same Phreeqc. Finally, the contaminant properties were defined. The model simulates the sorption of As on the surface of HFO colloids. The model assumes formation of colloids as an introduction of the As in the system and their concentration variation is described with respect to the distance. The maximum size at which the colloids can exist in the drainage is also defined, thereby partially incorporating the aspect of aggregation and deposition.

6.2.3 Theoretical estimation of aggregation and deposition

An estimation of the particle size of the colloids is key to clarifying the colloid transport behaviour, since the deposition of the colloids highly depends on the aggregate size. Hence, the size of Fe bearing nanoparticles was theoretically estimated using aggregation kinetics. Mass transport coefficients for aggregation (coagulation) were derived from physical considerations of the transport mechanisms of suspended particles (Aquatic Chemistry). The theoretical framework of the aggregation process was derived in 1917 by Smoluchowski and has been expanded over the years.

A detailed explanation of the equations used for the calculation are explained in Koide, MS2018, however, below is a run through of the equations used for the aggregation calculation. Primarily, the Smoluchowski equation was used to estimate the time evolution of the nanoparticle aggregation using the below equation.

$$\frac{dn_k}{dt} = \frac{1}{2} \sum_{i=1, i+j=k}^{i=k-1} k_{ij} n_i n_j - n_k \sum_{j=1}^{\infty} k_{kj} n_j \quad (6-1)$$

The equation covers both the formation of the aggregates and their loss. However, since the Brownian diffusion was considered as the primary process governing the aggregation, the rate constant for the brown diffusion was calculated using the below equation.

$$k_{ij} = \frac{2 k_B T (d_i + d_j)^2}{3 \eta d_i d_j} \quad (6-2)$$

where η is viscosity and $k_B T$ is the thermal energy. However, when considering the rate constant of brown diffusion for uniform particles, $d_i = d_j$, therefore the equation becomes

$$k_{ij} = \frac{8 k_B T}{3 \eta} \quad (6-3)$$

The average aging variation in concentration of particles is given by

$$\frac{dN(t)}{dt} = -\frac{1}{2} k_{11} N(t)^2 \quad (6-4)$$

Detailed assumptions made to support the calculation are that, (i) disaggregation does not occur following colloid formation, (ii) aggregation occurred in four main patterns, (iii) the initial particles size was set (based on field observations), and (4) all the particles became homogenous after aggregation. Finally, using the stokes equation, the particle size at which the colloids are deposited to the drainage bed following aggregation was calculated.

$$v = \left[\frac{g(\rho - \rho_0)}{18\eta} \right] \times d^2 \quad (6-5)$$

where g is gravity, ρ is the density of solid (the density of ferrihydrite is $3.77 \times 10^6 \text{ g/m}^3$ (Mineralogy Database)), ρ_0 is the density of liquid (the density of water is $9.997 \times 10^6 \text{ g/m}^3$), η is viscosity (the viscosity of water is $0.890 \text{ g/(m} \cdot \text{s)}$), and d is the particle size which can precipitate. The resulting estimates were about $32 \text{ } \mu\text{m}$ at P1.

6.3 Results

6.3.1 Geochemical simulations of Ainai mine drainage and Shojin river

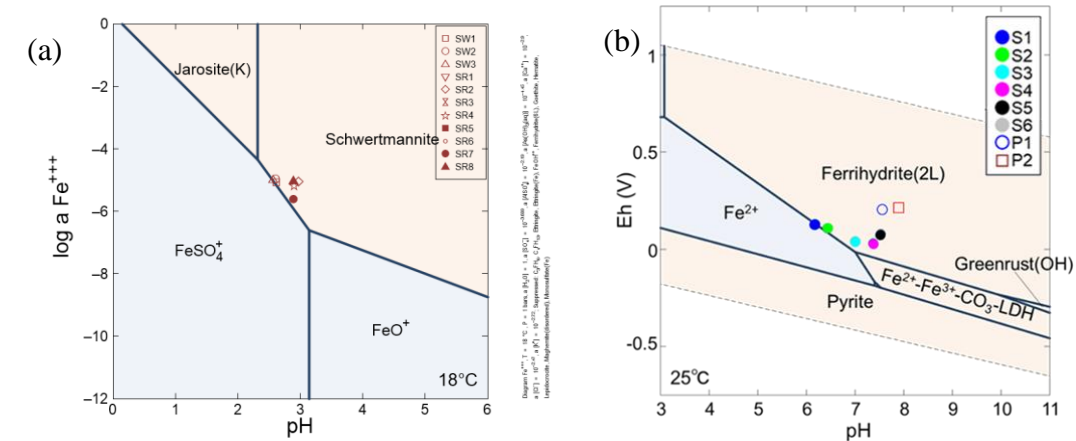


Figure 6-1. (a) Solubility diagram of Shojin river and (b) Stability diagram of Fe species in Ainai mine drainage.

The geochemical properties of the mine drainages that were investigated are summarized in Figure 6-1 a and b. From the diagram, given the concentration of Fe and

pH, Shojin samples plot within the boundary of schwertmannite and FeSO_4^+ . On the other hand, at the near neutral pH, ferrihydrite dominates the system, along with Fe^{2+} - Fe^{3+} - CO_3 -LDH. In the diagram, S3 and S4 plots near the equivalence state between ferrihydrite and Fe^{2+} - Fe^{3+} - CO_3^{2-} -LDH.

6.3.2 Simulation of colloid transportation by Phreeqc

The results from the model are plotted in Figure 6-2. Colloids transported from the upstream as a function of distance. Figure 6-3. In Figure 6-2, the Fe and As concentrations measured in the field increase drastically from the upstream, then decrease rapidly from mid to downstream. The colloids then reach significantly low concentrations, towards the downstream. The modelled data displays a similar trend from upstream to downstream.

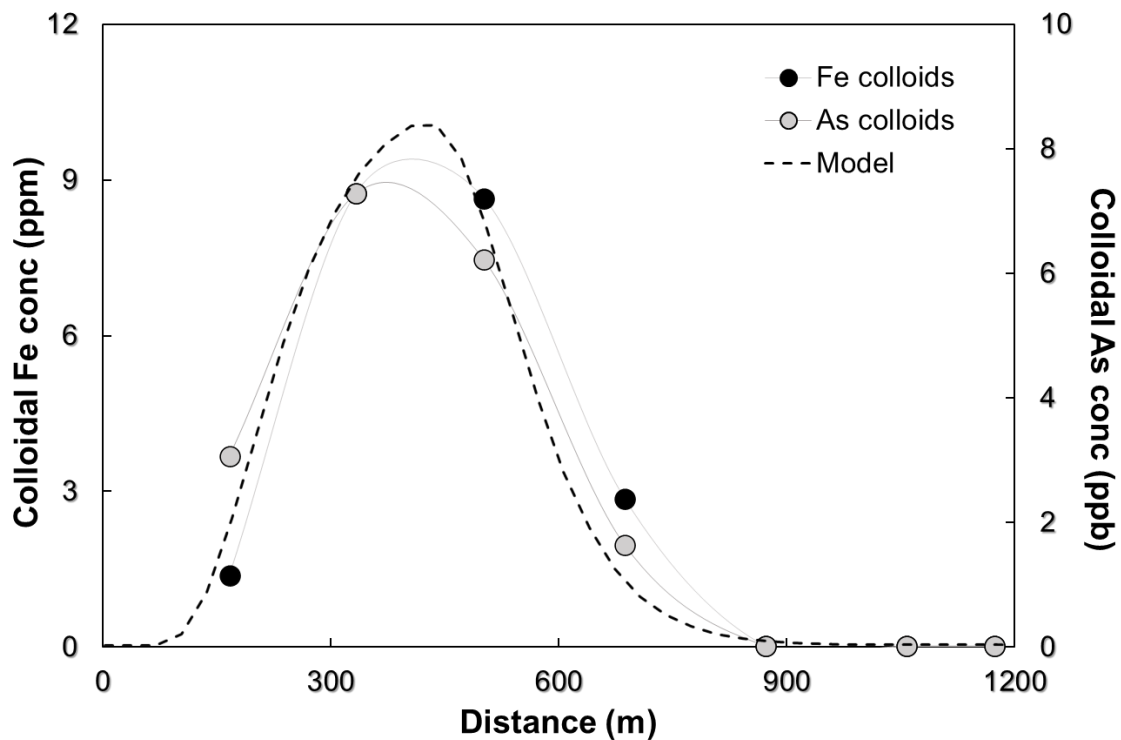


Figure 6-2. Colloids transported from the upstream as a function of distance.

In Figure 6-3, the transport behavior is compared for both Ainai and Shojin. The trend of the colloids at Ainai fits very well with that of the model, unlike the one for Shojin. At Shojin, no colloids are reported for the model in the upstream, while field data reports the presence of the colloids. Furthermore, the colloids are quickly removed from the modelled case but remain in the system all the way to the downstream. In the field data, colloids gradually decrease towards the downstream of the river.

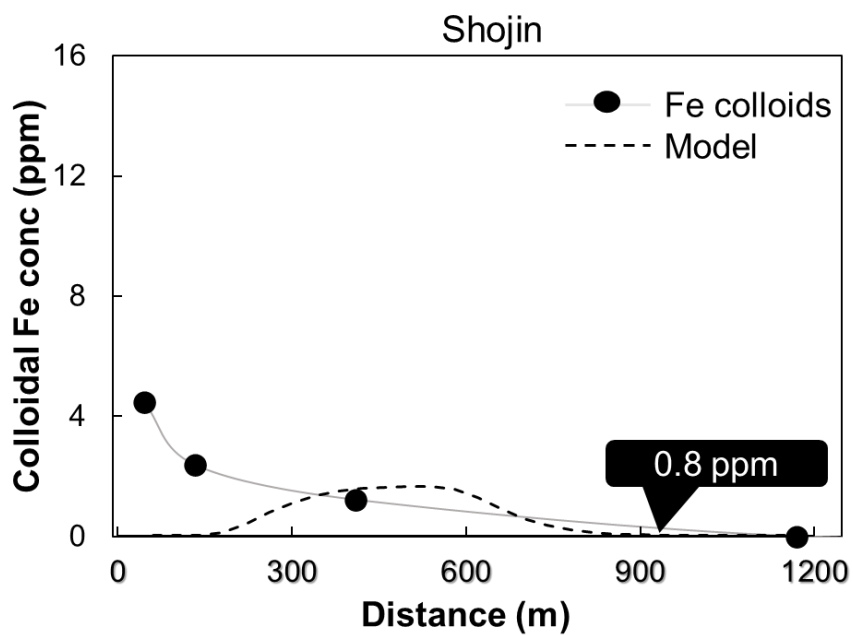
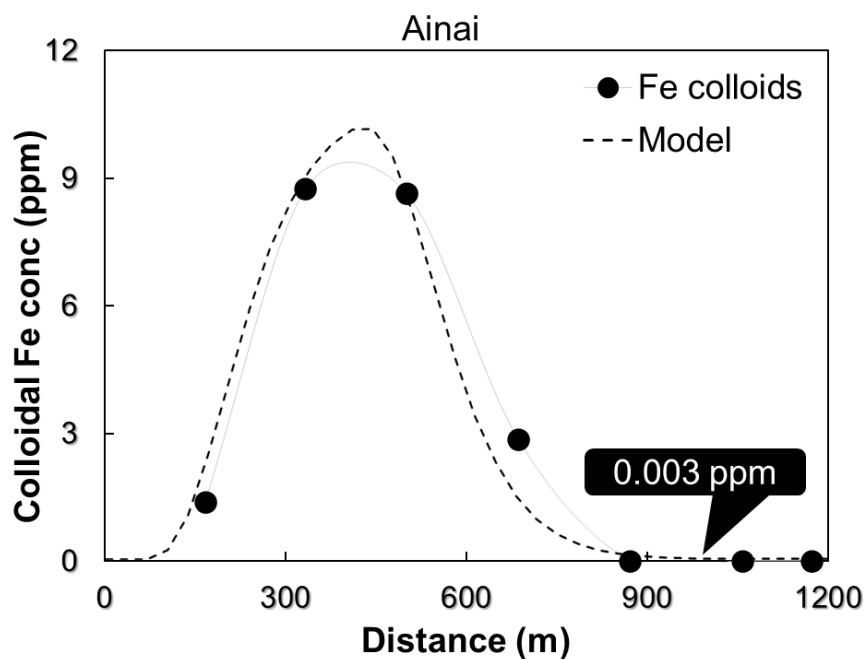


Figure 6-3. Comparison of field and modelling data of colloid formation and transportation of Fe colloids at Ainai mine drainage and Shojin river.

6.3.3 Theoretical estimations of aggregation and deposition kinetics

The results of the calculation are summarized in Figure 6-4. A variation in the aggregation rates at Ainai mine drainage and Shojin river. The calculation was done for both Ainai and Shojin river drainage, in each case defining parameters to suit the geochemical properties of the site. The aggregation rate of the colloids at Ainai mine drainage is a relatively steadily increasing trend, compared to that of Shojin. At Ainai, an initial particle size of 3 nm was defined while 55 nm was used for the initial size of the schwertmannite colloids as reported by Zhang et al., 2018. As a result of the different parameters such as pH and aggregation rate, the particle sizes, which represent the aggregation rates, vary at the two sampling sites. At Ainai, the aggregation is rapid in the upstream, then reaches a steady point at about 350 nm to unlike at Shojin where the aggregation is slow in the upstream then quickly increases towards the downstream without reaching a steady point as the case in at Ainai. Figure 6-4 summarizes the relationship between the aggregation rates and Fe concentrations at each sampling site, highlighting the correlation that exist between the aggregation displayed by the Fe concentrations with those from the theoretically calculated aggregation rates.

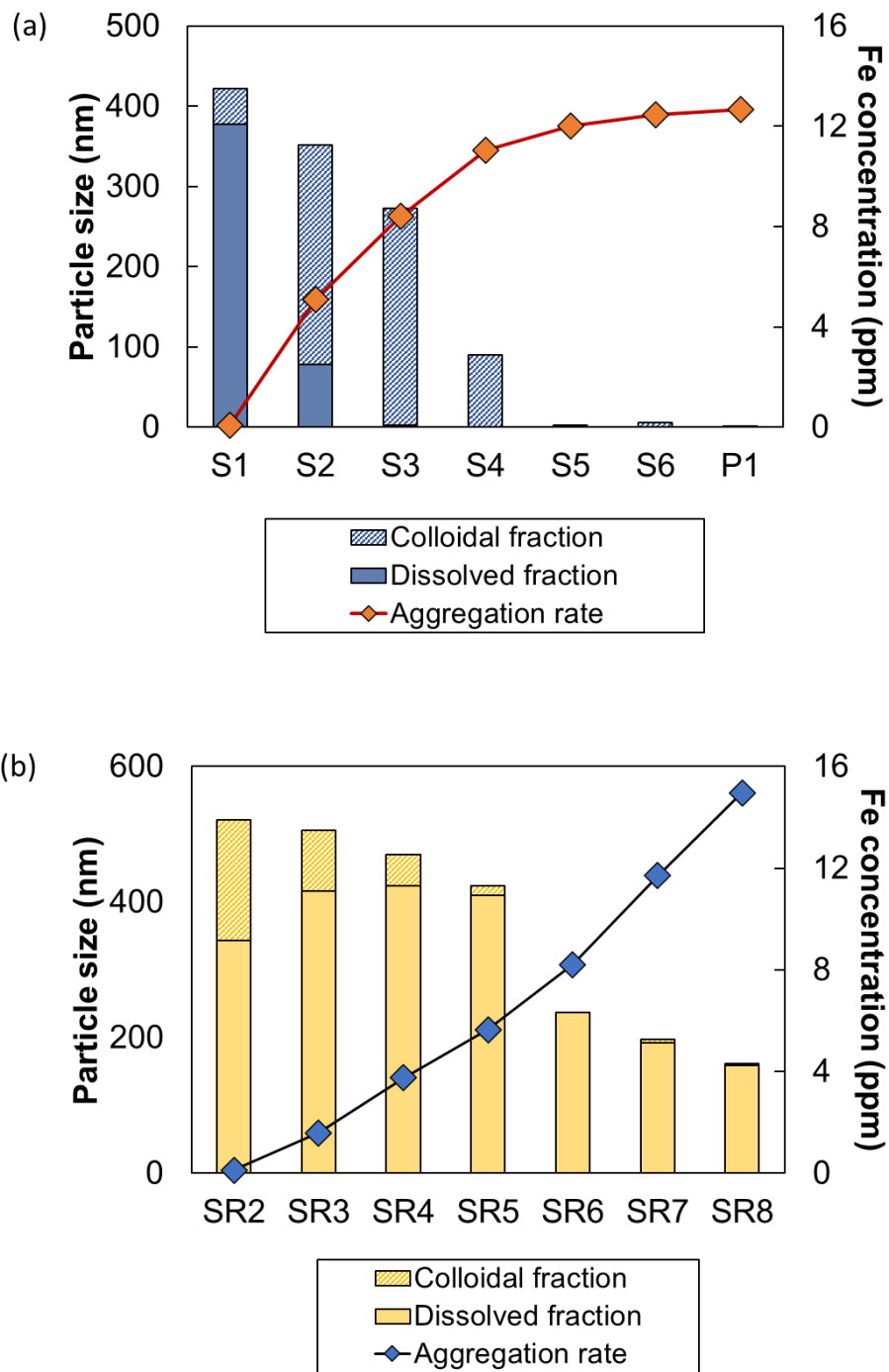


Figure 6-4. A variation in the aggregation rates at Ainai mine drainage and Shojin river.

Table 6-1. Parameters used to calculate aggregation rate at Ainai and Shojin.

	Initial Diameter (nm)	Calculated diameter	V0(m3)	Fh concentration (mg/L)	Fh density(g/m3)	Mass of 1 particle	N(Quantity/m3)	Time (s)	βp
S1	0.000000003	3.00	1.413E-26	4.86	3770000	5.32701E-20	9.12526E+19	0	6.06037E-18
S2	1.59744E-07	159.74	2.1333E-21	4.86	3770000	8.04255E-15	6.04415E+14	273	6.06037E-18
S3	2.62517E-07	262.52	9.4678E-21	7.52	3770000	3.56936E-14	2.10716E+14	273	1.24081E-17
S4	3.45662E-07	345.66	2.16139E-20	11.08	3770000	8.14843E-14	1.36001E+14	430.2	6.06037E-18
S5	3.75685E-07	375.69	2.77492E-20	11.08	3770000	1.04614E-13	1.05931E+14	344.4	6.06037E-18
S6	3.89048E-07	389.05	3.08168E-20	11.08	3770000	1.16179E-13	9.53864E+13	172.2	6.06037E-18
P1	3.95594E-07	395.59	3.23988E-20	11.08	3770000	1.22143E-13	9.0729E+13	88.8	6.06037E-18
	Initial Diameter (nm)	Calculated diameter	V0(m3)	Sch concentration (mg/L)	Sch density(g/m3)	Mass of 1 particle	N(Quantity/m3)	Time (s)	βp
SR2	0.000000008	60	1.1304E-22	8.94	3620000	4.09205E-16	2.1843E+16	0	6.06037E-18
SR3	0.000000006	60	1.1304E-22	8.94	3620000	4.09205E-16	2.1843E+16	0	6.06037E-18
SR4	1.41256E-07	135.78	1.47501E-21	8.94	3620000	5.33954E-15	1.67398E+15	91.0	6.06037E-18
SR5	1.26784E-07	194.53	1.06653E-21	1.91	3620000	3.86084E-15	4.95742E+14	234.2	6.06037E-18
SR6	1.84193E-07	252.21	3.27039E-21	1.91	3620000	1.18388E-14	1.6167E+14	687.7	6.06037E-18
SR7	2.62708E-07	359.73	9.48847E-21	1.91	3620000	3.43483E-14	5.57227E+13	1940.5	6.06037E-18
SR8	3.35641E-07	459.59	1.97881E-20	1.91	3620000	7.16328E-14	2.67193E+13	3214.3	6.06037E-18

6.4 Discussion

6.4.1 Fe systematics of Ainai mine drainage with Shojin river system with respect to their geochemical characteristics

The stability diagrams made for each drainage best describe the nature of the drainage and provide insight into the processes occurring in the drainages. The nature of Shojin is seen to be dominated by ferric Fe unlike the Shojin river system. At low to high activities as well as all pH ranges, the existing species in the drainage are in the ferric state of Fe and this correlates with the findings reported in the Chapter 3. Shojin samples also along the equilibrium boundary, somewhat falling in between the dissolved Fe state and the schwertmannite region. Their presence on the boundary is controlled by the pH, which is too low to allow precipitation of schwertmannite, however, the samples SR2 onwards, plot inside the schwertmannite region. This correlates very well with the field observations and analysis findings.

In Figure 6-1b, Ainai systematics are summarized. Unlike the acidic Shojin river drainage, Ainai mine drainage is relatively neutral and the Eh vs pH diagram well summarizes this. The major minerals i.e. ferrihydrite, Fe LDH and minor green rust, that dominate such nature of drainages are shown. Ainai samples plot along the equilibrium boundary of ferrous Fe and ferrihydrite, but as we progress towards the downstream, the samples fall further into ferrihydrite region. This also correlates and summarizes very well, the trend observed through analyses and observations. A major finding from the modelling of Ainai, was the clarity obtained with regards to the confirmation of the formation of Zn-Fe LDH in the drainage, to remediate Zn from the drainage.

The formation and stability of a $\text{Fe}^{2+}\text{-Fe}^{3+}\text{-CO}_3^{2-}$ LDH were considered at various pH values by thermodynamic modeling using the GWB software. In order to efficiently elucidate the Zn remediation approach, measured elemental concentrations in water samples at site S2 were used as input parameters for modeling to account for the effect of coexisting cations and anions on colloid solubility and separation. Bravo-Suarez (Bravo-Suárez, Páez-Mozo and Oyama, 2004) estimated solubility products of LDHs with different anions, based on their chemical compositions and thermodynamic data for their end-products. These data were used to model the formation of LDHs in the mine drainage. A gradual decrease in Fe^{2+} concentration occurs from the upper to lower drain, particularly at S3. In the Eh-pH stability diagram, S3 and S4 plot near the equivalence state between ferrihydrite and the $\text{Fe}^{2+}\text{-Fe}^{3+}\text{-CO}_3^{2-}$ LDH, implying that the LDH might have formed near S3 where pH and Eh are inferred to be controlled by coexisting ferrihydrite and $\text{Fe}^{2+}\text{-Fe}^{3+}\text{-CO}_3^{2-}$ LDH. Although the possibility of Green rust (OH) formation is observed, the pH in this drainage does not reach 11, hence its formation is

eliminated. The model is consistent with the inference that the low amounts of Zn-bearing minerals in natural drainage samples reflect that LDH formation is highly pH- and redox-dependent. A combination of the experiments, with geochemical modelling, indicate the formation of particles similar to a $\text{Fe}^{2+}\text{-Fe}^{3+}\text{-CO}_3^{2-}$ LDH that incorporate a considerable amount of Fe^{2+} from the source, which later incorporate Zn to form Zn-Fe LDH.

In summary, from the geochemical descriptions understood through the modelled plots, the major mineralogy expected, that is responsible for remediation can easily be understood. In this case, Ainaí due to its neutral state is dominated by ferrihydrite, because of the stability that the mineral has at neutral pH. Consequently, it is the remediation path taken for the drainage, allowing the ferrihydrite colloids to sorb As, while on the other hand, the presence of Zn initiates the formation of Zn-Fe LDH as the remediation approach. On the contrary, Shojin is dominated by ferric Fe, and at the low pH, schwertmannite colloids form and are the main remediation approach for the As in the drainage. More importantly, through the modelling approaches, it can be determined if the pH adjustments are enough or need further work to ensure efficient treatment in the mine drainages.

6.4.2 Transportation of the colloids as a function of pH

Colloids have also been reported to easily be transported through drainage systems, thereby affecting the efficiency of treatment approaches applied for drainage systems. Colloid transport is an important concept when looking at the behavior of colloids. This is because colloids are resistant to settling by gravity and can easily be transported in the drainage towards rivers and even oceans (Bunn et al., 2002). Seeing as the colloids play a significant role in scavenging other toxic elements, they can act as transport media for the toxic elements to other aquatic systems and may release these toxic elements in the other drainages (Corapcioglu and Jiang, 1993), thereby raising the need to explore the transportation behavior in detail. The transportation behavior of the colloids is reported from the geochemical modelling done by Phreeqc.

At the two river systems, correlation between Fe and As is evident, hence, understanding the behavior of Fe would highlight the fate of As and other associated toxic elements in the drainage. Colloid transport has been reported to vary with, among other geochemical characteristics, pH, ionic strength, bulk chemistry of the water and flowrate. The two sites under study vary in most of these characteristics, thereby (quantitatively) understanding their colloid transport behavior would highlight the significant factors that control colloid transport in mine drainages of varying characteristics. Seeing as the colloid transportation may vary widely, a geochemical simulation was also carried to assist in the correlation of field studies with the model, further increasing the understanding and applicability of the colloid transport model.

Remediation processes at the two drainage systems differ and the main controlling factors are the geochemical characteristics. In either case, remediation occurs in the drainages, allowing sorption of As from the drainage. Previous studies have shown that Fe minerals, being the strongly sorbing elements that they are, have various methodologies with which they sorb toxic elements from contaminated water (Crawford et al., 1993). Geochemical trends, modelling and experimental studies have been used to clarify which method dominates the sorbing process. Under consideration may be co-precipitation of the Fe mineral with the contaminant, adsorption of contaminant by the Fe mineral and several other processes. All these processes occur when the two, i.e. contaminant and the Fe mineral come into contact in a system. In this section, the sorbing processes, which are generalized as surface complexation for simplicity are considered along with their mobility. The significance of this approach is that it highlights the rate at which sorption occurs, and the estimated transported distance of the contaminants in the mine drainages. Understanding the modelling approach would assist in understanding colloid transportation behavior thereby ensuring that colloids are not transported further to other systems, and hence carrying with them contaminants.

A comparison of the model with the behaviors of Ainaï mine drainage Fe and As colloids is plotted in Figure 6-2. The detailed datafile for the model is also provided in the appendix. As seen in the diagram, there is a good correlation between the general trends of the colloids in the drainage and those of the model. At the neutral pH, the As colloids are introduced a few meters away from the drainage, drastically increase in the drainage, and finally decrease towards the downstream of the drainage. After estimating the transportation behavior of the colloids at Ainaï with the modelled case, a comparison of the behavior of the colloids in the two systems, i.e. Ainaï and Shojin river was done. The main goal was to differentiate, using the model, how their varying geochemical characteristics, formation pathways and settling rates, among others, would influence their transportation behaviors. In the comparison modelled result (Figure 6-3), the case of Ainaï is well depicted, accurately simulating the formation of the colloids, and when they reach a peak, then finally begin to decrease due to aggregation and removal by sedimentation or depositing to the system bed. On the other hand, Shojin system is predicted to have minimal colloid formation compared to those at Ainaï. None the less, the formed colloids seem to remain in the drainage unlike those at Ainaï.

Colloid transportation is investigated from field measurements and the modelling aspect. A comparison of the model with transport behavior at Ainaï mine drainage displayed a good correlation. One significant aspect that is occurring in the mine drainages is learnt from the model is displayed in Figure 6-3. Since the pH at Shojin varies significantly, an appropriate estimation of the model was difficult to attain, therefore, a comparison of field data and the model is reported only for Ainaï mine drainage. Fe colloid formation rate with respect to distance was simulated to estimate how much colloids form in the drainage, and what distance they may be transported. A major determining factor for the variation in the colloid formation and transportation is attributed to the reaction rate controlled by the pH. It is seen in the comparison model that colloid formation at Ainaï proceeds more vigorously than that at Shojin, attributing to the pH. As earlier observed

in the previous chapters, oxidative precipitation occurs at the neutral pH at Ainai, while hydrolysis is responsible for the As colloid formation at Shojin. Consequently, the number of colloids formed in the two drainages differ significantly. At Ainai, almost all the Fe introduced in the system forms the colloidal fraction, while only a small portion proceeds to form colloids at Shojin.

Furthermore, the colloids are deposited since an ideal set settling size that was defined in the model is reached, thereby displaying removal of the colloids. Majorly, the model comparison stipulates that at neutral pH, colloid formation is proceeds vigorously, while reaction is resisted at lower pH. More importantly though is the fact that the colloids still form at the low pH. Finally, from the model comparison, it may be deduced that colloid transport in these drainages occurs, however, efficient removal is achieved due to efficient aggregation of the colloids, which allows their deposition to the bed of the drainage. A modification in the model is required in terms of the processes at Shojin since the reaction process is high underestimated. So, although at pH 3.1, colloid formation was observed, it is not depicted in the model, as the reaction rate at that pH is significantly low. Furthermore, the colloids at Shojin settle much earlier than those of Ainai, because of the lower aggregation size that was defined, and therefore stipulates that the colloids are removed within a short distance following their formation. None the less, the general concept and trend displayed by the model is reliable but can be modified to better predict the behavior of the colloids at the Shojin river.

The estimates of both the concentration and distance fit very well, depicting that under such conditions i.e. pH and element concentration, this trend is expected and highly predictable. From the model, an incorporation of the size is made, allowing for a visible decrease in the colloid concentration. A minor misfit is observed in an overestimation of the As colloids, which do not form in the drainage as some As remains in the dissolved form, which the model does not recognize. The deposition rate of the colloids by the model is also slightly over estimated, i.e. a faster deposition is predicted most likely because the model reaches a saturation of colloids in the water, thereby increasing the estimated rate at which colloids settle. On the contrary, the colloid behaviors at Shojin required more complex definition of the colloid formation with respect to pH adjustment and was therefore investigated only by colloid formation based on the rate of reaction difference of the drainages.

Modelling the colloid behavior also gave a picture of the behavior of the colloids in the two drainages, and from the capacity of modelling carried out, it is evident that pH is the primary factor that affects the colloid transportation, since at low pH, sorption processes were lower, along with colloid formation. Therefore, minimal colloids were formed, and transported a longer distance, since they were not saturated in the wastewater, thereby slowing aggregation, and settling.

To summarize, it is seen that the model accurately demonstrates colloid formation and transport in Ainai mine drainage. Once formed the colloids are transported about 900 m before being deposited to the bed of the drainage, thereby removing both Fe and As from the drainage. It is therefore safe to say, reaction rate during the sorbing process, which is

well connected to the pH, a size definition of the colloids, and an ideal distance estimation is relevant to clearly estimate how much of the colloids are transported following their formation in mine drainages.

6.4.3 Aggregation and deposition kinetics of Ainai mine drainage and Shojin river

Three major forces, i.e. Brownian diffusion, fluid flow, and gravity were the major existing forces when considering nanoparticle aggregation. The clusters grow due to a sequential repetition of these processes. The aggregation process of nanoparticles is thorough as aging variation of distribution of clusters' diameters.

Aggregation of Fe colloids was quantitatively investigated using thermodynamic calculations. The reason for the detailed calculation, was to unveil in detail, the aggregation rate of the colloids. This gives insight on the rate at which the colloids will reach a point at which they are efficiently removed from the mine drainages. These calculations were carried out based on the series of equations compiled by Koide, MS2018. In this calculation, Brownian collisions are considered the primary process that induces the collisions of the colloidal particles, as these forces are most dominant when considering nanoparticles (Petosa et al., 2010). Since the interactions are the cause of increasing size, consequently repulsive forces are significantly overcome and result in the gradual increase in particle size. The hypothesis that the calculation was built on was based on, is summarized in Figure 6-5. The aggregation process of colloids based on Brownian's motion. With increased interactions from the Brownian motion, the colloid particles increase in interactions and the result in the aggregation of the colloid particles.

It is seen that at Ainai (Figure 6-4), right from the upstream when the colloids are forming, they are aggregating and the aggregation increases towards the downstream most likely because the colloids are saturating in the drainage towards the downstream, thereby increasing the interactions. A combination of the water chemistry and thermodynamic calculation further shows that the primary process in the upstream is the formation of the colloids whereas from mid to downstream dominantly aggregation of the colloids occurs.

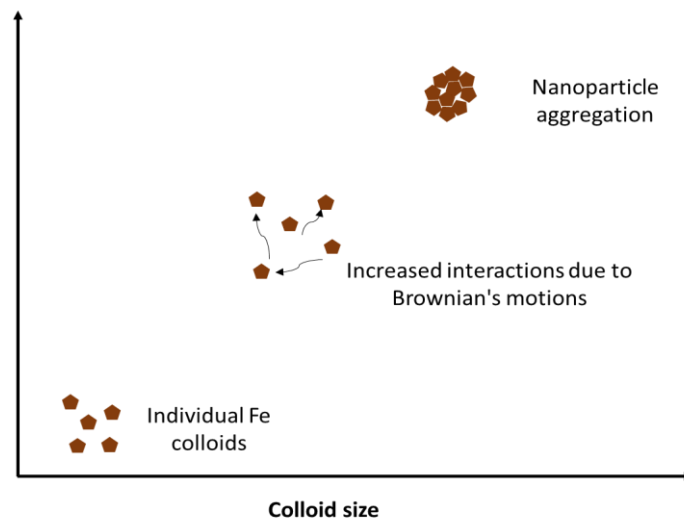


Figure 6-5. The aggregation process of colloids based on Brownian's motion.

On the other hand, aggregation is seen to be slow in the upstream of Shojin river, then quickly picks up from mid to downstream. This confirms the observation that the minor dissolution occurs around SR2 to SR3, but towards the downstream, the aggregation is rampant so much so that the colloids are hardly observed. The quick aggregation, however, does not reach a steady point, and this might be reflecting the increasing aggregation rate as result of undersaturation and hence continuous aggregation of the colloids towards the downstream. It implies that the colloids are efficiently aggregating and being removed from the drainage towards the downstream.

From the modelling of the aggregation behaviors, combined with estimated distance of a drainage, a design may be drawn to estimate how much of the colloids are aggregated at a particular distance and pH. At Shojin, a slight pH increase significantly improves aggregation and hence the removal rate. This proves that these aggregation estimates are useful for understanding colloid behaviors and even for mine design.

Although theoretical estimations can estimate the sizes of colloids at which deposition occurs, it is important to note that the parameters that are considered are quite limited and therefore leave out some factors that may play significant roles in the controlling of the aggregation behaviors. As shown in Table 6-1, parameters used to calculate the aggregation rate with time, are listed, and although some of the parameters were estimated from the field, such as the time from one point to another, colloid concentrations, some other parameters such as colloid mass and density are theoretically estimated, thereby acting as a limitation that exists with the calculation. Other crucial parameters such as pH, are also not considered directly in the calculation. Nonetheless, these estimations give a good insight on the aggregation behaviors displayed by the colloids in the drainages, since

a variation is also seen in the two drainages compared in this study, however, for more detailed simulations, more parameters are best to take into consideration.

6.5 Summary

This chapter provides insight on the formation mechanisms of Fe colloids in the drainages, their aggregation and transportation behavior. It is through modelling, that the dominant mineralogy and impacting parameters are seen. At Ainai, the ferrous rich, oxidative and near neutral nature allows for the formation of the ferrihydrite colloids. Furthermore, this enhances the aggregation rate, allowing for the colloids to reach a size of over 300 nm, which easily settles by gravity, thereby removed from the drainage. On the other hand, the low pH, ferric rich nature of Shojin slows down aggregation of the schwertmannite colloids. However, due to an increase in pH towards the downstream, the colloids quickly aggregate and are efficiently and abruptly decreased in the drainage to low concentrations. Thus, further correlates with the transport behavior, which shows that Ainai colloids are less transported than the Shojin colloids.

7 Chapter 7: General conclusions and implications

7.1 Conclusions from the study

The increasing abundance of wastewater from mining activities is raising the need to develop efficient passive treatment systems. These passive treatment systems are cheap and more importantly sustainable; however, their efficiency is highly dependent on the geochemical properties of the mine drainage system. Mine drainages vary from acidic to near neutral or even neutral pH, and vary widely in other properties, such as the general geology, target elements and organic matter among other properties. These properties affect and alter the processes that will be responsible for remediation of toxic elements in the drainage, therefore, this study was carried out at two mine drainages with contrasting characteristics, particularly pH, to elucidate the remediation processes occurring in the drainage systems.

One novel aspect of the study was the focus on the role of nanoparticles in the remediation process. The investigation at the Ainai mine drainage highlighted that, similar to most mine drainages, which are a result of oxidation of Fe containing minerals, Fe is commonly an abundant element in mine drainages. Consequently, the thermodynamics of Fe allow it to exist in its ferrous state at reducing conditions, which rapidly oxidizes to ferric state, forming octahedral Fe clusters, that then form colloids. At Ainai, the circumneutral pH, oxidative environment and abundance of ferrous Fe, allowed for this process to proceed and result in the formation of ferrihydrite colloids. These colloids, formed as an aggregation of the F_{13} Keggel clusters, which during their formation incorporated arsenic, which was a target element in the drainage. Following the formation of the colloids and sequestration of the As, the colloids aggregate to about 400 nm, reaching a size that can be deposited to the drainage bed by gravity, thereby achieving efficient remediation. Another target element in the drainage was Zn, which, through synthetic experiments, it was observed that Zn-Fe LDH were responsible for the its remediation at pH over 7.5.

On the other hand, schwertmannite colloids formed in the acidic Shojin mine drainage. Unlike the system at Ainai, where wastewater flows from an underground tunnel to the surface and proceeds without any kind of mixing, Shojin wastewater is released from underground, then mixes with neutral river water, which plays a significant role in the remediation process. Despite the lower buffering capacity of the background river water, the dilution effect is an important phenomenon on reducing the toxic element concentrations. Following which, the minor increase in pH and the saturation of the of the elements in the drainage, allow for the formation of the schwertmannite colloids. Minor dissolution of the colloids is observed in the colloids at Shojin, due to the low pH, which results in relatively unstable colloids in comparison with the Ainai colloids. The

aggregation rate of the colloids is also relatively slow, and although deposition is observed towards the downstream, therefore efficiently removing the schwertmannite colloids, along with the As that they co precipitated with and adsorbed during their formation.

Furthermore, Fe isotopic fractionations were applied as a second novel aspect of the study. Global Fe cycle has been studied for a while and especially with regards to Fe supply to oceans. Although many sources of Fe to oceans exist, rivers are reportedly the highest sources of Fe to oceans, and in turn, these rivers are highly supplied by mine drainages. Therefore, isotopic fractionations were utilized to trace the phases and transportation of the Fe, that is sourced from the mine drainages of varying characteristics. It was established from the $\delta^{56}\text{Fe}$ values that the Fe in the near-neutral Ainai drainage was transported mainly as colloids towards the downstream, but later settled to the bottom of the drainage efficiently. On the other hand, in the acidic conditions, dissolution of some colloids resulted in the transportation of both colloidal and dissolved form, and some Fe remained in the dissolved form longer than at neutral pH.

Finally, using modelling, the drainage systems were theoretically simulated thereby allowing us to understand the processes occurring in the drainages using the obtained parameters. Qualitative calculations were also carried out to quantify the aggregation behavior of the colloids in the drainage, parameters that need to be highlighted and well understood when constructing mine drainage systems.

Using the approach taken in the study, i.e. a synthesis of water chemistry studies with isotopic signatures and geochemical modelling, the study provides deep understanding on colloid behavior, which also affects other elements in the mine drainages. It is clear that the respective processes that the mine drainages undergo, leave signature isotopic fractionations, which can be traced back and used to follow the behavioral trend of the Fe. Processes such as oxidative precipitation and (in)stability of colloids can be monitored using the fractionation patterns displayed by Fe. Additionally, a distinction between dissolved and colloidal phases of Fe is highlighted once their isotopic fractionations are monitored. Dissolved fractions usually having lighter isotopic signatures, vary distinctly from their colloidal counterparts, thereby clarifying the major phase in which Fe is dominant in a system. Synthesizing this understanding with geochemical modelling gives an insight on the number of colloids that are transported, along with the distance that they are transported. At Ainai, for instance, about 23% of the colloids, i.e. about 1.4 ppm of the colloids, are transported a distance of 200 m, a trend that is seen through both the isotopic patterns and the geochemical modelling. Overall, the processes followed in the mine drainage, particularly at circumneutral pH where oxidative precipitation prevails, large fractionations of $\sim 4\text{‰}$ have been recorded, which correspond to the size fraction analysis approach of Fe that was taken into consideration in this study. Fe colloid transportation results in a fractionation of $\sim +0.75\text{‰}$, which results from the

transportation of colloids from upstream, thereby modify isotopic signatures towards the downstream.

Therefore, it is evident that Fe colloid behavior can be clearly understood from the geochemical trends and Fe isotopic fractionations. Geochemical modelling provides insight on the processes occurring in the drainages as well, and all these together, aid in understanding the formation, aggregation, transportation and depositional behaviors of Fe colloids in mine drainages. This can also be used to trace the behavior of Fe in other systems further than the mine drainages, thereby providing insight of Fe release and circulation in rivers and oceans.

7.2 Implications of the study

The study carried out leaves a wide range of implications relating to mine drainage design and maintenance, studying Fe mobility utilizing Fe isotopes and Fe cycle in general.

(i) During mine design, the size fraction considered to transport toxic elements varies, but is commonly 0.2 microns. Particles under 0.2 microns are considered dissolved and the wastewater filtered to 0.2 microns is considered clean. However, from our study, it is evident that there a lower cut off fraction is necessary to deem wastewater clean and preferably, that which considers the colloids. These colloids are under 0.2 microns, but due to their large surface area have high reactivity which allows them to uptake toxic elements. If not properly considered, these colloids may act as transportation media, taking toxic elements to other systems and contaminating other water resources, especially due to the risk of release of the toxic elements. Therefore, during mine design, approaches that allow colloids to settle to before mixing of wastewater with other resources is important.

A direct implication of the study can be applied to the design of Ainaí mine drainage. The 1 km stretch through which water flows allows the formation and aggregation of the colloids to about 350 nm, a size that is large enough to settle by gravitational force. Seeing as the geochemical conditions, i.e., Fe concentration, pH, ionic strength among others favor these processes, so that the target elements, specifically Fe and As reduce to concentrations below the WHO stipulated standard by the time the water reaches S5, room for modification is available. The current design includes a reservoir pond, followed by a sedimentation pond, however, most parameters are within standard before reaching the reservoir pond. Furthermore, following the estimate by the colloid transport, a shorter drainage length would be enough to settle the colloids out of the wastewater. Therefore, a modified system of the Ainaí mine drainage would efficiently function without a sedimentation pond, since most of the waste is already remediated by the downstream of

the drainage (Figure 7-1). However, the reservoir pond would still be necessary for an extensive removal by settling in the case of trace colloids that may be transported further than the downstream.

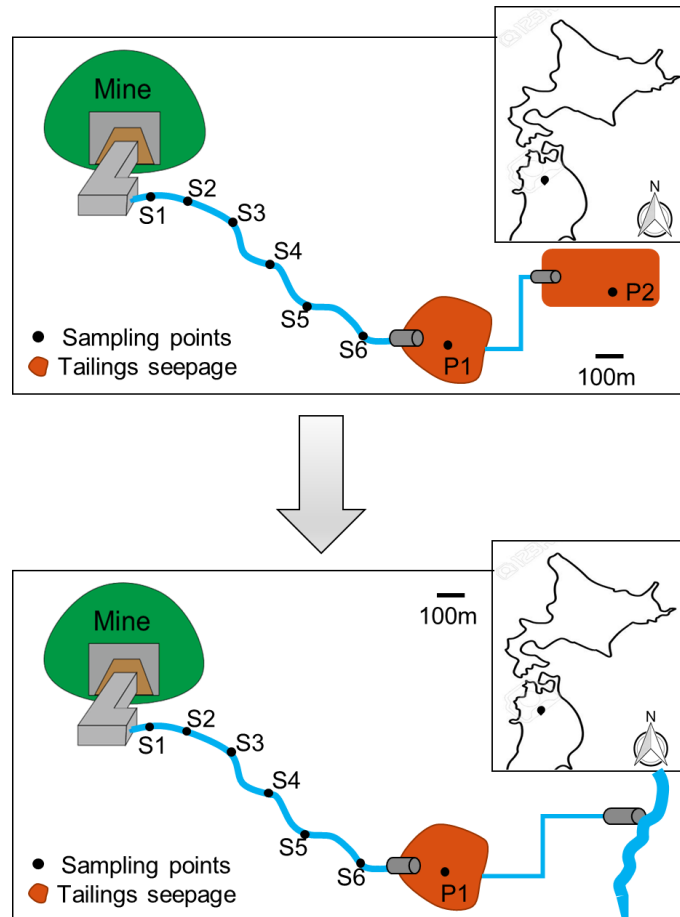


Figure 7-1. New proposed design for Ainai mine drainage implied from our findings.

Given that the pond specifics are relevant to building the design and ensuring efficient treatment, the below design (Figure 7-2) is suggested. The keypoints of the design velow are the forebay, which will act as an initial sink for the sludge, and the actual pond's size which can accommodate sludge for long periods of time. The suggested style will ensure efficient treatment at minimal cost.

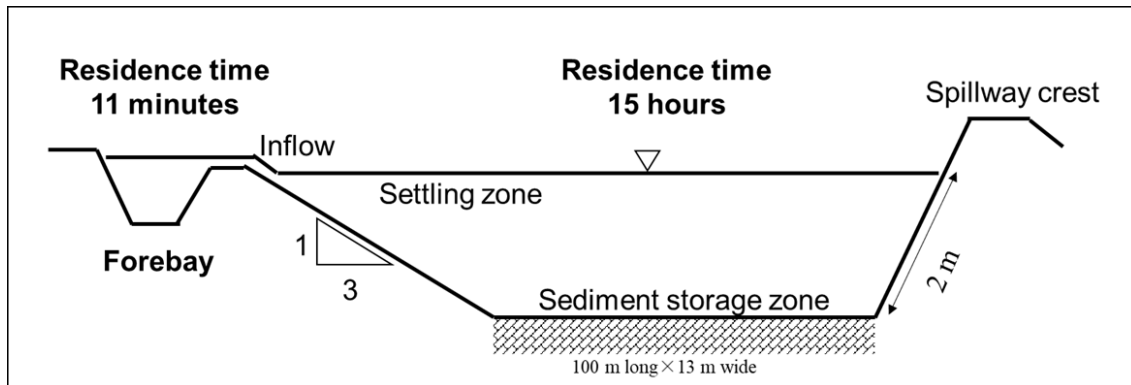


Figure 7-2. The proposed design of the sedimentation pond at Ainai mine drainage.

(ii) Seasonal variations need to be considered seriously in the mine drainages, as well as flow rate and other parameters.

(iii) Acidic mine wastewater treatment has considered the increase of pH to neutral, however, although minor dissolution may occur, the increase in pH does not necessarily have to be to neutral pH. At low pH, formation of the colloids is also observed, implying that even at such low pH, remediation is possible. It is however important to consider the effectiveness of the process responsible i.e. whether coprecipitation, adsorption or complexation, and how the processes are affected at the low pH.

(iv) Mobility of Fe is very important to various life sustaining cycles. Therefore, the use of Fe isotopes to highlight these phases, mobility and general behaviors of Fe in mine drainages can be applied to other systems in order to assist with understanding the behaviors of Fe. In the case of mine drainages, neutral pH enhanced the aggregation of colloids and improves the deposition rate of the colloids from the wastewater. On the contrary, at low pH, colloids are transported further and display dissolution patterns thereby increasing Fe mobility (Figure 7-3).

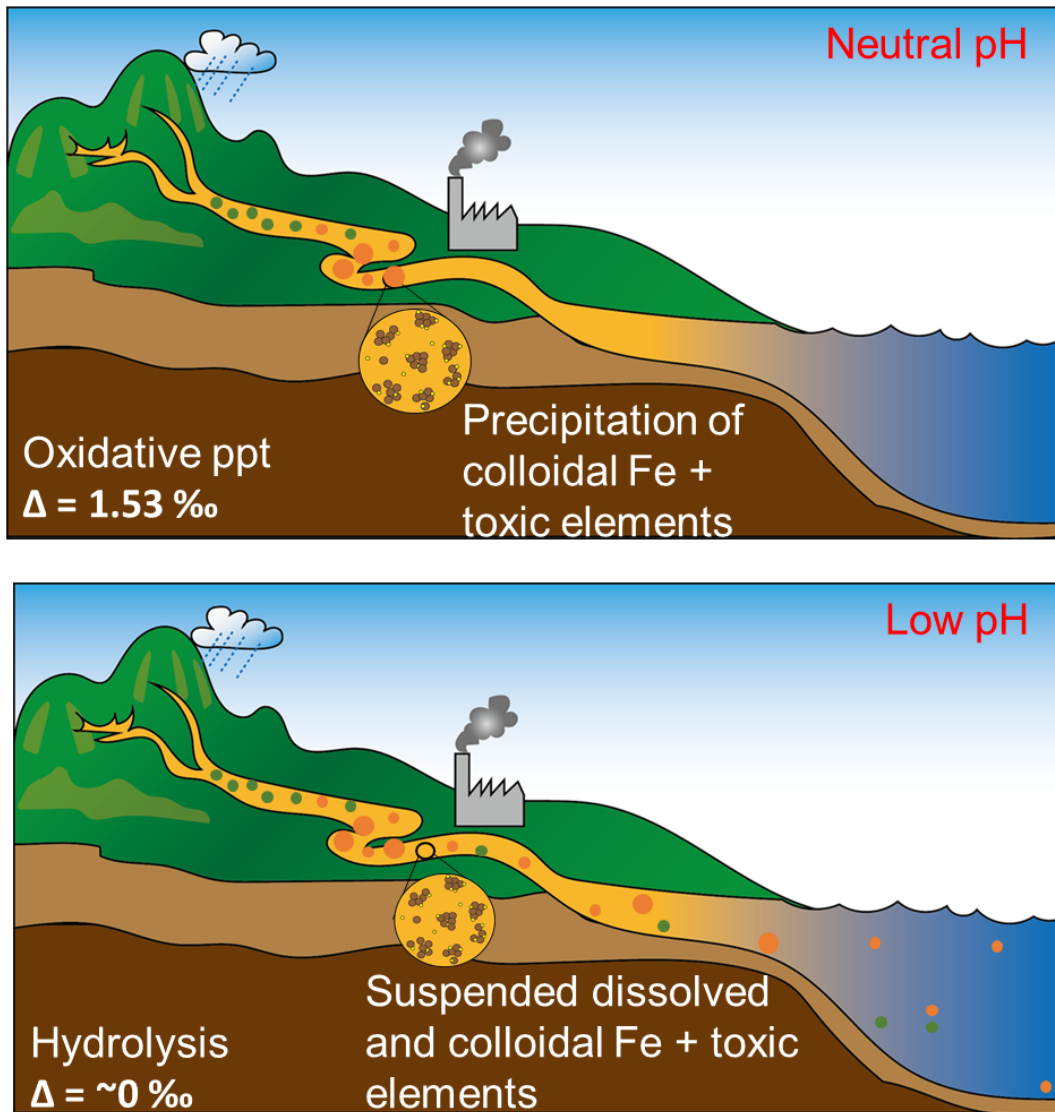


Figure 7-3. Colloid mobility at circumneutral and acidic pH mine drainages along with their isotopic signatures.

References

- Akcil, A. and Koldas, S. (2006) Acid Mine Drainage (AMD): causes, treatment and case studies. *Journal of Cleaner Production*, 14, pp. 1139–1145. doi: 10.1016/j.jclepro.2004.09.006.
- Allada, R. K., Peltier, E., Navrotsky, A., Casey, W.H., Johnson, C.A., Berbeco, H. L., Sparks, D.L. (2006) Calorimetric determination of the enthalpies of formation of hydrotalcite-like solids and their use in the geochemical modeling of metals in natural waters. *Clays and Clay Miner.* 54, pp. 409–417. doi: 10.1346/CCMN.2006.0540401.
- Babakhani, P. (2019). The impact of nanoparticle aggregation on their size exclusion during transport in porous media: One- and three-dimensional modelling investigations. *Scientific Reports*, 9(1), pp. 1–12. doi: 10.1038/s41598-019-50493-6.
- Bergquist, B. A. and Boyle, E. A. (2006) Dissolved iron in the tropical and subtropical Atlantic Ocean. *Global Biogeochemical Cycles*, 20(1), pp. 1–14. doi: 10.1029/2005GB002505.
- Bigham, J. M., Schwertmann, U., Traina, S. J., Winland, R. L., Wolf, M. (1996) Schwertmannite and the chemical modeling of iron in acid sulfate waters. *Geochimica et Cosmochimica Acta*, 60(12), pp. 2111–2121. doi: 10.1016/0016-7037(96)00091-9.
- Bigham, J. M., Carlson, L. and Murad, E. (1994) Schwertmannite, a new iron oxyhydroxy-sulfate from Pyhasalmi, Finland and other localities. *Min. Mag.* 58(12), pp. 641–648.
- Bowles, J. F. W. (2021) Hydroxides-Ferrihydrite in Soil and Environmental Chemistry. Volume 1. 2nd Ed, pp. 442-451.
- Boyd, P. W. and Ellwood, M. J. (2010) The biogeochemical cycle of iron in the ocean. *Nature Geoscience*. Nature Publishing Group, 3(10), pp. 675–682. doi: 10.1038/ngeo964.
- Boye, M., Nishioka, J., Croot, P., Laan, P., Timmerman, K. R., Strass, V. H., Takeda, S. and Baar, H. (2010) Significant portion of dissolved organic Fe complexes in fact is Fe colloids. *Marine Chemistry*. 122(1–4), pp. 20–27. doi: 10.1016/j.marchem.2010.09.001.
- Bravo-Suárez, J. J., Páez-Mozo, E. A. and Oyama, S. T. (2004) Models for the estimation of thermodynamic properties of layered double hydroxides: Application to the study of their anion exchange characteristic. *Quimica Nova*, 27(4), pp. 574–581. doi: 10.1590/S0100-40422004000400011.
- Bunn, R. A., Magelky, R. D., Ryan, J. N. and Elimelech, M. (2002) Mobilization of natural colloids from an iron oxide-coated sand aquifer: Effect of pH and ionic strength. *Environmental Science and Technology*, 36(3), pp. 314–322. doi: 10.1021/es0109141.
- Byrne, P. (2019) The impairment of river systems by metal mine contamination: A review including remediation options. *Environmental Science and Technology*, 11(1).
- Christian, P., Kammer, F., Hofmann, T. (2008) Nanoparticles: Structure, properties, preparation and behaviour in environmental media. *Ecotoxicology*, 17(5), pp. 326–343. doi: 10.1007/s10646-008-0213-1.
- European Commission. (2006) Scientific committee on emerging and newly identified health risks (SCENIHR) modified Opinion on the appropriateness of existing methodologies to

assess the potential risks associated with engineered and adventitious.

- Conrad, S., Ingri, J., Gelting, J., Nordblad, F., Engstrom, E. and Anderson, P. S. (2019) Distribution of Fe isotopes in particles and colloids in the salinity gradient along the Lena River plume, Laptev Sea. *Biogeosciences*, 16(6), pp. 1305–1319. doi: 10.5194/bg-16-1305-2019.
- Conrad, S. (2019) Iron isotopes in aquatic systems. Doctoral Thesis submitted to Lulea University of Technology.
- Corapcioglu, M. Y. and Jiang, S. (1993) Colloid-facilitated groundwater contaminant transport. *Water Resources Research*, 29(7), pp. 2215–2226. doi: 10.1029/93WR00404.
- Crawford, R. J., Harding, I. H. and Mainwaring, D. E. (1993) Adsorption and Coprecipitation of Multiple Heavy Metal Ions onto the Hydrated Oxides of Iron and Chromium. *Langmuir*, 9(11), pp. 3057–3062. doi: 10.1021/la00035a052.
- Cruz-Hernández, P., Pérez-López, R. and Nieto, J. M. (2017) Role of Arsenic During the Aging of Acid Mine Drainage Precipitates. *Procedia Earth and Planetary Science*. 17, pp. 233–236. doi: 10.1016/j.proeps.2016.12.079.
- Dauphas, N. and Rouxel, O. (2006) Mass spectrometry and natural variations of iron isotopes. *Mass Spectrometry Reviews*, 25(4), pp. 515–550. doi: 10.1002/mas.20078.
- Dold, B. (2014) Evolution of acid mine drainage formation in sulphidic mine tailings. *Minerals*, 4(3), pp. 621–641. doi: 10.3390/min4030621.
- Dold, B. and Fontboté, L. (2002) A mineralogical and geochemical study of element mobility in sulfide mine tailings of Fe oxide Cu - Au deposits from the Punta del Cobre belt, northern Chile. *Chemical Geology*, 189(3–4), pp. 135–163. doi: 10.1016/S0009-2541(02)00044-X.
- Dzombak, D. A. and Morel, F. M. M. (1993) Surface complexation modeling: Hydrated ferric oxide. *Journal of Colloid and Interface Science*, 141(2), pp. 595–596. doi: 10.1016/0021-9797(91)90361-b.
- Escoube, R., Rouel, O.J., Pokrovsky, O.S., Schroth, A, Holmes, R. M. and Donard, O. F. X. (2015) Iron isotope systematics in Arctic rivers. *Comptes Rendus - Geoscience. Academie des sciences*, 347(7–8), pp. 377–385. doi: 10.1016/j.crte.2015.04.005.
- Fantle, M. S. and DePaolo, D. J. (2004) ‘Iron isotopic fractionation during continental weathering’, *Earth and Planetary Science Letters*, 228(3–4), pp. 547–562. doi: 10.1016/j.epsl.2004.10.013.
- Federation, I. A. (2011) *Encyclopedia of Astrobiology*, Encyclopedia of Astrobiology. doi: 10.1007/978-3-642-11274-4.
- Fernandez-Martinez, A. Roman-Ross, G., Timon, V. and Cuello, G. (2010) The structure of schwertmannite, a nanocrystalline iron oxyhydroxysulfate. *American Mineralogist*, 95(8–9), pp. 1312–1322. doi: 10.2138/am.2010.3446.
- Friedrich, A. J. Beard, B. L. Reddy, T. R. and Johnson, C. M. (2014) Iron isotope fractionation between aqueous Fe(II) and goethite revisited: New insights based on a multi-direction

- approach to equilibrium and isotopic exchange rate modification. *Geochimica et Cosmochimica Acta*. Elsevier Ltd, 139, pp. 383–398. doi: 10.1016/j.gca.2014.05.001.
- Fritzsche, A., Rennert, T. and Totsche, K. U. (2011) Arsenic strongly associates with ferrihydrite colloids formed in a soil effluent. *Environmental Pollution*, 159(5), pp. 1398–1405. doi: 10.1016/j.envpol.2011.01.001.
- Fu, D., Keech, P. G., Sun, X. and Wren, C.J. (2011) Iron oxyhydroxide nanoparticles formed by forced hydrolysis: Dependence of phase composition on solution concentration. *Physical Chemistry Chemical Physics*, 13(41), pp. 18523–18529. doi: 10.1039/c1cp20188c.
- Fu, F. and Wang, Q. (2011) Removal of heavy metal ions from wastewaters: A review. *Journal of Environmental Management*. Elsevier Ltd, 92(3), pp. 407–418. doi: 10.1016/j.jenvman.2010.11.011.
- Fukushi, K., Sasaki, M., Sato, T., Yanase, . and Ikeda, H. (2003) A natural attenuation of arsenic in drainage from an abandoned arsenic mine dump. *Applied Geochemistry*, 18(8), pp. 1267–1278. doi: 10.1016/S0883-2927(03)00011-8.
- Geological Survey of Japan (2019) Water Quality Survey. Hokkaido Research Organisation.
- Gilbert, B., Lu, G. and Kim, C. S. (2007) Stable cluster formation in aqueous suspensions of iron oxyhydroxide nanoparticles. *Journal of Colloid and Interface Science*, 313(1), pp. 152–159. doi: 10.1016/j.jcis.2007.04.038.
- Gledhiir, M. and Buck, K. N. (2012) The organic complexation of iron in the marine environment: A review. *Frontiers in Microbiology*, 3(FEB), pp. 1–17. doi: 10.3389/fmicb.2012.00069.
- Hao, L., Liu, M., Wang, N. and Li, G. (2018) A critical review on arsenic removal from water using iron-based adsorbents. *RSC Advances*. Royal Society of Chemistry, 8(69), pp. 39545–39560. doi: 10.1039/c8ra08512a.
- Hase, H., Nishiuchi, T., Sato, T., and Otake, T. (2017) A novel method for remediation of nickel containing wastewater at neutral conditions. *Journal of Hazardous Materials*. Elsevier B.V., 329, pp. 49–56. doi: 10.1016/j.jhazmat.2017.01.019.
- Henkel, S., Kasten, S., Poulton, S. W. and Staubwasser, M. (2016) Determination of the stable iron isotopic composition of sequentially leached iron phases in marine sediments. *Chemical Geology*, 421, pp. 93–102. doi: 10.1016/j.chemgeo.2015.12.003.
- Herbert, R. B. and Schippers, A. (2008) Iron isotope fractionation by biogeochemical processes in mine tailings. *Environmental Science and Technology*, 42(4), pp. 1117–1122. doi: 10.1021/es071616s.
- Heyden, B. P. and Roychoudhury, A. N. (2015) A review of colloidal iron partitioning and distribution in the open ocean. *Marine Chemistry*. 177, pp. 9–19. doi: 10.1016/j.marchem.2015.05.010.
- Hochella, M. F., Mogk, D. W., Ranville, J., Allen, I. C., Maruyama, M., Schroeder, P. A., Rosso, K. M. and Yang, Y. (2019) Natural, incidental, and engineered nanomaterials and their impacts on the Earth system. *Science*, 363(6434). doi: 10.1126/science.aau8299.

- Hockridge, J. G., Jones, F., Loan, M. and Richmond, W. R. (2009) An electron microscopy study of the crystal growth of schwertmannite needles through oriented aggregation of goethite nanocrystals. *Journal of Crystal Growth*, 311(15), pp. 3876–3882. doi: 10.1016/j.jcrysgr.2009.06.023.
- Hongo, T., Iemura, T. and Yamazaki, A. (2008) Adsorption ability for several harmful anions and thermal behavior of Zn-Fe layered double hydroxide. *Journal of the Ceramic Society of Japan*, 116(1350), pp. 192–197. doi: 10.2109/jcersj2.116.192.
- Ingri, J., Baxter, D. C., Widlund, A., Andersson, P. and Ohlander, B. (2006) Iron isotope fractionation in river colloidal matter. *Earth and Planetary Science Letters*, 245(3–4), pp. 792–798. doi: 10.1016/j.epsl.2006.03.031.
- Ishii Yasuo (1964) Geological structures and characteristics of black ore deposits of the ainai mine. Yasuo Ishii Nitto Mining Company report.
- Ito, A., Otake, T., Shin, K., Ariffin, K. S., Yeoh, F. and Sato, T. (2017) Geochemical signatures and processes in a stream contaminated by heavy mineral processing near Ipoh city, Malaysia. *Applied Geochemistry*, 82, pp. 89–101. doi: 10.1016/j.apgeochem.2017.05.007.
- Japan Meteorological Agency (2018) Japan Meteorological Agency (ed) Climate Change Monitoring Report 2017. *Climate in Japan*, 12, pp. 16–21.
- Jung, H. B., Yun, S., Kwon, J. and Zheng, Y. (2012) Role of iron colloids in copper speciation during neutralization in a coastal acid mine drainage, South Korea: Insight from voltammetric analyses and surface complexation modeling. *Journal of Geochemical Exploration*. Elsevier B.V., 112, pp. 244–251. doi: 10.1016/j.gexplo.2011.09.002.
- Kappler, A., Johnson, C. M., Crosby, H. A., Beard, B. L. and Newman, D.K. (2010) Evidence for equilibrium iron isotope fractionation by nitrate-reducing iron(II)-oxidizing bacteria. *Geochimica et Cosmochimica Acta*, 74(10), pp. 2826–2842. doi: 10.1016/j.gca.2010.02.017.
- Khamphila, K., Kodama, R., Sato, T. and Otake, T. (2017) Adsorption and Post Adsorption Behavior of Schwertmannite with Various Oxyanions. *Journal of Minerals and Materials Characterization and Engineering*, 05(02), pp. 90–106. doi: 10.4236/jmmce.2017.52008.
- Koide, A. (2018) Formation and aggregation processes of colloids during natural remediation in Ainai mine drainage, Akita Prefecture Master thesis 2018 Division of Cooperative Program for Resources Engineering, Graduate School of Engineering, Hokkaido University.
- Legg, B. A., Zhou, M., Gilbert, B. and Banfield, J. (2014) Impacts of ionic strength on three-dimensional nanoparticle aggregate structure and consequences for environmental transport and deposition. *Environmental Science and Technology*, 48(23), pp. 13703–13710. doi: 10.1021/es502654q.
- Liao, P., Li, W., Wu, J., Yuan, S. and Clammar, D. E. (2017) Formation, aggregation, and deposition dynamics of non-iron colloids at anoxic-oxic interfaces. *Environmental Science and Technology*. American Chemical Society, 51(21), pp. 12235–12245. doi: 10.1021/acs.est.7b02356.

- Lotfi-Kalahroodi, E., Wickmann, A. P., Roussel, O. and Davrache, M. (2021) Does ultrafiltration kinetics bias iron isotope compositions? *Chemical Geology*, 566(November 2020), pp. 1–7. doi: 10.1016/j.chemgeo.2021.120082.
- Lu, Q., Bian, Z. and Tsuchiya, N. (2019) Hydrotransport-oriented zn, cu, and pb behavior assessment and source identification in the river network of a historically mined area in the Hokuroku basin, Northeast Japan. *International Journal of Environmental Research and Public Health*, 16(20). doi: 10.3390/ijerph16203907.
- Mohod, C. V and Dhote, J. (2013) Review of Heavy Metals in Drinking Water and Their Effect on Human Health. *International Journal of Innovative Research in Science, Engineering and Technology*, 2(7), pp. 2992–2996.
- Mokhter, M., Magnenet, C., Lakard, S., Euvrard, M., Aden, M., Clement, S., Lakard, B. (2018) Use of Modified Colloids and Membranes to Remove Metal Ions from Contaminated Solutions. *Colloids and Interfaces*, 2(2), p. 19. doi: 10.3390/colloids2020019.
- Morimoto, K., Tamura, K., Anraku, S., Sato, T., Suzuki, M., Yamada, H. (2015a) Synthesis of Zn-Fe layered double hydroxides via an oxidation process and structural analysis of products. *Journal of Solid State Chemistry*. Elsevier, 228, pp. 221–225. doi: 10.1016/j.jssc.2015.04.045.
- Morimoto, K. (2015b) Synthesis of Zn-Fe layered double hydroxides via an oxidation process and structural analysis of products. *Journal of Solid State Chemistry*. Elsevier, 228, pp. 221–225. doi: 10.1016/j.jssc.2015.04.045.
- Nakashima, R. N., Haraguchi, T. H. and Tanaka, A. T. (2012) Classification of Groundwater According to Water Quality in Saga Prefecture. *Bul. Fac. Agric. Saga. Univ.* 97, 27-35.
- Nguyen, K.M., Nguyen, B., Hai, N.T. and Nguyen, T.H.H. (2019) Adsorption of arsenic and heavy metals from solutions by unmodified iron-ore sludge. *Applied Sciences (Switzerland)*, 9(4). doi: 10.3390/app9040619.
- Nordstrom, D. Kirk (2011) Mine waters: Acidic to circumneutral. *Elements*, 7(6), pp. 393–398. doi: 10.2113/gselements.7.6.393.
- Norsuzila Y., Mardina A. and Mahamod I. (1989) Impact of Wastewater on Surface Water Quality in Developing Countries: A Case Study of South Africa. *Intech*, 32, pp. 137-144.
- Okamoto, H., Morimoto, K., Anraku, S., Sato, T. and Yoneda, T., (2010) A novel remediation method learnt from natural attenuation process for Cu- and Zn-bearing wastewater. *Clay science*, 14(5), pp. 203–210. Doi: 10.11362/jcssjclayscience.14.5_203.
- Oleinikova, O. V., Poitrasson, F., Shirokova, L. S. and Porokrovsky, O. S. (2019) Iron isotope fractionation during bio- And photodegradation of organoferric colloids in boreal humic waters. *Environmental Science and Technology*. American Chemical Society, 53, pp. 11183–11194. doi: 10.1021/acs.est.9b02797.
- Parida, K. M. and Mohapatra, L. (2012) Carbonate intercalated Zn/Fe layered double hydroxide: A novel photocatalyst for the enhanced photo degradation of azo dyes. *Chemical Engineering Journal*. Elsevier B.V., 179, pp. 131–139. doi: 10.1016/j.cej.2011.10.070.
- Petosa, A.R., Jaisi, D.P., Quevedo, I.R., Elimelech, M. and Tufenkji, N. (2010) Aggregation

and deposition of engineered nanomaterials in aquatic environments: Role of physicochemical interactions. *Environmental Science and Technology*, 44(17), pp. 6532–6549. doi: 10.1021/es100598h.

- Plumlee, G. S., Logsdon, M. J. and Filipek, L. F. (1997) Metal Sorption on Mineral Surfaces. *The Environmental Geochemistry of Mineral Deposits*, pp. 161–182. doi: 10.5382/rev.06.07.
- Poitrasson, F. (2006) On the iron isotope homogeneity level of the continental crust. *Chemical Geology*, 235(1–2), pp. 195–200. doi: 10.1016/j.chemgeo.2006.06.010.
- Pokrovsky, O. S., Viers, J., Shirokova, L.S and Shevchenko, V.P. (2010) Dissolved, suspended, and colloidal fluxes of organic carbon, major and trace elements in the Severnaya Dvina River and its tributary. *Chemical Geology*. Elsevier B.V., 273(1–2), pp. 136–149. doi: 10.1016/j.chemgeo.2010.02.018.
- Pokrovsky, O. S. and Schott, J. (2002) Iron colloids/organic matter associated transport of major and trace elements in small boreal rivers and their estuaries (NW Russia). *Chemical Geology*, 190(1–4), pp. 141–179. doi: 10.1016/S0009-2541(02)00115-8.
- Raiswell, R., Hawkings, J., Elsenousy, A., Death, R. and Wadham, J (2018) Iron in Glacial Systems: Speciation, Reactivity, Freezing Behavior, and Alteration During Transport. *Frontiers in Earth Science*, 6(12). doi: 10.3389/feart.2018.00222.
- Raiswell, R. and Canfield, D. E. (2012) The iron biogeochemical cycle past and present. *Geochemical Perspectives*, 1(1), pp. 1–232. doi: 10.7185/geochempersp.1.1.
- Ritter, K., Aiken, G. R., Ranville, J. F. and Macaldy, D. L. (2006) Evidence for the aquatic binding of arsenate by natural organic matter-suspended Fe(III). *Environmental Science and Technology*, 40(17), pp. 5380–5387. doi: 10.1021/es0519334.
- Roberts, D. R., Scheinost, A. C. and Sparks, D. L. (2002) Zinc speciation in a smelter-contaminated soil profile using bulk and microspectroscopic techniques. *Environmental Science and Technology*, 36(8), pp. 1742–1750. doi: 10.1021/es015516c.
- Sánchez España, Lopez Pamo, E., Santofimia, E. and Martin Rubi, J.A. (2006) The removal of dissolved metals by hydroxysulphate precipitates during oxidation and neutralization of acid mine waters, Iberian Pyrite Belt. *Aquatic Geochemistry*, 12(3), pp. 269–298. doi: 10.1007/s10498-005-6246-7.
- Santos Pinheiro, G. M., Poitrasson, F., Sondag, F., Vieira, L. C. and Pimentel, M. M. (2013) Iron isotope composition of the suspended matter along depth and lateral profiles in the Amazon River and its tributaries. *Journal of South American Earth Sciences*. 44, pp. 35–44. doi: 10.1016/j.jsames.2012.08.001.
- Schemel, L. E., Kimball, B. A. and Bencala, K. E. (2000) ‘Colloid formation and metal transport through two mixing zones affected by acid mine drainage near Silverton, Colorado’, *Applied Geochemistry*, 15(7), pp. 1003–1018. doi: 10.1016/S0883-2927(99)00104-3.
- Sharma, P., Ofner, J. and Kappler, A. (2010) Formation of binary and ternary colloids and dissolved complexes of organic matter, Fe and As. *Environmental Science and Technology*, 44(12), pp. 4479–4485. doi: 10.1021/es100066s.

- Skousen, J., Zipper, C. A., Rose, A., Nairn, R. and McDonald, L. M. (2017) Review of Passive Systems for Acid Mine Drainage Treatment. *Mine Water and the Environment*. Springer Berlin Heidelberg, 36(1), pp. 133–153. doi: 10.1007/s10230-016-0417-1.
- Song, L., Liu, C., Wang, Z., Tang, S., Teng, Y., Liang, L. and Li, J. (2011) Iron isotope fractionation during biogeochemical cycle: Information from suspended particulate matter (SPM) in Aha Lake and its tributaries, Guizhou, China. *Chemical Geology*. Elsevier B.V., 280(1–2), pp. 170–179. doi: 10.1016/j.chemgeo.2010.11.006.
- Sverjensky, D. A. and Fukushi, K. (2006) A predictive model (ETLM) for As(III) adsorption and surface speciation on oxides consistent with spectroscopic data. *Geochimica et Cosmochimica Acta*, 70(15), pp. 3778–3802. doi: 10.1016/j.gca.2006.05.012.
- Swanner, E. D. et al. (2015) ‘Fractionation of Fe isotopes during Fe(II) oxidation by a marine photoferrotroph is controlled by the formation of organic Fe-complexes and colloidal Fe fractions’, *Geochimica et Cosmochimica Acta*. Elsevier Ltd, 165, pp. 44–61. doi: 10.1016/j.gca.2015.05.024.
- Swanner, E. D., Bayer, T., Hao, L., Obst, M., Kleinhanns, I.C. and Schonberg, R. (2017) Iron Isotope Fractionation during Fe(II) Oxidation Mediated by the Oxygen-Producing Marine Cyanobacterium *Synechococcus* PCC 7002. *Environmental Science and Technology*, 51(9), pp. 4897–4906. doi: 10.1021/acs.est.6b05833.
- Tagliabue, A., Bowie, A. R., Boyd, P.W., Buck, K. N. and Johnson, K. S. (2017) The integral role of iron in ocean biogeochemistry. *Nature*. Nature Publishing Group, 543(7643), pp. 51–59. doi: 10.1038/nature21058.
- Wang, Z., Zhang, L., Zhao, J. and Xing, B. (2016) Environmental processes and toxicity of metallic nanoparticles in aquatic systems as affected by natural organic matter. *Environmental Science: Nano*. Royal Society of Chemistry, 3(2), pp. 240–255. doi: 10.1039/c5en00230c.
- Weatherill, J. S., Morris, K., Stawski, T. M., Blackham, R. and Shaw, S. (2016) Ferrihydrite formation: The role of Fe₁₃ Keggin clusters. *Environmental Science and Technology*, 50(17), pp. 9333–9342. doi: 10.1021/acs.est.6b02481.
- Webster, J. G., Swedlund, P. J. and Webster, K. S. (1998) Trace metal adsorption onto an acid mine drainage iron(III) oxy hydroxy sulfate. *Environmental Science and Technology*, 32(10), pp. 1361–1368. doi: 10.1021/es9704390.
- Whitney King, D. (1998) Role of carbonate speciation on the oxidation rate of Fe(II) in aquatic systems *Environmental Science and Technology*, 32(19), pp. 2997–3003. doi: 10.1021/es980206o.
- Wiley, J. Stumm, W., Morgan, J. J., 2006, *Aquatic Chemistry*, third edition. John Wiley and Sons.
- Williamson, M. A., Kirby, C. S. and Rimstidt, J. D. (2006) Iron dynamics in acid mine drainage. 7th International Conference on Acid Rock Drainage 2006, ICARD - Also Serves as the 23rd Annual Meetings of the American Society of Mining and Reclamation, 3(June 2006), pp. 2411–2423. doi: 10.21000/jasmr06022411.

- World Health Organization (2018) A global overview of national regulations and standards for drinking-water quality. Verordnung über die Qualität von Wasser für den menschlichen Gebrauch (Trinkwasserverordnung -TrinkwV 2001), p. 100.
- Wu, B., Amelung, W., Xing, Y., Bol, Y. and Berns, A. E. (2019) Iron cycling and isotope fractionation in terrestrial ecosystems. *Earth-Science Reviews*. 190(12), pp. 323–352. doi: 10.1016/j.earscirev.2018.12.012.
- Wu, L., Beard, B. L., Roden, E. E. and Johnson, Clark, M. (2011) Stable iron isotope fractionation between aqueous Fe(II) and hydrous ferric oxide, *Environmental Science and Technology*, 45(5), pp. 1847–1852. doi: 10.1021/es103171x.
- Wu, W., Swanner, E. D., Pan, Y. and Kappler, A. (2017) Fe isotope fractionation during Fe(II) oxidation by the marine photoferrotroph *Rhodovulum iodolum* in the presence of Si – Implications for Precambrian iron formation deposition. *Geochimica et Cosmochimica Acta*. Elsevier Ltd, 211, pp. 307–321. doi: 10.1016/j.gca.2017.05.033.
- Xu, Y. (2013) Sorption of metal cations on layered double hydroxides. *Colloids and Surfaces A: Physicochemical and Engineering Aspects*. Elsevier B.V., 433(31), pp. 122–131. doi: 10.1016/j.colsurfa.2013.05.006.
- Yamada, R. and Yoshida, T. (2011) Relationships between Kuroko volcanogenic massive sulfide (VMS) deposits, felsic volcanism, and island arc development in the northeast Honshu arc, Japan. *Mineralium Deposita*, 46(5), pp. 431–448. doi: 10.1007/s00126-011-0362-7.
- Zhang, Z., Bi, X., Li, X. and Chen, H. (2018) Schwertmannite: occurrence, properties, synthesis and application in environmental remediation', *RSC Advances*. Royal Society of Chemistry, 8(59), pp. 33583–33599. doi: 10.1039/C8RA06025H.
- Zipper, C. and Skousen, J. (2014) Passive Treatment of Acid Mine Drainage', *Acid Mine Drainage, Rock Drainage, and Acid Sulfate Soils: Causes, Assessment, Prediction, Prevention, and Remediation*. doi: 10.1002/9781118749197.ch30.

Appendix

Appendix A

Behavior of Fe colloids at Amemasu river

Shojin river flows in a region along with Amemasu river as shown in Figure X. The two rivers flow through similar deposits and were both being mined around a similar timeframe and were then closed, but the need for their remediation remains. As chapter 3 shows, natural remediation occurs at Shojin river, where schwertmannite colloids form and aid in the removal of other toxic elements. However, Amemasu river does not self-remediate, thereby posing a risk of releasing toxic elements to the nearby river and later the Japan sea. Colloid formation was also investigated at Amemasu river and Orito river and is explained below. A schematic of the river systems is shown in. Multiple wastewaters are released to the Amemasu river, before finally mixing and flowing downstream. Below are also photos of the drainage taken during sampling, and in particular, Am 3 and Am 3_2 are a mixing point, whose waste and river water have distinct color variations, with the river water having reddish precipitates that are absent in the wastewater.

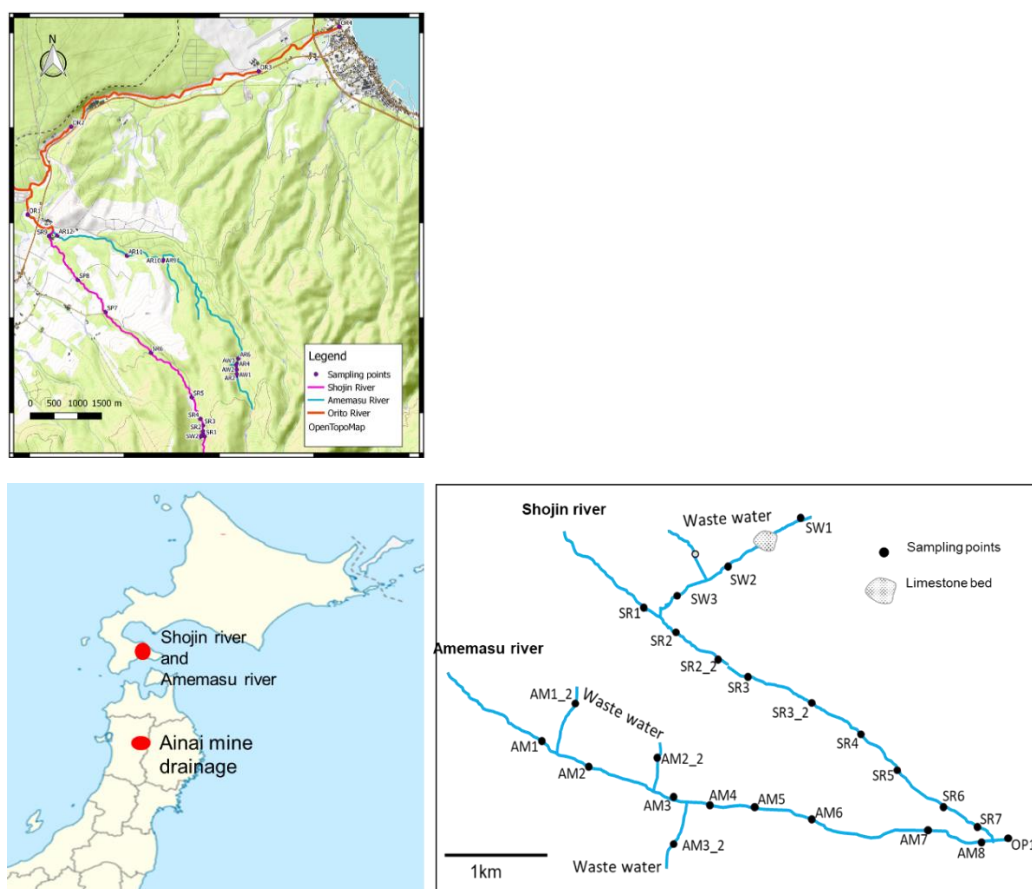


Figure A-1. Locations and schematic diagram of Amemasu, Orito and Shojin rivers

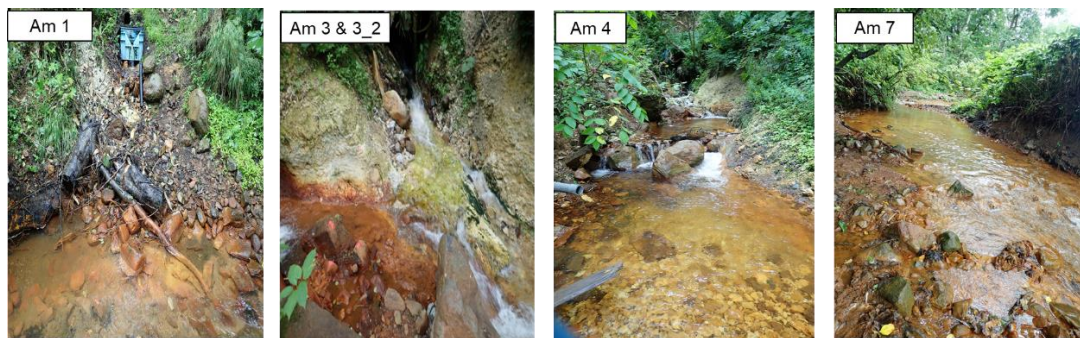


Figure A-2. Pictures taken from the Amemasu river drainage.

The geochemical characteristics of Amemasu river are summarized in the below figure. pH fluctuates significantly with immediate decreases in the wastewater pH, which then quickly rises, before decreasing again at another wastewater entry point. The Fe²⁺ concentration is also very low and fluctuates similarly to the pH. On the other hand, also fluctuates at the upstream, but is relatively low. Once at the downstream, a sudden increase in turbidity is observed implying an increase in the nanoparticles presenting the wastewater. Overall, the general characteristics at Amemasu were relatively like those of Shojin but a major variation is the lower pH at Amemasu than Shojin, which is the cause for the different behaviors of metals at Amemasu.

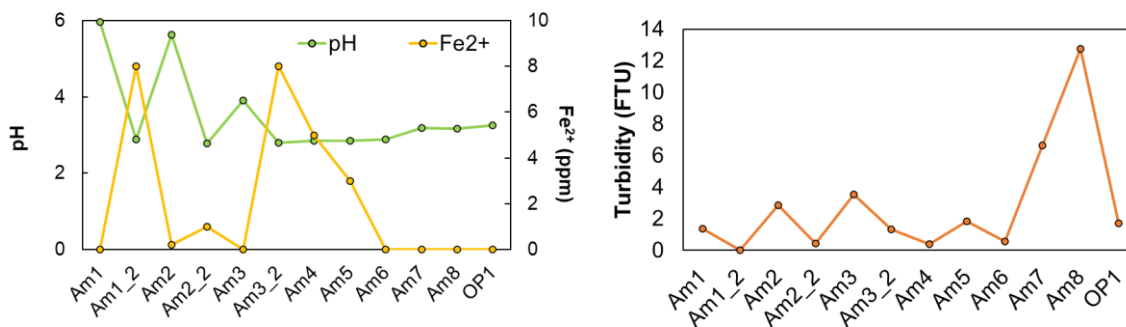


Figure A-3. Variation in pH, ferrous Fe and turbidity at the Amemasu river

The Fe and As concentrations at Amemasu river are plotted in the below figure. All samples with _2 symbolize the wastewater. The input of Fe is similar to Shojin, i.e. around 40 ppm. The river water has almost no Fe and has high pH, which results in drastic decreases in the Fe and almost a complete removal of the Fe once mixing occurs. The Fe concentration then decreases towards the downstream at a very slow rate until Am7 and 8 where drastic decreases are observed. As behaves similar to Fe and shows similar trends,

however, the input of As at Amemasu is significantly higher than that of Shojin. Amemasu As concentrations are about 500 ppb (5 times higher than Shojin), while the Fe supply is the very similar, hence towards the downstream, As concentrations still surpass the stipulated standard of 10 ppb. The precipitation after mixing is however very quick such that all the Fe is consumed, however, at Am7 and 8, the Fe concentration decrease is slower, and colloid formation is observed in both Fe and As. Further remediation is required to ensure that colloids are not transported to the nearby river or sea, since not all of the colloids are removed from the the drainage, particularly of As.

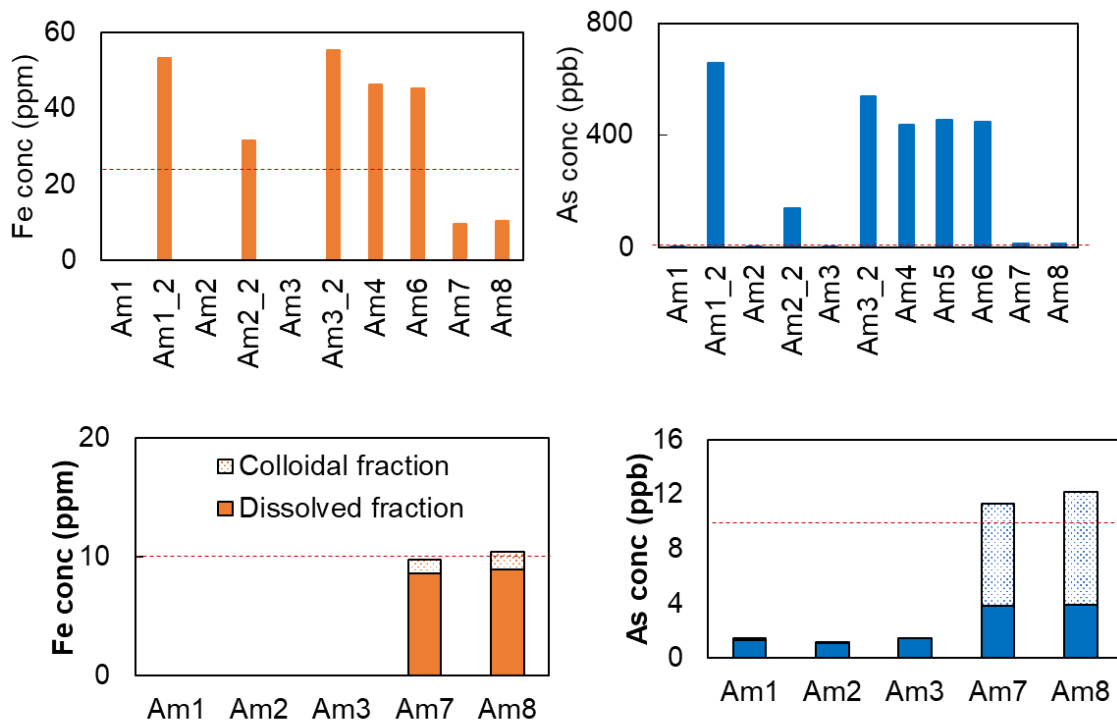


Figure A-4. Dissolved and colloidal fractions of Fe and As at Amemasu river.

Finally, data from Orito river is plotted below to show that colloids formed in the Shojin and Amemasu rivers are not transported towards further downstream, and therefore toxic elements are efficiently removed and not transported to the nearby sea.

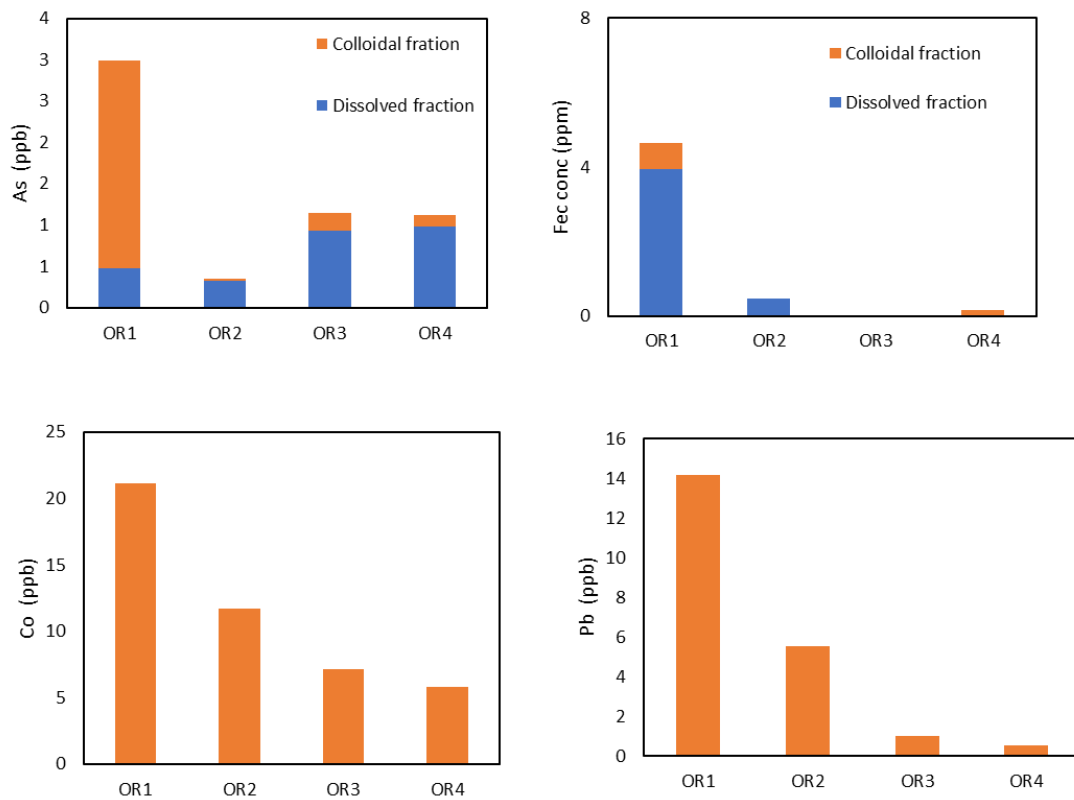


Figure A-5. Concentrations of As, Fe, Co and Pb concentrations at Orito river.

Appendix B

Transport modelling was carried out for the Fe colloids using Phreeqc. Phreeqc incorporated a one dimensional transport model with surface complexation. The model

was developed based on the written code, through which the significant parameters were defined. The detailed code is reported in figure

```

DATABASE c:\phreeqc\database\wateq4f.dat
SOLUTION_SPECIES
Na+ = Na+; -log_k 0; -gamma 1e10 0
Ca+2 = Ca+2; -log_k 0; -gamma 1e10 0
Cl- = Cl-; -log_k 0; -gamma 1e10 0
H2O + 0.01e- = H2O-0.01; -log_k -9
H3AsO4 = AsO4-3 + 3H+; -log_k -20.7
SURFACE_MASTER_SPECIES /* define sorbed form of Hfo = Sfo */
Sfo_s Sfo_sOH; Sfo_w Sfo_wOH
As H3AsO4 -1.0 74.9216 74.9216
SURFACE_SPECIES
Sfo_sOH = Sfo_sOH; log_k 0.0
Sfo_sOH + H+ = Sfo_sOH2+; log_k 7.29
Sfo_sOH = Sfo_sO- + H+; log_k -8.93
Sfo_wOH = Sfo_wOH; log_k 0.0
Sfo_wOH + H+ = Sfo_wOH2+; log_k 7.29
Sfo_wOH = Sfo_wO- + H+; log_k -8.93
# Calcium
Sfo_sOH + Ca+2 = Sfo_sOHCa+2; log_k 4.97
Sfo_wOH + Ca+2 = Sfo_wOCa+ + H+; log_k -5.85
# Zinc
Sfo_sOH + Zn+2 = Sfo_sOZn+ + H+; log_k 0.99
Sfo_wOH + Zn+2 = Sfo_wOZn+ + H+; log_k -1.99
#Arsenic
Sfo_sOH + AsO4-3 + 3H+ = Sfo_sH2AsO4 + H2O; log_k 29.31
Sfo_wOH + AsO4-3 + 2H+ = Sfo_wHAsO4- + H2O; log_k 23.51
SOLUTION 1-21
pe 14 O2(g) -0.58
Na 1; Ca 1; Cl 1 charge
SURFACE 1-21 # define small conc's
Hfo_w 97.5e-15 600 88e-13 Dw 1e-13
Hfo_s 2.5e-15
Sfo_w 97.5e-15 600 88e-13 Dw 0
Sfo_s 2.5e-15
-donnan 1e-10
-equil 1
END
SOLUTION 0
pe 14 O2(g) -0.58
Na 10; Ca 1; As 13; Cl 100 charge
SURFACE 0
Hfo_w 97.5e-5 600 88e-3 Dw 1e-13
Hfo_s 2.5e-5
-donnan 1e-10 #d 1 | 0.99 v 1# 1e-9
-equil 0
END
PRINT; -reset false; -status false

RATES
Sorb_hfo
-start
10 rate = -40 * tot("Hfo_w") else rate = 400 * tot("Sfo_w")
20 save rate * time

-end
KINETICS 1-21
Sorb_Hfo; -formula Hfo_w 0.975 Hfo_s 0.025 Sfo_w -0.975 Sfo_s -0.025
USER_GRAPH
-head As_Hfo As_tot
-axis_titles "Distance" "ug/L"
-chart_title "Arsenic colloid formation and transport in the presence of Ferrihydrite"
-axis_scale x_axis 0 3
-axis_scale y_axis 0 0.2
-plot_concentration_vs t
-start
10 PV = (step_no + 0.5) / 1 / cell_no
12 if sim_no > 4 then PV = PV + 1.0
20 As_sol = 1e3 * tot("As")
30 As_col = 1e3 * (mol("Hfo_sH2AsO4") + mol("Hfo_wHAsO4-"))
40 plot_xy PV, get(99), color = Green, symbol = None, y_axis = 2
50 plot_xy PV, (tot("Hfo_w") + tot("Hfo_s")) * 1e3, color = Orange, symbol = Circle,
symbol_size = 10, line_width = 0
60 plot_xy PV, As_col, color = Magenta, symbol = Circle, symbol_size = 6, line_width = 0

-end
TRANSPORT
-cells 20
-length 0.1; -disp 0.066
-shifts 10 1
-punch_fr 1
-punch_c 10
-time 0.5e-2
-bcon 3 3
-diffc 0.3e-9
-multi_d true 1e-9 0.3 0 1
END
PRINT; -user_graph false
SURFACE 0
SOLUTION 0
pe 14 O2(g) -0.58
Na 1; Ca 0; Cl 1 charge
END
PRINT; -user_graph true
TRANSPORT
-shifts 30 1
END

```



```

DATABASE c:\phreeqc\database\wateq4f.dat
SOLUTION_SPECIES
Na+ = Na+; -log_k 0; -gamma 1e10 0
Ca+2 = Ca+2; -log_k 0; -gamma 1e10 0
Cl- = Cl-; -log_k 0; -gamma 1e10 0
H2O + 0.01e- = H2O-0.01; -log_k -9
H3AsO4 = AsO4-3 + 3H+; -log_k -20.7
SURFACE_MASTER_SPECIES /* define sorbed form of Hfo = Sfo */
Sfo_s Sfo_sOH; Sfo_w Sfo_wOH
As H3AsO4 -1.0 74.9216 74.9216
SURFACE_SPECIES
Sfo_sOH = Sfo_sOH; log_k 0.0
Sfo_sOH + H+ = Sfo_sOH2+; log_k 7.29
Sfo_sOH = Sfo_sO- + H+; log_k -8.93
Sfo_wOH = Sfo_wOH; log_k 0.0
Sfo_wOH + H+ = Sfo_wOH2+; log_k 7.29
Sfo_wOH = Sfo_wO- + H+; log_k -8.93
# Calcium
Sfo_sOH + Ca+2 = Sfo_sOHCa+2; log_k 4.97
Sfo_wOH + Ca+2 = Sfo_wOCa+ + H+; log_k -5.85
# Zinc
Sfo_sOH + Zn+2 = Sfo_sOZn+ + H+; log_k 0.99
Sfo_wOH + Zn+2 = Sfo_wOZn+ + H+; log_k -1.99
#Arsenic
Sfo_sOH + AsO4-3 + 3H+ = Sfo_sH2AsO4 + H2O; log_k 29.31
Sfo_wOH + AsO4-3 + 2H+ = Sfo_wHAsO4- + H2O; log_k 23.51
SOLUTION 1-21
pe 14 O2(g) -0.58
Na 1; Ca 1; Cl 1 charge
SURFACE 1-21 # define small conc's
Hfo_w 97.5e-15 600 88e-13 Dw 1e-13
Hfo_s 2.5e-15
Sfo_w 97.5e-15 600 88e-13 Dw 0
Sfo_s 2.5e-15
-donnan 1e-10
-equil 1
END
SOLUTION 0
pe 14 O2(g) -0.58
Na 10; Ca 1; As 100; Cl 100 charge
SURFACE 0
Hfo_w 97.5e-5 600 88e-3 Dw 1e-13
Hfo_s 2.5e-5
-donnan 1e-10 #d 1 | 0.99 v 1# 1e-9
-equil 0
END
PRINT; -reset false; -status false

RATES
Sorb_hfo
-start
10 rate = -100 * tot("Hfo_w") else rate = 400 * tot("Sfo_w")
20 save rate * time

-end
KINETICS 1-21
Sorb_Hfo; -formula Hfo_w 0.975 Hfo_s 0.025 Sfo_w -0.975 Sfo_s -0.025
USER_GRAPH
-head As_Hfo As_tot
-axis_titles "Distance" "ug/L"
-chart_title "Arsenic colloid formation and transport in the presence of Schwertmannite"
-axis_scale x_axis 0 3
-axis_scale y_axis 0 0.2
-plot_concentration_vs t
-start
10 PV = (step_no + 0.5) / 1 / cell_no
12 if sim_no > 4 then PV = PV + 1.0
20 As_sol = 1e3 * tot("As")
30 As_col = 1e3 * (mol("Hfo_sH2AsO4") + mol("Hfo_wHAsO4-"))
40 plot_xy PV, get(99), color = Green, symbol = None, y_axis = 2
50 plot_xy PV, (tot("Hfo_w") + tot("Hfo_s")) * 1e3, color = Orange, symbol = Circle,
symbol_size = 10, line_width = 0
60 plot_xy PV, As_col, color = Magenta, symbol = Circle, symbol_size = 6, line_width = 0

-end
TRANSPORT
-cells 20
-length 0.1; -disp 0.066
-shifts 10 1
-punch_fr 1
-punch_c 10
-time 0.5e-2
-bcon 3 3
-diffc 0.3e-9
-multi_d true 1e-9 0.3 0 1
END
PRINT; -user_graph false
SURFACE 0
SOLUTION 0
pe 14 O2(g) -0.58
Na 1; Ca 0; Cl 1 charge
END
PRINT; -user_graph true
TRANSPORT
-shifts 30 1
END

```

Figure B-1 top and bottom. Phreeqc modelling code for the surface complexation of colloids and incorporation of the transport model for Ainai (left) and Shojin (right).

Appendix C

The contents of this part of the appendix are yet to be submitted to Malawi Journal of Science and Technology

Environmental assessment report for the Lisungwi and Kaphamtengo rivers in Manondo, Central Malawi

Frances Chikanda¹, Tsubasa Otake², Jones Mwatseteza³, Tsutomu Sato²

¹Division of Sustainable Resource Engineering, Graduate School of Engineering, Hokkaido University, N13W8, Kita-ku, Sapporo, 0608628, Japan

²Division of Sustainable Resource Engineering, Faculty of Engineering, Hokkaido University, N13W8, Kita-ku, Sapporo, 0608628, Japan

³Department of Chemistry, Chancellor College, University of Malawi, P.O. Box 280, Zomba, Malawi

Abstract

Mining activities can be one of the most impactful sources of water contamination. In Malawi, gold deposits occur in the basement rocks of the Lisungwi-Manondo region. As a result, a boom in small scale artisanal mining has occurred as residents have settled in the area. Despite the development of mining activities, few studies have investigated the water quality of the main rivers in the region (i.e., the Lisungwi and Kaphamtengo rivers), upon which local residents are highly dependent for daily use. This study provides baseline data for water quality in the region. The river water has a moderate buffering capacity due to its high alkalinity, along with high Ca, Si, Mg, and Cl concentrations sourced from the gneiss and calcsilicate rocks in the region. Further analysis of the water quality based on the physiochemical parameters (e.g. pH, turbidity, electric conductivity), major and trace element concentrations, showed that the river waters were in accordance with guidelines set by the Malawi Bureau of Standards (MBS) and the World Health Organization (WHO) for river water quality, with all analyzed parameters being below

the recommended standards. Our results indicated that the regional geology exerts a significant control on water chemistry, but the impact on the river water leaves the water in an uncontaminated state.

1. Introduction

Reports of artisanal gold mining in Malawi date back to the 1930s, and an interest in the exploration of economically significant gold (Au) occurrences persists until today (British Geological Survey, 2009). A few exploration programs focus on previously known Au occurrences. Key sites for further development include the Lisungwi Valley-Kirk Range, the Nathenje region in Lilongwe, and the Dwangwa River in Nkhotakota (Japan International Cooperation Agency [JICA], 2013). However, the progress made on such exploration programs has varied.

Recently, Malawi has experienced a boom in alluvial/placer gold mining (Malunga, 2012). The main mining areas include Mangochi, Chitipa, Kasungu, Lilongwe, Ntcheu, Neno, and Balaka. Among them, the Ntcheu-Neno-Balaka block, in the Lisungwi Valley-Kirk Range, is the largest hotspot and attracts hundreds of miners, a significant proportion of which are small scale artisanal miners (Catholic Commission for Justice and Peace [CCJP], 2012; Etter-Phoya, 2015). Such mining booms have the potential to ravage landscapes, disturb natural ecosystems, and contribute to the loss of agricultural and farmland. Increased human activities in mining areas can undermine the availability and quality of natural resources such as water (Wilson et al., 2015; Funoh, 2014). Despite the widespread use of groundwater from boreholes in rural areas of Malawi, a significant portion of the population continues to rely on surface water (including rivers) for domestic

use such as drinking. Measurements of the chemical composition of these water sources in most areas are either scarce or non-existent (Addison et al., 2020; Mkwate et al., 2017; Sajidu et al., 2007). The risks associated with mining activity are high due to (a) the potential exposure of the population to unsafe water sources, and (b) the inability to monitor the impact of artisanal gold mining on the availability and quality of water resources. Kanyerere et al. (2012) discuss the effects of water contamination by microbial pathogens, physical agents, chemical compounds, and radiologic agents. Such effects include environmental and health concerns for millions of people and can be associated with increased morbidity and mortality, especially in vulnerable populations most at risk of water-related diseases. Consequently, unregulated gold mining in the country is of great concern for farmers, government officials, and environmental experts.

To address the scarcity of physicochemical datasets of water in Malawian artisanal gold mining hotspots, we conducted measurements in the Lisungwi River in the Manondo area, within the Ntcheu-Neno-Balaka block. Due to widespread artisanal mining activities in the region, we also sampled the Lisungwi tributary, Kaphamtengo River. Our research addresses the absence of crucial water quality data in the area, where water from the Lisungwi and Kaphamtengo rivers are used for domestic purposes by local communities.

2. Location and geology of the study area

The study area is located at the boarder of the Neno, Balaka, and Ntcheu districts in southern Malawi (Figure 1). The Lisungwi River forms the boundary between the Balaka and Neno districts, while the Kaphamtengo River separates Ntcheu from Balaka. The Malawi–Mozambique border lies a few kilometers to the west of the study area.

(bottom left (British Geological Survey, 2019)) and enlarged geological map of the study area showing sampling points as green dots (bottom right).

3. Materials and methods

3.1. Sampling and on-site field measurements

Water was sampled from eight locations on the Lisungwi and Kaphamtengo rivers in September 2019. September is a dry season and precedes the driest season of October when temperatures are the highest in the region. Four samples were collected at each location in pre-rinsed 50 mL plastic polyethylene bottles: (i) an unfiltered sample for on-site measurements; (ii) a 0.2 μm polytetrafluoroethylene (PTFE) membrane-filtered, non-acidified sample for anion analyses; (iii) a 0.2 μm PTFE membrane-filtered sample acidified with 1 vol% HNO_3 (ultrapure grade, Kanto Chemicals, Japan) for cation analyses; and (iv) a 0.45 μm PTFE membrane filtered sample for alkalinity titration. The three latter samples were kept at $\sim 4^\circ\text{C}$ and analyzed at the Laboratory of Environmental Geology, Hokkaido University, Japan.

The dissolved oxygen (DO), pH, electrical conductivity (EC), turbidity, temperature, oxidation–reduction potential (ORP), and alkalinity of the water samples were measured on-site. Alkalinity was measured by titrating HNO_3 into the 50 mL water samples that had been filtered through a 0.45 μm PTFE membrane filter. The bicarbonate ion (HCO_3^-) concentration was obtained from alkalinity using the Gran function plot method (Rounds, 2006). The Geochemist's Workbench (GWB14) software was used to calculate the charge balance and construct the Piper diagrams for water classification.

3.2. Analytical methods

Non-acidified water samples were diluted 10 times and analyzed for anion concentrations by ion chromatography (Metrohm Advanced Compact IC 861). Anion mixture standard solution 1 (Multi-anion Standard Solution 1, Wako Pure Chemical Industries, Ltd) was used as the calibration standard. Acidified water samples were diluted 40 times and analyzed for major and trace element concentrations by inductively coupled plasma–atomic emission spectroscopy (ICP–AES; Shimadzu ICPE-9000) and ICP–mass spectroscopy (ICP–MS; Thermo Scientific iCap Qc). Multi-element standard solutions were prepared using a multi-standard solution (Wako Pure Chemical Industries, Ltd.). Ruthenium, Rh, and Ir were used as internal standards for the ICP–MS analyses. Oxide formation during measurements was monitored by the CeO/Ce ratio, which remained below 0.5% to minimize the mass interference of Ba-oxides on Eu.

4. Results and Discussion

4.1. Water and socio-economic factors

During the field work activities, observations and verbally communicated information from the locals was obtained and combined with informal reports to have an overview of the river water usage at Lisungwi and Kaphamtengo rivers. Water from the Lisungwi and Kaphamtengo rivers is used for domestic purposes. These rivers constitute the main source of water for cooking, bathing, and washing, as well as drinking for local residents and farmed animals. Fertilizers are used on cropland—mainly maize, groundnuts and soybeans—near the rivers to improve yields. The rivers' water levels fluctuate significantly, as attested by layered marks left by high waters during the rainy season and recordings of flooding events. Informal communications with local residents suggested

that the quality of the river water was satisfactory, and that no foul taste or coloration had been observed in and outside of the rainy season. High turbidity has been recorded during the rainy season, mainly due to storm water inflow and the mixing of water with sediments. However, once settled, the river water quickly returns to an easily usable form. Despite the absence of stringent community rules to protect water resources, the river water appears to be fit for consumption and daily use.

4.2. Physicochemical characteristics of the river water

The physicochemical parameters of the two rivers measured on site are reported in Table 1. All results were compared to the guidelines from the Malawi Bureau of Standards (MBS describe title of standard) and the World Health Organization (WHO describe title of standard) to determine the quality-based use of the water. The pH of the water in the rivers was neutral for all samples (7.30 to 7.68), in accordance with MBS and WHO standards for stream and river waters. DO values were relatively uniform (with an average of ~7.31 mg/L), although DO at L1 was slightly lower than at other sites. Similarly, EC and temperature were relatively homogeneous, varying from 16.15 to 22.50 mS/m, and from 22.87 to 29.47°C, respectively. The rivers are relatively oxidizing according to ORP values that range from 183 to 282 mV. Turbidity values were similar between sites (22.40 to 41.63 FTU), except in the visibly brown colored water at K1, where turbidity reached 169 FTU. The high turbidity at this site was most likely due to re-construction of a bridge activities that were observed during sample collection. The bridge had been destroyed due to previous flooding events, prompting people to cross through the river directly, thereby contributing to the high turbidity of the river water. Anion concentrations

measured in these water samples were all below WHO and MBS standards, and the average charge balance was calculated as $\pm 12\%$.

Table 2. Physicochemical characteristics of the Lisungwi and Kaphamtengo Rivers.

	pH	DO (mg/L)	EC (mS/m)	ORP (mV)	Turbidity (FTU)	Temp. (°C)	Alkali. (mg/L)	NO ₃ (mg/L)	Cl ⁻ (mg/L)
K1	7.30	7.45	16.15	282.00	169.00	22.87	35.10	14.2	21.2
K2	7.56	7.21	19.11	211.67	41.63	26.33	50.70	16.6	20.6
K3	7.61	7.14	18.74	234.33	27.28	26.93	50.70	14.6	29.5
L1	7.57	6.96	22.07	201.00	35.71	29.47	50.70	12.6	22.4
L2	7.53	7.31	19.82	183.00	27.51	27.33		12.4	24.0
L3	7.51	7.32	20.14	196.33	29.45	29.33	50.70	12.4	23.9
L4	7.53	7.65	19.70	242.33	32.90	23.63		12.2	25.5
L5	7.68	7.33	22.50	247.00	25.33	24.87	50.70	12.3	27.7
L6	7.51	7.04	21.67	233.67	22.40	28.70	58.60	12.4	38.8
WHO								50	
MBS								45	

DO: dissolved oxygen; EC: electric conductivity; ORP: oxidation-reduction potential; Temp.: Temperature; Alkali.: Alkalinity; WHO: World Health Organization; MSB: Malawi Bureau of Standards.

4.3. Geological controls on water quality

Understanding the quality of surface waters has been done using various approaches, with the aim of highlighting the controlling factors for their chemistry. Surface waters have a wide range of controlling factors, that range from groundwater quality and compositions, the bedrock of the area and anthropogenic processes such as farming, industrial use and mining. Appello and Postma (2005) summarized the controlling parameters, using plots that compare surface waters from around the world. Besides the major factors, taking into consideration the hydrological cycle highlights the complexity of the factors that affect the surface waters, such as rainfall, mixing of various waters, evaporation and uptake by

vegetation among other factors (Pagano and Sorooshian, 2014; Kumambala, 2010). Specifically, the decay of organic matter, weathering, and dissolution of minerals, mixing of different water qualities and anthropogenic activities are the processes that underlie the major factors affecting water quality. Since the amount of organic matter to be taken into consideration at Lisungwi and Kaphamtengo rivers is very minimal, redox reactions of organic matter are not considered as a controlling factor for the river quality. Furthermore, the main anthropogenic activities that are carried out in the area are domestic use, feeding of cattle and small scale artisanal mining. However, since these activities are carried at a very small scale and by a small population, anthropogenic factors may not really be controlling the water chemistry at the site. Therefore, that leaves the major controlling factor for the water quality at Lisungwi and Kaphamtengo to be the underlying geology, which allows for interaction with existing bedrock and dissolution of minerals.

Lisungwi and Kaphamtengo rivers flow through metamorphic rocks. Metamorphic dolomitic marble, minor calcite, granite, and minor diopside occur in the region, in addition to gold-bearing quartz, pyrite among other occurrences. Rock fragments, gravel, sand, and sub-sand are also found in the wider region. Given the mineral composition of the main mineral occurrences in the region, a correlation between the river water and bedrock is investigated using water classification plot, which is presented in Figs 2. High (bi)carbonate, Ca, and Mg concentrations indicate a strong buffering capacity of the water and are indicative of a dominant geological control on water quality. Furthermore, elevated Cl concentrations in the Piper diagram suggest the influence of calcsilicate rocks on water chemistry. The total dissolved salts were about 135 mg/L on average, with high amounts of Ca, Mg and HCO_3 . Underlying bedrock mainly controls the water chemistry through dissolution of the existing minerals.

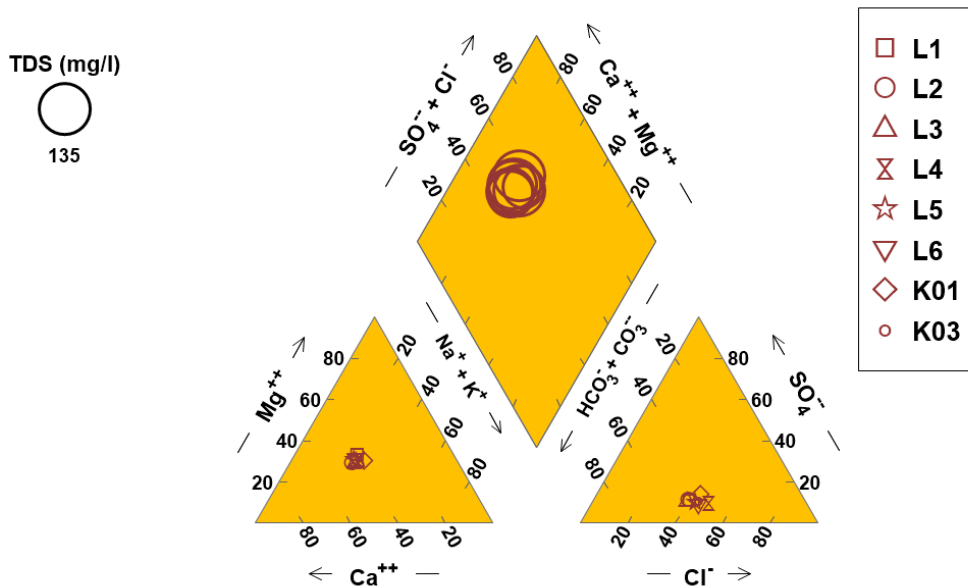


Figure 0-2. Piper diagram displaying the chemical compositions of the Lisungwi (L01–L06) and Kaphamtengo (K01–K03) rivers.

A comparison of the Lisungwi and Kaphamtengo rivers with other world surface waters is shown in Figure 0-3. The plots suggested by (Gibbs, 1970) give a reflection of the nature of groundwater that interacts with the surface water. Na and Cl are ions that are mainly contributed from rainwater, whereas on the other hand, elements like Ca and HCO_3^- are a result of dissolution by Ca-silicates, calcite and other carbonate minerals. According to the plots, it is seen that Lisungwi and Kaphamtengo rivers plot almost in the middle of Ca and Na rich waters, but more inclined towards the Ca region, thereby highlighting the impact from dissolution of the underlying minerals. And to complement the possibility of mineral-rock interaction, the Lisungwi and Kaphamtengo rivers are also

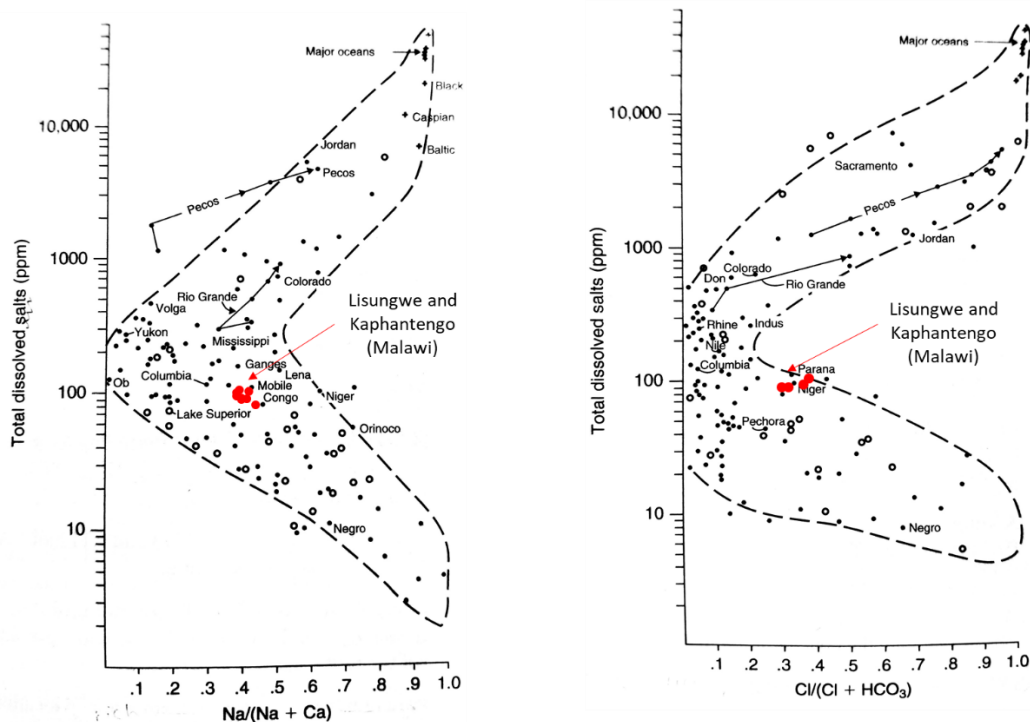


Figure 0-3. The chemistry of Lisungwi and Kaphantengo rivers in comparison with other world surface waters, expressed as a function of total dissolved salts (TDS) and the relative contribution of Na^+ , Ca^{2+} , and Cl^- and HCO_3^- .

high in HCO_3^- , thereby conquering with the initial suggestion that highlights the mineral dissolution as a major factor controlling the water chemistry. It is therefore reasonable to conclude that the water chemistry at the two rivers is controlled by the dissolution of the minerals from the bedrock, thereby giving the water the carbonate nature.

Major element concentrations of the river water are presented in Figure 0-5. All concentrations were below MBS and WHO standards, and were relatively similar at all sites.

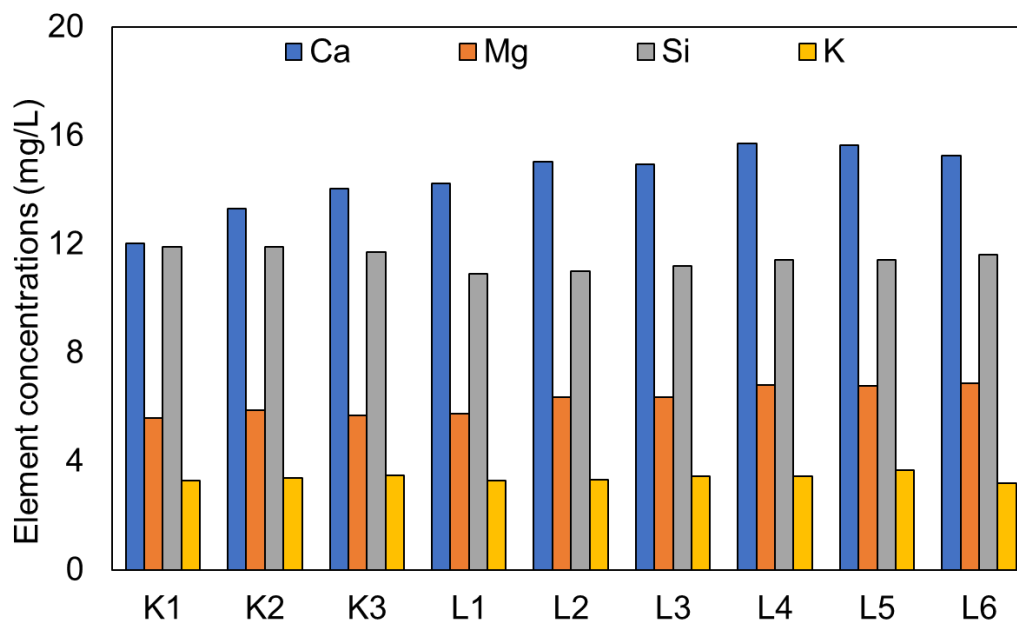


Figure 0-4. Major element concentrations in the Lisungwi and Kaphamtengo rivers.

All elements present in our standard (Al, Ba, Ca, Fe, K, Mg, Mn, Na, Si) were analyzed, but most of them were below the detected limit, therefore those reported in Figure 0-5 are those whose concentrations were high enough to analyze. Elevated Si concentrations, possibly from the presence of the (Ca)- silicate minerals, in the region, also supported a geological control on the elemental composition of the river water. The Ca concentrations in Kaphamtengo river ranged from 12 to 13 mg/L while in the Lisungwi river were slightly elevated, with their values ranging from 13 to 16 mg/L. Mg concentrations were within 4 to 7 mg/L in both rivers. Similarly, other major elements such Si and K were within similar ranges in the two rivers. Despite all of the elements being under the recommended standard, a trend in geological control is observed. The Ca and Mg concentration and the highest major elements present in the water, evidently from the interaction of the water with the bedrock which consists of calcsilicates, dolomites and

other carbonate rocks. From the major elemental concentrations, it is evident that the regional geology has a significant impact on water chemistry, however, this does not result in contaminated water.

4.4. Concentration of hazardous elements

The insight obtained from the major chemistry was then complemented by investigating the trace elements (As, Ba, Cd, Co, Cr, Cs, Cu, Ni, Pb, Sr and Zn), in order to identify any potentially hazardous elements that may have been present in the river waters. All the trace elements that were analyzed had concentrations below 1.5 $\mu\text{g/L}$, and most of them, except some (discussed below) were below the detection limit. The low concentrations in the water samples shows that the water in the Lisungwi and Kaphamtengo rivers is uncontaminated. Despite the low concentrations, a notable trend was observed for the elements whose concentrations were within observable limits, i.e., As, Cr and Cu. These concentrations, despite being very low, are slightly higher in the Lisungwi unlike the Kaphamtengo river (Figure 0-5). This trend is similar to that displayed by Ca. Although the difference is minor, it might be an indicator of the impact of the different geologies that the rivers flow through (Figure 0-1, bottom). The underlying bedrock may be responsible for releasing more Ca, and possibly As and Cr, that results in the slightly elevated values in the Lisungwi and not Kaphamtengo rivers. Evidently, these results show that the anthropogenic activities occurring at the two rivers have thus far not influenced the water chemistry in the rivers, therefore, our dataset may be considered a baseline to monitor future changes in land uses and their effect on water chemistry.

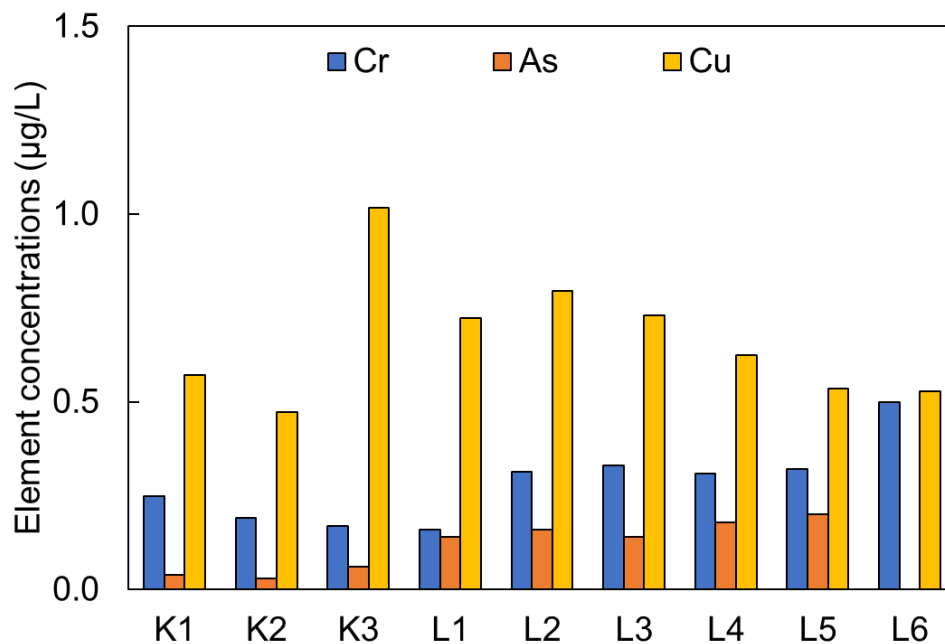


Figure 0-5. Major and trace element concentrations in the Lisungwi and Kaphamtengo rivers.

5. Conclusions

The potential for gold mining in the Lisungwi catchment area warranted an environmental study to provide background data on river water quality. The Lisungwi and Kaphamtengo rivers flow through metamorphic rock that currently hosts widespread artisanal gold mines. Alluvial sediments containing gold are collected using buckets and panned multiple times to extract gold. Although the land is slightly disturbed, evidence for no contamination was seen based on the elemental composition of the river water, with most metal concentrations below the WHO standards. Physicochemical parameters were also in line with natural river water that had not been contaminated by mining activities. Potential contamination by other anthropogenic activities, such as farming and bathing,

were also explored in our study. We found that the water did not appear to be contaminated by anthropogenic activities, likely because the overall use of the rivers for these activities was low, and because any potential contamination may have been quickly transferred downstream.

6. Acknowledgements

The authors would like to thank Mr. Edward Hlane and Ms. Ayaka Murofushi for his assistance during the field work and the chief as well as the residents of the area for welcoming us to investigate the river water. This research was supported by the Japan Society for the Promotion of Science (JSPS) KAKENHI (17H03502; 20H00184) to T.O.; and the Japan International Cooperation Agency (JICA).

7. References

- Addison, M. J., Rivett, M., Robinson, H., Fraser, A., Miller, A.M., 2020. Fluoride occurrence in the lower East African Rift System, Southern Malawi. *Sci. of the Total Environ.* 712. 136260. doi: 10.1016/j.scitotenv.2019.136260.
- Appelo, C.A.J., Postma, D. 2005. *Geochemistry, groundwater and pollution*. 2nd Edition. Balkema Publishers, The Netherlands. pp 40-51
- British Geological Survey, United Kingdom, 2009. Mineral deposits associated with the basement metamorphic and igneous rocks (precious and base metals, gemstones and industrial minerals), Ministry of Energy and Mines, Republic of Malawi. <http://www.malawi.gov.mw/Mines/Energy>.

- CCJP, 2012. Mapping of Extractive companies in Malawi. available at <https://mininginmalawi.com>
- Etter-Phoya, R., 2015. Formalising for Development: Artisanal and Small-Scale Mining in Malawi's Draft Mining Legislation: Unpublished assignment, Centre for Energy, Petroleum and Mineral Law and Policy, University of Dundee, available at <https://miningmalawi.com>
- Funoh, K., 2014. The impacts of artisanal gold mining on local livelihoods and the environment in the forested areas of Cameroon. CIFOR Working Paper, 150. Doi: <http://doi.org/10.17528/cifor/005089>
- JICA, 2013. Final Report of the Project for Establishment of Integrated Geographic Information System (GIS) Database for Mineral Resources Abridgment: Sumiko Resources Exploration and development company limited.
- Kanyerere, T., Levy, J., Xu, Y., Saka, J., 2012. Assessment of microbial contamination of groundwater in upper Limphasa River catchment, located in a rural area of northern Malawi. *Water SA*, 38, pp. 581–596. doi: 10.4314/wsa.v38i4.14.
- Kumambala, P. G. (2010) ‘Sustainability of water resources development for Malawi with particular emphasis on North and Central Malawi’, *Water Resources*. Available at: <http://theses.gla.ac.uk/1801/>.
- Malunga, G. W. P., 2012. Gold mining potential in Malawi. *Mining and Trade Review*, 69, pp. 10.
- Mkwate, R. C., Chidya, R. C. G. and Wanda, E. M. M., 2017. Assessment of drinking water quality and rural household water treatment in Balaka District, Malawi. *Physics and*

Chemistry of the Earth. 100, pp. 353–362. doi: 10.1016/j.pce.2016.10.006.

Onuma, T., 2013. Final Report of the Project for Establishment of Integrated Geographic Information System (GIS) Database for Mineral Resources Abridgment. pp. 1–118.

Pagano, T. C. and Sorooshian, S., 2014. Hydrologic cycle. Encyclopedia of global environmental change. pp. 450–464.

Rajae, M., Obiri, S., Green, A., 2015. Integrated assessment of artisanal and small-scale gold mining in Ghana—Part 2: Natural Sciences Review. International Journal of Environmental Research and Public Health, 12, 8, pp. 8971–9011. doi: 10.3390/ijerph120808971.

Rivett, M. Robinson, H.L., Melville, J., McGrath, L., Flink, J., Wanangwa, G.J., Mleta, P., Kalin, R.M., 2019. Arsenic occurrence in Malawi groundwater. Journal of Applied Sciences and Environmental Management, 22, 11, pp. 1807. doi: 10.4314/jasem.v22i11.16.

Rounds, S. A., 2006. Alkalinity and acid neutralising capacity (ver. 3.0): US Geological Survey Techniques of Water-Resources Investigations, book 9, chap. A6, sec. 6.6.

Sajidu, S. M. I., Masamba, W.R.I., Henry, E.M.T., Kuyeli, S.M., 2007. Water quality assessment in streams and wastewater treatment plants of Blantyre, Malawi. Physics and Chemistry of the Earth, 32(15–18), pp. 1391–1398. doi: 10.1016/j.pce.2007.07.045.

Wilson, M. L., Renne, E., Roncoli, C., Agyei-Baffour, P., Tenkorang, E.Y., 2015. Integrated assessment of artisanal and small-scale gold mining in Ghana - Part 3: Social sciences and economics. International Journal of Environmental Research and Public Health, 12(7), pp. 8133–8156. doi: 10.3390/ijerph120708133.

Appendix

Table A1. Metal concentrations of the Lisungwi and Kaphamtengo Rivers.

Site	Concentrations (mg/L)						Concentrations (µg/L)						
	Ca	Fe	K	Mg	Si	P	Pb	Zn	Cr	As	Co	Ni	Cu
K1	12.01	0.09	3.28	5.59	11.9	b.d.	b.d.	b.d.	0.25	0.04	0.06	0.14	0.57
K2	13.30	0.02	3.36	5.87	11.9	b.d.	b.d.	b.d.	0.19	0.03	0.08	0.15	0.47
K3	14.02	0.14	3.47	5.69	11.7	b.d.	b.d.	0.01	0.17	0.06	0.14	0.15	1.02
L1	14.22	0.02	3.28	5.76	10.9	b.d.	b.d.	b.d.	0.16	0.14	0.06	0.13	0.72
L2	15.01	0.01	3.30	6.37	11.0	b.d.	b.d.	b.d.	0.32	0.16	0.05	0.14	0.80
L3	14.94	0.02	3.45	6.37	11.2	b.d.	b.d.	b.d.	0.33	0.14	0.06	0.12	0.73
L4	15.70	0.02	3.43	6.81	11.4	b.d.	b.d.	0.03	0.33	0.18	0.05	0.13	0.62
L5	15.64	b.d.	3.66	6.76	11.4	b.d.	b.d.	b.d.	0.31	0.20	0.16	b.d.	0.54
L6	15.26	b.d.	3.19	6.86	11.6	b.d.	b.d.	0.01	0.50	b.d.	0.05	b.d.	0.53
WHO	75–200	10		-				5.00					
MBS	250	3		200									

b.d.: Below detection limit; **WHO:** World Health Organization; **MBS:** Malawi Bureau of Standards.